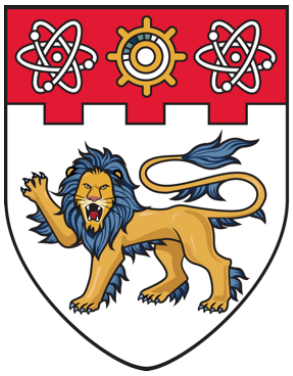

NANYANG TECHNOLOGICAL UNIVERSITY
SINGAPORE

DEVELOPMENT OF SELF-ASSEMBLED SUPRAMOLECULAR DENDRITIC DNA HYDROGEL FOR 3D CELL CULTURE PLATFORM

BELLA ROSA LIYARITA

SCHOOL OF PHYSICAL AND MATHEMATICAL SCIENCES

2022

DEVELOPMENT OF SELF-ASSEMBLED SUPRAMOLECULAR DENDRITIC DNA HYDROGEL FOR 3D CELL CULTURE PLATFORM

BELLA ROSA LIYARITA

SCHOOL OF PHYSICAL AND MATHEMATICAL SCIENCES

A thesis submitted to the Nanyang Technological University in partial fulfilment of the requirement for the degree of Doctor of Philosophy

2022

Statement of Originality

I hereby certify that the work embodied in this thesis is the result of original research done by me except where otherwise stated in this thesis. The thesis work has not been submitted for a degree or professional qualification to any other university or institution. I declare that this thesis is written by myself and is free of plagiarism and of sufficient grammatical clarity to be examined. I confirm that the investigations were conducted in accord with the ethics policies and integrity standards of Nanyang Technological University and that the research data are presented honestly and without prejudice.

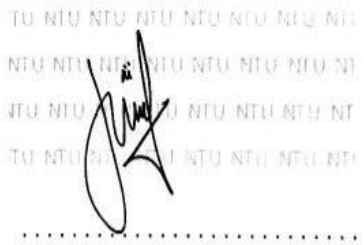

2 August 2021
.....
Date

.....
Bella Rosa Liyarita

Supervisor Declaration Statement

I have reviewed the content and presentation style of this thesis and declare it of sufficient grammatical clarity to be examined. To the best of my knowledge, the thesis is free of plagiarism and the research and writing are those of the candidate's except as acknowledged in the Author Attribution Statement. I confirm that the investigations were conducted in accord with the ethics policies and integrity standards of Nanyang Technological University and that the research data are presented honestly and without prejudice.

Tianhu Li

2 Aug. 2021

.....

Date

.....

Assoc. Prof. Li Tianhu

Authorship Attribution Statement

This thesis contains material from one paper published in the following peer-reviewed journal in which I am listed as an author.

Chapter 2 is published as J. Wu, B.R. Liyarita, H. Zhu, M. Liu, X. Hu, and F. Shao. Self-Assembly of Dendritic DNA into a Hydrogel: Application in Three-Dimensional Cell Culture. *ACS Appl. Mater. Interfaces* **13**, 49705-49712 (2021). DOI: doi.org/10.1021/acsami.1c14445

The contributions of the co-authors are as follows:

- Assoc. Prof. Shao Fangwei and Prof. Hu Xiao provided the initial project direction and edited the manuscript drafts
- Dr. Wu Jingyuan and I performed the experiments
- I conducted the experiments on the effect of crosslinking ratio, thermal stability, cell viability in 3D cell culture, cell re-harvesting, and regeneration
- Dr. Wu Jingyuan wrote the initial manuscript draft and I added the additional experiments
- Dr. Ming Liu assisted in performing the rheology measurement
- Ms. Zhu Haishuang revised the manuscript

3 February 2022
Date

.....
Bella Rosa Liyarita

Abstract

DNA is gaining favorable attention as the versatile building block material for hydrogel formation due to its unique properties such as sequence programmability, multifunctional tunability, precise recognition, structural rigidity, and biocompatibility. The DNA hydrogel self-assembly is formed purely by the supramolecular interaction between the complementary DNA base pairs which results in the dynamic interaction in the hydrogel and confers to the thixotropic properties and designable responsiveness of the hydrogel. Thus, allowing the DNA building block as the competitive alternative for the formation of hydrogel with tailored function and precise molecular structure design. By taking advantage of these features, DNA hydrogels have been developed for application in tissue engineering such as 3D cell culture and bioprinting. However, some challenges still remain, such as the complex design of the DNA building block to load functionalities into the hydrogel and the low mechanical strength of the pure DNA hydrogel.

In this thesis, we focus on the development of the self-assembled dendritic DNA hydrogel design to offer tailored bio-functionality and enhanced mechanical property to suit the different needs of *in vitro* 3D cell culture platform. Most DNA hydrogel building blocks require complex design for functionalization and high gelation concentration to form the hydrogel. Hence, in chapter 2 we design a dendritic DNA structure to have a defined composition and offer simultaneous multifunction of bio-cue loading and gelation by independently programming the DNA branches. Tunable mechanical property and cell re-harvesting and regeneration into a new DNA hydrogel can be achieved due to the dynamic nature of the DNA hydrogel.

In addition, the hydrogel scaffold for 3D cell culture should offer a versatile design to cater to the different cell line needs. Thus, in chapter 3 we aim to functionalize the DNA hydrogel with integrin-targeting ligand to control the cell attachment and spreading. Furthermore, the potential of employing supramolecular hydrogel for 3D cell culture still presents a challenge of the low mechanical stiffness due to the weaker interaction as compared to the covalently crosslinked hydrogel. Therefore, in chapter 4, we present a strategy to enhance the mechanical property of the DNA hydrogel by incorporating the interpenetrating double network into the dendritic DNA hydrogel structure. The double network hydrogel was self-assembled purely based on the supramolecular interaction of DNA base pairing. Enhancement of the mechanical property was observed in the double network dendritic DNA and distinct cell morphology was achieved as compared to that of the parent single-network DNA hydrogels.

Acknowledgements

My PhD journey would not be possible without the presence and support of all these important people. First and foremost, I would like to convey my deepest gratitude to my supervisors, Assoc. Prof. Shao Fangwei, Prof. Hu Xiao from MSE, and Assoc. Prof. Li Tianhu for their kind support, guidance, motivation, and encouragement both in research and life. They always welcome me for discussion and be supportive every time I reach out for help. I would also like to extend my gratitude to Asst. Prof. Qiao Yuan for helping me with the necessary administrative requirement for my thesis submission.

Secondly, I would like to thank my groupmates, past and present, Dr. Wu Jingyuan, Dr. He Lei, Dr. Wang Liying, Dr. Zhang Hao, Dr. Ba Sai, Ms. Lee Yiqin Jasmine, and Dr. Wang Tianxiang. Also Dr. Liang Yen Nan, Dr. Lim Song Kiat Jacob, Dr. Bao Yueping, Dr. Mya Mya Khin, and Ms. Nupur Gupta from MSE. I am grateful for all the assistance and discussion we have shared during my PhD study.

I would also like to thank my TAC members, Prof. Zhao Yanli and Assoc. Prof. Lu Lei from SBS for their insights and advice for my research.

Deeper appreciation and gratitude are also expressed for the staff at the CBC department and SPMS who have assisted me in administrative stuff and lab matters.

I would also like to thank the Division of Chemistry and Biological Chemistry, Nanyang Technological University for the financial support and opportunity to realize my dream by pursuing research study in this department.

Lastly, a very special mention to thank my loved ones, my family, and friends. Thank you for being a support system for me and being there through my ups and downs during this PhD journey. Their support and presence have always been motivating me to keep moving on and pick the rewards of this challenging journey.

Table of Contents

CHAPTER 1

Introduction

1.1 3D Cell Culture

The process of drug development and discovery involves preclinical testing of the drug candidates *in vitro* in the appropriate cell lines, followed by *in vivo* studies in animal models. These studies are performed to analyse the safety and performance of the drug candidates by investigating the toxicity, distribution, metabolism, and excretion properties of the drugs. Once both *in vitro* and *in vivo* studies show promising results, the clinical trials of the drugs are performed in human through various phases. In practice, many drug candidates fail after it advances to the clinical trials mainly due to the lack of efficacy and intolerable toxicity.[1] Therefore, it is important that the ineffective candidates are dismissed as early as possible, preferably during *in vitro* study for a more efficient drug discovery process. To do so, the *in vitro* assay should be improved to mimic the environment of the target cells in the body to provide more reliable information about the performance of the drug.[2-3]

3D cell cultures models have been extensively developed over the past two decades. It was evident that the 3D cell cultures could establish the cell-cell and cell-ECM interaction and serve as the platform to mimic the living tissue with better physiological relevance in comparison to 2D cell culture.[4-5] For example, Discher and coworkers showed that the human mesenchymal stem cells (hMSCs) differentiation depends on the mechanical stiffness of the cell culture platform.[6] The 3D environment could provide suitable mechanical support for the cells. In addition, the normal human breast cell grows like malignant cells in 2D culture, but they returned to their normal growth when cultured in the 3D models.[7] Interestingly, it was observed that the chondrogenesis of the embryonic stem cells was improved when cultured in the 3D environment as compared to the 2D cell culture.[8] Furthermore, when the cells are cultured in a 3D environment, the cells interact with each other to form aggregates/spheroids.

The cell-cell and cell-ECM interactions in spheroids closely resemble the cellular process and cell morphology *in vivo*.[9] These findings show that growing the cells in a three-dimensionally environment would be more analogous to the living condition *in vivo* and could serve as a more predictive culture model to the native tissue.

1.1.1 Cell Microenvironment

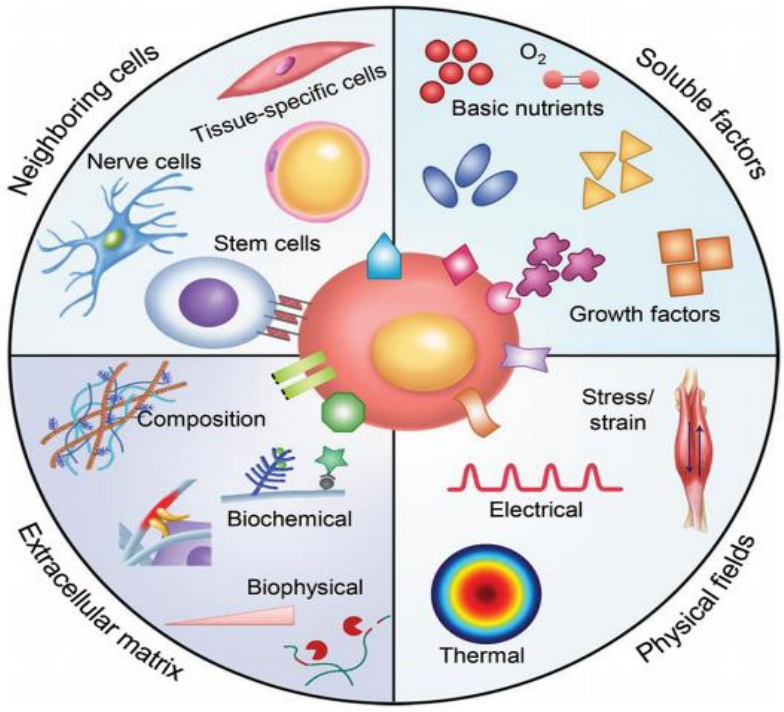

Figure 1.1 Illustration of the main components constructing the cell microenvironment in vivo. [3]

In our body, the cells reside in the extracellular matrix (ECM) which consists of a 3D architecture to support the cells and interact with each other through mechanical and biochemical cues.[5] However, in 2D cell culture, the cells are seeded onto the surface of the culture flask where they would adhere only to one side of the surface. This lack of cell-cell and cell-ECM interaction would limit the ability to mimic the cell condition in native tissue such as cell morphology, viability, differentiation, gene expression, and overall cellular architecture.[10]

In developing the 3D cell culture that would best imitate the cell condition *in vivo*, understanding the cell microenvironment is important. Cells reside in the environment with the heterotypic, dynamic, and complex set of biophysical and biochemical cues signaling pathways, also known as "niche" in the stem cells.[11-12] Most cell microenvironments of the multicellular animals share the common features and composition such as surrounding ECM to provide structural integrity to the cells, cell-cell interaction with the neighboring cells, soluble factors to support the cell growth, and biophysical cues to regulate the dynamic cell behavior including cell differentiation, migration, and spreading (**Figure 1.1**).[3]

The cells do not exist in isolation *in vivo* but dynamically interact with neighboring multicellular cells, both similar and different cell types. They interact in a diverse and complex cell-cell interaction that plays an important role in cell and tissue function and morphogenesis.[13-14] The signaling pathways at which the neighboring cells interact include direct and indirect via cell-cell contact and soluble factors mediation, respectively. In direct cell-cell interactions, physical contact between neighboring cells occurred through the anchoring junctions, tight junctions, and distant cell-cell interaction via a long-distance mechanical signaling pathway through the ECM interconnecting network.[15-16] However, most studies of the cell-cell interaction were investigated on a specific cell type over its lifecycle. Hence, the focus shifts to study the interaction between multicellular different cell types by using the co-culture model and also organ-on-a-chip to further precisely mimic the complex cell microenvironment *in vivo*.[17-18] Furthermore, cells encounter various soluble factors in their aqueous environment, such as signaling molecules (growth factors, hormones, and cytokines) as the bio-cue to control the cell response, and basic nutrients (amino acids, oxygens, and

glucose) to support the cell growth. Therefore, designing the 3D cell culture platform that can provide and control this environment is important.[19-20]

The widely explored ECM is a critical factor to determine the physiology and fate of the cells. ECM does not only provide the physical support for the cell but also serves as the cell-cell or cell-matrix crosstalk across the ECM network.[21] Most studies investigated the role of ECM in supporting the cell structural integrity by encapsulating the cell in a bulk ECM with the function that can direct the cell to exhibit certain functions or morphologies based on demand.[22-23] This method relies on the cell themselves to "do the work" creating their own local 3D microenvironment similar to *in vivo*. However, the local 3D cell microenvironment is considerably different than the bulk ECM microenvironment.[21, 24-26] Hence, there is a growing opportunity to explore the design of biomaterial that can mimic the relevant cell microenvironment *in vivo*.

1.1.2 In Vitro 3D Cell Culture Model

Various 3D cell culture platforms have been developed to accommodate the high demand for 3D cell culture. The 3D cell culture models are broadly categorized into scaffold-free (anchorage-independent) and scaffold-based (anchorage-dependent) systems

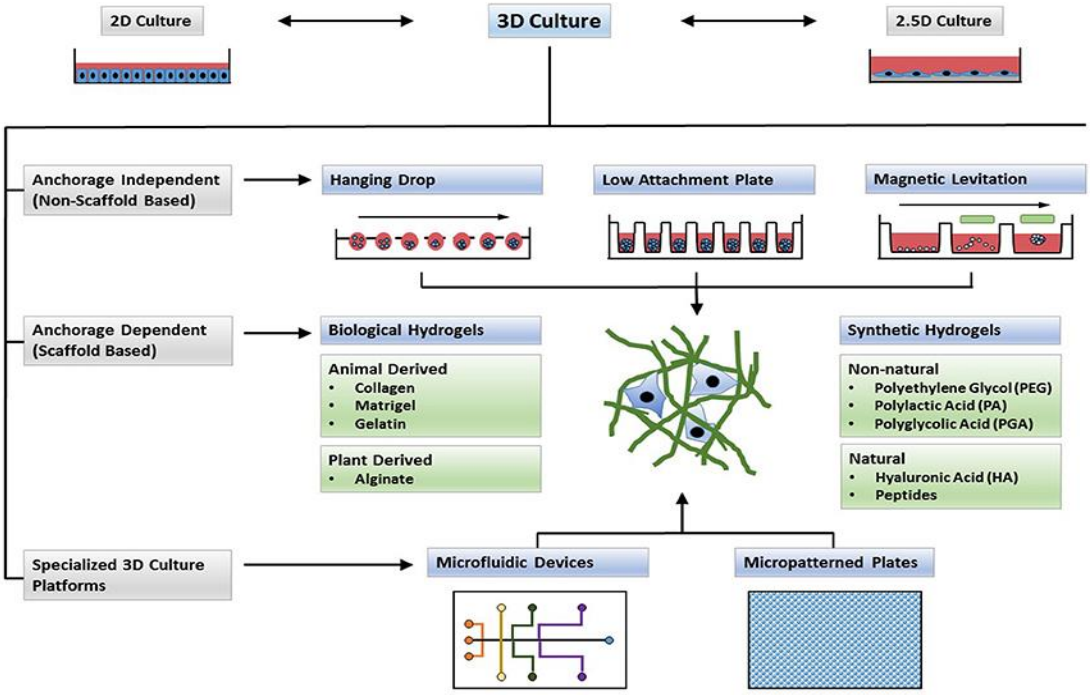

Figure 1.2. Different platform and techniques for in vitro 3D cell culture.[27]

(**Figure1.2**).[27] The basic scaffold-free system employs cellular aggregates which are cultured in suspension or modified culture plates without matrix-based substrate. The most commonly used methods are hanging drop, micropatterned plates for microfluidic cell culture, and ultra-low attachment coating on the low adhesion plates. These methods are all used to promote the cell spheroid formation.[1, 27-28] Cell spheroids exhibit physiological properties of tissues and tumors based on the cell-cell interaction. In the scaffold-free systems, the spheroid relies on the cell themselves to secrete their own ECM for the cell-matrix interaction.

In the hanging drop method, the cells aggregate into the spheroids because of the lack of the cell attachment site. The culture plate is specially modified to incorporate bottomless wells for the formation of a small cell suspension droplet, sustaining the cell culture for several days to manipulate the cell into spheroid due to the tight space.[29] Some applications of the hanging drop cell culture are for the formation of hepatocytes spheroid for toxicity testing,[30] formations of the cardiac spheroid,[31] and co-culture of iPSC-derived cardiomyocytes with

endothelial and fibroblast cells.[32] However, the hanging drop method raises questions on the cell viability after culture due to the direct physical manipulation of the cell spheroid.

The alternative scaffold-free method, the low-adhesion plate, applies the same principle as the hanging drop cell culture by utilizing the lack of cell attachment site on the culture platform to promote the cell aggregation to further form the spheroid. The non-adherent coating on the culture platform prevents the cell to attach and promote the cell-cell interaction to form the cell spheroid.[33-34] This method gives an advantage compared to the hanging drop technique as the culture plate offers higher volume capacity and enables the co-culture of multicellular cells.

The more complex 3D cell culture system employs the scaffold-based system. The scaffolds provide support for the cells and facilitate nutrients, gas, and waste transport due to the porosity in their structure. Moreover, the cells can migrate, proliferate, and adhere within the scaffold mesh.[35] A wide variety of materials and fabrications techniques has been used to develop the scaffolds with varying biological and physical requirements for different cell conditions in the native tissue. Of the different methods available for 3D cell culture, a hydrogel-based system is the most commonly used for the *in vitro* application.[36]

1.2 Hydrogel for 3D Cell Culture Platform

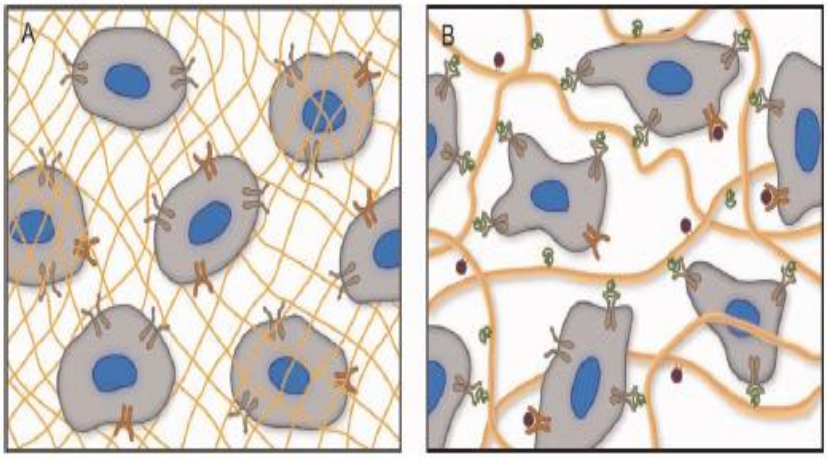

Figure 1.3. A) Synthetic hydrogel crosslinking network (yellow mesh) can be incorporated with integrin (brown) and another surface receptor (orange). B) Natural hydrogel. Integrin-binding sites (green) and growth factor (red) are naturally present in the ECM (yellow fibre).[38]

Hydrogels, the water-swollen network of cross-linked polymer chains, have emerged as the promising platform for 3D cell culture due to their ability to mimic biophysical properties similar to soft tissues.[37] Hydrogels are suitable to investigate the influence of ECM on cells because the components of the biomimetic hydrogels can be precisely modified and altered systematically to suit the different needs of 3D cell culture applications. The high-water content and the good permeability allow them for effective transport of oxygen, nutrients, wastes, and other soluble factors.[38] The mechanical properties of hydrogels are important to support the cells in a 3D environment and influence the mechanotransduction in cells, which is the process of converting mechanical signals from the microenvironment of the cells into biochemical cues.[39] In addition, the inner structure of the hydrogel can also be tuned to accommodate the different requirements of cell culture. The mesh size of the hydrogel should be on the order of tens micrometers, a scale smaller than most of the cell size, but larger than most of the growth

factors, chemokines, and cytokines. Therefore, the accessibility of these small molecules and proteins to the cells is not hindered.[40]

The fabrication of a hydrogel cell culture platform for cellular experiments is usually by encapsulation of the cells within the material or seeding the cells into the hydrogels that are already fabricated using molds to provide tightly crosslink support to sustain the cells. Overall, there are two broad types of hydrogel based on the source, natural-derived and synthetic hydrogels (**Figure 1.3**).[38, 41]

1.2.1 Synthetic Polymer Based Hydrogel

Synthetic polymer hydrogel is biologically inert, simple to process with high reproducibility, and able to tune the mechanical properties to provide structural support for various cell types. Moreover, bio-cue can be grafted into the polymer chain to provide biological property as needed. [42-43] Various synthetic-based hydrogels have been widely developed for constructing the cell microenvironment, such as poly(2-hydroxyethyl methacrylate) (PHEMA), poly(acrylamide) (PA), and the most commonly explored poly(ethylene glycol) (PEG).[44]

In some studies, poly(ethyleneglycol) (PEG) hydrogels could maintain cell viability and allow for ECM deposition while they degrade, demonstrating that the hydrogels could serve as the 3D cell culture platform without the integrin-binding ligand.[45] Polyacrylamide (PA) hydrogels do not interact with cell surface receptors or integrins, hence they are suitable for mechanobiology study where the hydrogel stiffness needs to be controlled.[10] In addition, polypeptide hydrogels can be engineered to show the advantages of the natural-derived

hydrogels such as interaction with the cells, degradability, and assembly into the hierarchical structure resembling the natural protein.[46] However, the high cost for polypeptide production is one factor to be considered for the large-scale 3D cell culture. Furthermore, similar to a natural-derived polymer, it would be difficult to form the hydrogel that does not degrade for long periods of time.

Furthermore, synthetic hydrogels can be integrated with biological components to properly mimic the ECM cell microenvironment. For example, the synthetic polypeptide hydrogel conjugated with laminin has been shown to support neuronal cell proliferation and differentiation.[47] Hyaluronic acid (HA) hydrogels do not support integrin-mediated cell adhesion, therefore it must be modified with adhesive ligands to permit cell attachment into the hydrogel.[48] In another example, gelatin macromer was modified with methacrylate for photoencapsulation of cells. The aortic valvular interstitial cells (VICs) were successfully cultured and achieved their native morphology using the hybrid hydrogel.[49] These observations demonstrate how the conjugation with appropriate biological components can enhance the biological properties of the synthetic hydrogels for 3D cell culture application. However, some disadvantages still shadow the use of synthetic-based hydrogel. One main concern is that the hydrogel fabrication usually requires a precursor which may be toxic for the cell, thus preventing the precise simulation of the cell microenvironment for 3D cell culture application.

1.2.2 Natural Polymer Based Hydrogel

Natural-based hydrogel is often considered a superior alternative to synthetic hydrogel for mimicking the *in vivo* cell microenvironment. Natural hydrogels for 3D cell cultures are usually formed of proteins and other natural materials existing in the ECM such as fibrin, laminin, collagen, hyaluronic acid, chitosan, alginate, and Matrigel®.[50] These hydrogels are essentially bioactive and biocompatible as they are derived from natural resources. In addition, they stimulate many cellular functions due to the presence of diverse endogenous factors to supports cell viability, proliferation, function, and other cellular behaviors. For example, cardiac cells were cultured in the peptide-modified chitosan-collagen hydrogel showed improved metabolic activity, morphology, and viability.[51] Another commonly used natural-based hydrogel is collagen, which is one of the major components in the ECM. Collagen is more abundantly exists in articular and bone tissue, hence the common use of this hydrogel for bone and cartilage regeneration.[52] Another study also reported the fabrication of hybrid silk fibroin/collagen hydrogel to tune the hydrogel mechanical property and subsequently culture the human mesenchymal stem cell.[53]

However, such natural-derived scaffolds do possess some disadvantages such as difficulties in tuning the mechanical and biochemical properties, risk of contamination due to isolation from the animal-derived resources, and the inherent batch-to-batch variability which could affect cell differentiation, proliferation, and migration. Furthermore, the complex and often ill-defined structure of the scaffold makes it difficult to determine the specific cell functions that are being investigated.

1.2.3 Supramolecular Hydrogel

Supramolecular hydrogels are gaining traction of research interest to explore the potential for cell culture application. Due to the dynamic nature of the supramolecular chemistry, the hydrogel can be custom-tailored to design tunable and responsive hydrogel. Most of the receptors on the cells and their surrounding environment interact using the non-covalent interaction, such as ligand-receptor interaction, DNA base-pair molecular recognition, and hydrophobic interaction.[54] Stimuli-responsive hydrogels can be used to dynamically engineer the cell microenvironment, which is beneficial for the study of cell interaction on the *in vitro* 3D cell culture model. In addition, biochemical and biophysical unique features of the biomolecule can be tailored into the supramolecular hydrogel network, which is often difficult to achieve on the natural and synthetic based hydrogel.[55-56]

For example, a hydrogel purely constructed by the DNA building block can encapsulate a single cell and responsively release the cell by enzyme digestion to study single cell analysis.[57] Hybrid supramolecular hydrogel was fabricated by utilizing the supramolecular assembly between double-stranded DNA crosslinker on the peptide chain to form a hydrogel with high mechanical stiffness and maintain the cell suspension for application in 3D bioprinting.[58] In addition, by custom-tailoring the design of the peptide sequence building blocks, supramolecular peptide hydrogel can replicate the structural features that control the cell adhesion, growth factor-binding, and biodegradability of that native-derived hydrogel.[59] Therefore, the supramolecular hydrogel offers the potential to design a responsive cell culture platform to better mimic the cell microenvironment. Due to the dynamic nature of the hydrogel, controlled release of therapeutic agents casted on the hydrogel platform can further be explored.

1.3 DNA Hydrogel

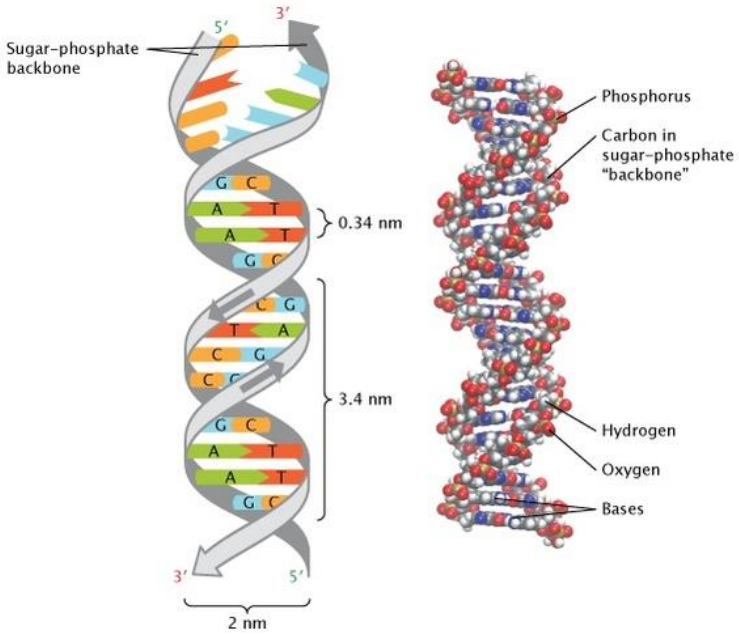

Figure 1.4 Structure of nucleic acid DNA. Nucleobase A-T and G-C form hydrogen bond interactions via Watson-Crick base pairing. © 2013 Nature Education.

Nucleic acid has been considered as an outstanding building block material for the construction of hydrogel due to its unique properties compared to most natural and synthetic hydrogels, such as multifunctional tunability, on-demand programmability, inherent biocompatibility and biodegradability, precise molecular recognition, and structural rigidity.[60] The study of the molecular structure of DNA as the information carrier or gene in our body has been developed into investigating the property of DNA hydrogel as a polymeric biomaterial.[61] In the DNA structure, there are four different nucleobases: Adenine (A), Guanine (G), Cytosine (C), and Thymine (T). A and G contain double-ringed structure and are classified into purines groups, while C and T contain single six-member ring and are classified as pyrimidines. These

nucleotides can specifically form hydrogen bonds interaction via Watson-Crick base pairing with A-T and G-C always complementary with each other (**Figure 1.4**).[62]

The unique properties of programmability and precise molecular recognition enable DNA hydrogel to be custom-tailored to design a hydrogel that mimics the cell microenvironment. Versatile tools of biomolecule functionalization can be applied to DNA hydrogel, such as aptamer, growth factor, peptide, and chemical group functionalization. Moreover, the physical properties of the DNA hydrogel can be easily tuned by systematically designing the crosslinking network system and the biodegradability of the hydrogel can be achieved via a wide range of enzymatic tools.[63]

1.3.1 Hybrid DNA Hydrogel

DNA can be used as the crosslinker by attachment to polymer side chain to form the hybrid hydrogel through physical entanglement or chemical reactions. Due to the dynamic nature of DNA supramolecular interaction, the programmable feature of the DNA hydrogel could be designed to be responsive to stimuli such as enzyme, temperature, pH, and metal ions by coding the loading with the desired sequence.[63] A dual responsive pH and thermal responsive hybrid DNA hydrogel were formed by copolymerization of NIPAM and acrylamide grafted with C-rich DNA. The DNA crosslinker can self-assemble into i-motif under low pH conditions and reversibly disassemble under basic pH solution.[64] Stimuli-responsive hybrid DNA-polymer network has also been explored to form the shape-memory hydrogel by incorporating the two DNA linkers as the bridging memory and stimuli-responsive, respectively. Switchable DNA sequence structure provides a rich “tool-box” to fabricate

stimuli-responsive hybrid polymer-DNA hydrogels, which is beneficial in the application for controlled drug delivery, biosensor, etc. [65]

In addition, nanomaterials can also be grafted into DNA hydrogels to gain desirable features as needed. A DNA-SWNT hydrogel was designed to responsively switch into gel-sol with controlled pH by grafting the single wall CNT as the crosslinker. By combining the DNA with CNT, the hybrid hydrogel displayed electronic and photonic nanomaterial system.[66] Furthermore, DNA structure can also be incorporated with silver nanoclusters, which can endow fluorescence and antibacterial function into the DNA-AgNCs hydrogel for biomedical application.[67]

The aforementioned DNA-hybrid structures offer the versatile application of DNA hydrogel for a wide range of applications, mostly in nanoparticle fields such as biosensors, nanomotors, bioimaging, and drug delivery. However, the application of hybrid-DNA hydrogel specifically for cell culture may be hindered by the biocompatibility properties of the hybrid-DNA hydrogel to sustain cells over days. Additionally, the preparation of the hybrid DNA hydrogel would also require multiple steps of modification and conjugation, therefore an easy and fast strategy to assemble designable DNA hydrogel is desired.

1.3.2 Pure DNA Hydrogel

In pure DNA hydrogels, DNA can be utilized as both backbone and crosslinker (**Figure 1.5)**. Besides exhibiting the previously mentioned characteristics, the long persistence length of DNA crosslinking in pure DNA hydrogel makes the network rigid and excludes the smaller mesh size at nanometer scale, thus the hydrogels are permeable to nutrients (~22kDa) for cell

proliferation in 3D cell culture. [68-69] In addition, the mechanical property of the DNA hydrogel can be easily tuned by adjusting the gelation concentration or the DNA sequence. [70-71]

Luo and coworkers developed a new approach to construct the pure DNA hydrogels by using well-designed single-stranded DNA to form branched DNA building blocks (X-tile, Y-tile, and T-tile) which assembles to form hydrogel via enzymatic ligation .[72] These branched DNA hydrogels can be applied for controlled drug release, cell encapsulation[72], and cell-free protein-producing hydrogels.[55] However, the assembly through enzymatic ligation would be time-consuming in terms of preparation and the gelation process. Nöll and coworkers demonstrated a strategy to assemble thermal-responsive DNA hydrogel by utilizing the DNA hybridization interaction. The DNA hydrogel was formed by self-assembly of short linear double-stranded DNA building blocks with sticky ends.[73] Another strategy to form DNA hydrogel was by assembling single-stranded DNA monomers containing multiple palindromic sites for cross-linking. The thermal stability, mechanical properties, and loading capacity of the DNA hydrogel were adjustable by modifying the DNA sequences while leaving the palindromic site unmodified for the crosslinking.[74]

DNA hydrogel with both thermal and enzyme responsive property was developed by Liu and coworkers.[75] The DNA hydrogel formation was completely based on self-assembly without any further chemical treatment. By properly adjusting the sticky ends of the DNA building blocks (Y-scaffold and linker), the pure DNA hydrogel can be formed rapidly under physiological condition by the principle of DNA hybridization. In further experiments, they

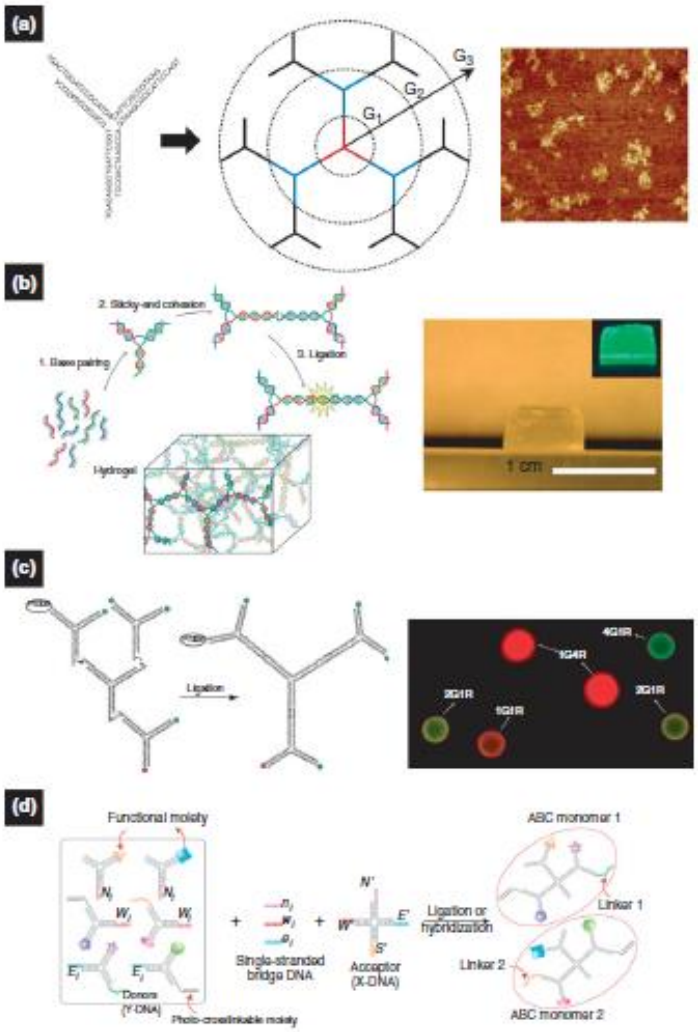

Figure 1.5. DNA hydrogels formed purely by DNA building block.[65]

demonstrated the permeability of the DNA hydrogels for small molecules and the application for single-cell encapsulation.[57] Furthermore, a tissue-like structure was fabricated by combining two DNA hydrogels with different cell types. The two DNA hydrogel bricks could merge due to the "self-healing" property of the hydrogel and the hydrogel permits cell migration in the 3D structure.[76]

The strategy to employ branched DNA such as X-tile and Y-tile has shown promising results as the platform for 3D cell culture. However, high concentration of DNA would be needed for the hydrogel self-assembly to provide desired mechanical property for the cell

culture platform. In addition, it would require a complex sequence design to introduce exogenous molecules or functionalization of DNA hydrogel. Therefore, a new approach to design a DNA hydrogel with inherent biocompatibility, programmable for multi-modulus loading, and low gelation concentration is required.

1.4 Research Objectives

3D cell culture platforms have been widely developed as a tool to mimic the cell microenvironment *in vivo*. The *in vitro* 3D cell culture tool must cater to the different criteria of cell culture study. Hydrogel scaffolds with high water content jelly-like structures provide potent physiological and structural support for cell growth three-dimensionally. Hydrogels can be designed to incorporate biophysical and biochemical properties to study and control cell behavior. Therefore, there is a need to design a hydrogel-based cell culture platform that can be custom-tailored to cater to the different cell study criteria. Though the synthetic and natural-based hydrogels offer compatibility for cell culture, they usually require synthesis difficulty, uncertain composition, and hard functionality.

On the other hand, while supramolecular hydrogel offers dynamic nature to design a responsive hydrogel platform, they still lack the mechanical strength to support the cell growth due to the weaker interaction between the building blocks. In addition, the pharmacokinetic study and kinetic study of the supramolecular hydrogel in response to the cell microenvironment still need to be well understood. Moreover, even though some supramolecular hydrogels such as peptide and Y-tile assembled DNA hydrogel offer biocompatibility, they require high gelation concentration, undefined composition, and complicated design to introduce functionality. Additionally, high cost and difficulty in the

large-scale preparation remain as the major obstacle in the development of the practical use of supramolecular-based hydrogel. Therefore, the future direction to develop the effective supramolecular hydrogel for tissue engineering application focus on the improvement in their mechanical properties and mass production method. Different approaches are still available for further investigations to address these concerns.

In this work, we aim to develop a versatile supramolecular hydrogel formed purely by DNA self-assembly. A dendritic DNA building block was designed to have a defined composition and offer simultaneous multifunction of bio-cue loading and gelation into the hydrogel network by independently programming the DNA branches. The dendritic DNA building was assembled into bulk DNA hydrogel and further explored for application in 3D cell culture. In chapter 2, we investigated the optimum condition for the DNA hydrogel crosslinking to form the hydrogel that can sustain the cells growth. In addition, owing to the DNA hydrogel thixotropy and self-healing characteristic, the cells can be re-harvested from the hydrogel and cultured into a new DNA hydrogel, allowing the cells to further proliferate in the new platform.

Additionally, the hydrogel scaffold for 3D cell culture should offer a versatile design to cater to the different cell line needs, such as cell attachment and mechanical stiffness to stimulate the cell microenvironment. Thus, in chapter 3 we aim to functionalize the DNA hydrogel with integrin-targeting ligand to control the cell attachment and spreading of fibroblast cells. Furthermore, the potential of employing supramolecular-based hydrogel for 3D cell culture is still hindered with the challenge of low mechanical stiffness and higher synthetic cost due to their weaker interaction as compared to the covalently crosslinked hydrogel. Therefore, a systematic study was performed to address these concerns in chapter 4. We presented a strategy

that can enhance the mechanical property of the DNA hydrogel by incorporating the interpenetrating double network into the dendritic DNA hydrogel structure. The double network DNA hydrogel was self-assembled purely by the supramolecular interaction of DNA hybridization. A systematic study was performed to determine the effect of bp length and GC-content composition of the dendritic DNA gelation branches on the mechanical properties of the resulting single network DNA hydrogel before further incorporating two DNA hydrogels network with rigid and flexible mechanical properties into a double network DNA hydrogel. The double network hydrogel was further applied for 3D cell culture and the performance of manipulating the cell morphology was assessed.

1.5 References

1. Breslin, S.; O'Driscoll, L., *Drug Discov Today* **2013,** *18* (5-6), 240-9.

2. Mazzoleni, G.; Di Lorenzo, D.; Steimberg, N., *Genes Nutr* **2009,** *4* (1), 13-22.

3. Huang, G.; Li, F.; Zhao, X.; Ma, Y.; Li, Y.; Lin, M.; Jin, G.; Lu, T. J.; Genin, G. M.; Xu, F., *Chemical Reviews* **2017,** *117* (20), 12764-12850.

4. Haycock, J. W., *Methods Mol Biol* **2011,** *695*, 1-15.

5. Lee, J.; Cuddihy, M. J.; Kotov, N. A., *Tissue Eng Part B Rev* **2008,** *14* (1), 61-86.

6. Engler, A. J.; Sen, S.; Sweeney, H. L.; Discher, D. E., *Cell* **2006,** *126* (4), 677-89.

7. Petersen, O. W.; Rønnov-Jessen, L.; Howlett, A. R.; Bissell, M. J., *Proc Natl Acad Sci U S A* **1992,** *89* (19), 9064-8.

8. Tanaka, H.; Murphy, C. L.; Murphy, C.; Kimura, M.; Kawai, S.; Polak, J. M., *J Cell Biochem* **2004,** *93* (3), 454-62.

9. Khaitan, D.; Chandna, S.; Arya, M.; Dwarakanath, B., *J Transl Med* **2006,** *4*, 12.

10. Caliari, S. R.; Burdick, J. A., *Nat Methods* **2016,** *13* (5), 405-14.

11. Li, L.; Xie, T., *Annual Review of Cell and Developmental Biology* **2005,** *21* (1), 605-631.

12. Wilson, A.; Trumpp, A., *Nature Reviews Immunology* **2006,** *6* (2), 93-106.

13. Mao, A. S.; Shin, J.-W.; Mooney, D. J., *Biomaterials* **2016,** *98*, 184-191.

14. Xin, T.; Greco, V.; Myung, P., *Cell* **2016,** *164* (6), 1212-1225.

15. Wang, H.; Abhilash, A. S.; Chen, Christopher S.; Wells, Rebecca G.; Shenoy, Vivek B., *Biophysical Journal* **2014,** *107* (11), 2592-2603.

16. Sarvestani, A. S.; Picu, C. R., *Polymer* **2004,** *45* (22), 7779-7790.

17. L. Berg, E.; Hsu, Y.-C.; Lee, J. A., *Advanced Drug Delivery Reviews* **2014,** *69-70*, 190-204.

18. Lind, J. U.; Busbee, T. A.; Valentine, A. D.; Pasqualini, F. S.; Yuan, H.; Yadid, M.; Park, S.-J.; Kotikian, A.; Nesmith, A. P.; Campbell, P. H.; Vlassak, J. J.; Lewis, J. A.; Parker, K. K., *Nature Materials* **2017,** *16* (3), 303-308.

19. Dingal, P. C. D. P.; Discher, D. E., *Nature Materials* **2014,** *13* (6), 532-537.

20. Cezar, C. A.; Mooney, D. J., *Advanced Drug Delivery Reviews* **2015,** *84*, 188-197.

21. Brassart-Pasco, S.; Brézillon, S.; Brassart, B.; Ramont, L.; Oudart, J.-B.; Monboisse, J. C., *Frontiers in Oncology* **2020,** *10* (397).

22. Lam, D.; Enright, H. A.; Cadena, J.; Peters, S. K. G.; Sales, A. P.; Osburn, J. J.; Soscia, D. A.; Kulp, K. S.; Wheeler, E. K.; Fischer, N. O., *Scientific Reports* **2019,** *9* (1), 4159.

23. Nallanthighal, S.; Heiserman, J. P.; Cheon, D.-J., *Frontiers in Cell and Developmental Biology* **2019,** *7* (86).

24. Henke, E.; Nandigama, R.; Ergün, S., *Frontiers in Molecular Biosciences* **2020,** *6* (160).

25. Reinhard, J.; Brösicke, N.; Theocharidis, U.; Faissner, A., *Int J Biochem Cell Biol* **2016,** *81* (Pt A), 174-183.

26. Gattazzo, F.; Urciuolo, A.; Bonaldo, P., *Biochim Biophys Acta* **2014,** *1840* (8), 2506-19.

27. Langhans, S. A., *Frontiers in Pharmacology* **2018,** *9* (6).

28. Sutherland, R., *Science* **1988,** *240* (4849), 177-184.

29. Stadler, M.; Walter, S.; Walzl, A.; Kramer, N.; Unger, C.; Scherzer, M.; Unterleuthner, D.; Hengstschläger, M.; Krupitza, G.; Dolznig, H., *Seminars in Cancer Biology* **2015,** *35*, 107-124.

30. Shri, M.; Agrawal, H.; Rani, P.; Singh, D.; Onteru, S. K., *Scientific Reports* **2017,** *7* (1), 1203.

31. Chitnis, T.; Weiner, H. L., *The Journal of Clinical Investigation* **2017,** *127* (10), 3577-3587.

32. Polonchuk, L.; Chabria, M.; Badi, L.; Hoflack, J.-C.; Figtree, G.; Davies, M. J.; Gentile, C., *Scientific Reports* **2017,** *7* (1), 7005.

33. Abe-Fukasawa, N.; Otsuka, K.; Aihara, A.; Itasaki, N.; Nishino, T., *Scientific Reports* **2018,** *8* (1), 3627.

34. Bresciani, G.; Hofland, L. J.; Dogan, F.; Giamas, G.; Gagliano, T.; Zatelli, M. C., *Frontiers in Endocrinology* **2019,** *10* (682).

35. Knight, E.; Przyborski, S., *J Anat* **2015,** *227* (6), 746-56.

36. Suparna, S. K., M. , Materials and assay systems used for three-dimensional cell culture. In *Technology Platforms for 3D Cell Culture*.

37. Peppas, N. A.; Hilt, J. Z.; Khademhosseini, A.; Langer, R., *Advanced Materials* **2006,** *18* (11), 1345-1360.

38. Tibbitt, M. W.; Anseth, K. S., *Biotechnol Bioeng* **2009,** *103* (4), 655-63.

39. Ingber, D. E., *Faseb j* **2006,** *20* (7), 811-27.

40. Lin, C. C.; Metters, A. T., *Adv Drug Deliv Rev* **2006,** *58* (12-13), 1379-408.

41. Cushing, M. C.; Anseth, K. S., *Science* **2007,** *316* (5828), 1133-1134.

42. DeForest, C. A.; Anseth, K. S., *Annual Review of Chemical and Biomolecular Engineering* **2012,** *3* (1), 421-444.

43. Lutolf, M. P.; Hubbell, J. A., *Nature Biotechnology* **2005,** *23* (1), 47-55.

44. Place, E. S.; George, J. H.; Williams, C. K.; Stevens, M. M., *Chemical Society Reviews* **2009,** *38* (4), 1139-1151.

45. Bryant, S. J.; Anseth, K. S., *J Biomed Mater Res* **2002,** *59* (1), 63-72.

46. Webber, M. J.; Tongers, J.; Newcomb, C. J.; Marquardt, K. T.; Bauersachs, J.; Losordo, D. W.; Stupp, S. I., *Proc Natl Acad Sci U S A* **2011,** *108* (33), 13438-43.

47. Ortinau, S.; Schmich, J.; Block, S.; Liedmann, A.; Jonas, L.; Weiss, D. G.; Helm, C. A.; Rolfs, A.; Frech, M. J., *Biomed Eng Online* **2010,** *9*, 70.

48. Burdick, J. A.; Prestwich, G. D., *Adv Mater* **2011,** *23* (12), H41-56.

49. Benton, J. A.; DeForest, C. A.; Vivekanandan, V.; Anseth, K. S., *Tissue Engineering Part A* **2009,** *15* (11), 3221-3230.

50. Gils, J.; Shalumon*, K. T.; Jyh-Ping, C., *Current Medicinal Chemistry* **2020,** *27* (16), 2734-2776.

51. Reis, L. A.; Chiu, L. L. Y.; Liang, Y.; Hyunh, K.; Momen, A.; Radisic, M., *Acta Biomaterialia* **2012,** *8* (3), 1022-1036.

52. Liu, M.; Zeng, X.; Ma, C.; Yi, H.; Ali, Z.; Mou, X.; Li, S.; Deng, Y.; He, N., *Bone Research* **2017,** *5* (1), 17014.

53. Nguyen, B.-N. B.; Moriarty, R. A.; Kamalitdinov, T.; Etheridge, J. M.; Fisher, J. P., *Journal of Biomedical Materials Research Part A* **2017,** *105* (4), 1123-1131.

54. Du, X.; Zhou, J.; Shi, J.; Xu, B., *Chemical Reviews* **2015,** *115* (24), 13165-13307.

55. Park, N.; Um, S. H.; Funabashi, H.; Xu, J.; Luo, D., *Nat Mater* **2009,** *8* (5), 432-7.

56. Gačanin, J.; Synatschke, C. V.; Weil, T., *Advanced Functional Materials* **2020,** *30* (4), 1906253.

57. Jin, J.; Xing, Y.; Xi, Y.; Liu, X.; Zhou, T.; Ma, X.; Yang, Z.; Wang, S.; Liu, D., *Advanced Materials* **2013,** *25* (34), 4714-4717.

58. Li, C.; Faulkner-Jones, A.; Dun, A. R.; Jin, J.; Chen, P.; Xing, Y.; Yang, Z.; Li, Z.; Shu, W.; Liu, D.; Duncan, R. R., *Angewandte Chemie International Edition* **2015,** *54* (13), 3957-3961.

59. O'Leary, L. E. R.; Fallas, J. A.; Bakota, E. L.; Kang, M. K.; Hartgerink, J. D., *Nature Chemistry* **2011,** *3* (10), 821-828.

60. Morya, V.; Walia, S.; Mandal, B. B.; Ghoroi, C.; Bhatia, D., *ACS Biomaterials Science & Engineering* **2020,** *6* (11), 6021-6035.

61. Li, F.; Tang, J.; Geng, J.; Luo, D.; Yang, D., *Progress in Polymer Science* **2019,** *98*, 101163.

62. Watson, J. D.; Crick, F. H., *Nature* **1953,** *171* (4356), 737-8.

63. Shao, Y.; Jia, H.; Cao, T.; Liu, D., *Accounts of Chemical Research* **2017,** *50* (4), 659-668.

64. Guo, W.; Lu, C.-H.; Qi, X.-J.; Orbach, R.; Fadeev, M.; Yang, H.-H.; Willner, I., *Angewandte Chemie International Edition* **2014,** *53* (38), 10134-10138.

65. Lu, C.-H.; Guo, W.; Hu, Y.; Qi, X.-J.; Willner, I., *Journal of the American Chemical Society* **2015,** *137* (50), 15723-15731.

66. Cheng, E.; Li, Y.; Yang, Z.; Deng, Z.; Liu, D., *Chemical Communications* **2011,** *47* (19), 5545-5547.

67. Geng, J.; Yao, C.; Kou, X.; Tang, J.; Luo, D.; Yang, D., *Advanced Healthcare Materials* **2018,** *7* (5), 1700998.

68. Baumann, C. G.; Smith, S. B.; Bloomfield, V. A.; Bustamante, C., *Proc Natl Acad Sci U S A* **1997,** *94* (12), 6185-90.

69. Smith, S. B.; Cui, Y.; Bustamante, C., *Science* **1996,** *271* (5250), 795-9.

70. Liu, H.; Cao, T.; Xu, Y.; Dong, Y.; Liu, D., *International Journal of Molecular Sciences* **2018,** *19* (6), 1633.

71. Xing, Z.; Caciagli, A.; Cao, T.; Stoev, I.; Zupkauskas, M.; O'Neill, T.; Wenzel, T.; Lamboll, R.; Liu, D.; Eiser, E., *Proceedings of the National Academy of Sciences* **2018**.

72. Um, S. H.; Lee, J. B.; Park, N.; Kwon, S. Y.; Umbach, C. C.; Luo, D., *Nat Mater* **2006,** *5* (10), 797-801.

73. Nöll, T.; Schönherr, H.; Wesner, D.; Schopferer, M.; Paululat, T.; Nöll, G., *Angewandte Chemie International Edition* **2014,** *53* (32), 8328-8332.

74. Jiang, H.; Pan, V.; Vivek, S.; Weeks, E. R.; Ke, Y., *ChemBioChem* **2016,** *17* (12), 1156-1162.

75. Xing, Y.; Cheng, E.; Yang, Y.; Chen, P.; Zhang, T.; Sun, Y.; Yang, Z.; Liu, D., *Advanced Materials* **2011,** *23* (9), 1117-1121.

76. Wang, Y.; Shao, Y.; Ma, X.; Zhou, B.; Faulkner-Jones, A.; Shu, W.; Liu, D., *ACS Applied Materials & Interfaces* **2017,** *9* (14), 12311-12315.

CHAPTER 2

In Vitro Tool: Dendritic DNA Hydrogel as The Platform For 3D Cell Culture

Chapter 2 is published as J. Wu, B.R. Liyarita, H. Zhu, M. Liu, X. Hu, and F. Shao. Self-Assembly of Dendritic DNA into a Hydrogel: Application in Three-Dimensional Cell Culture. *ACS Appl. Mater. Interfaces* **13**, 49705-49712 (2021). DOI: doi.org/10.1021/acsami.1c14445

2.1 Introduction

In our body, the cells reside in the extracellular matrix (ECM) which adopts a 3D architecture to support the cells and interact with each other through mechanical and biochemical cues. However, in 2D monolayer cell culture, the cells are seeded onto the surface of the culture flask where they would adhere only to one side of the surface. This lack of cell-cell and cell-ECM interaction would limit the ability to mimic the overall cellular architecture in native tissue and even aberrant especially for pathological study.[1-2]

To overcome these limitations, various 3D cell cultures models have been extensively developed over the past decades to suit the different needs of the culture platform. It was evident that the 3D cell cultures could establish the cell-cell and cell-ECM interaction and serve as the platform to mimic the living tissue with better physiological relevance in comparison to 2D cell culture. Of the different methods available for 3D cell culture, the hydrogel-based system is the most commonly used for the *in vitro* application.[3-5]

Hydrogel offers high water content and jelly-like structure to provide the physiological and structural support for the cells to grow in three-dimension, similar to those seen *in vivo*.[6] Hydrogels composed of natural biomacromolecules such as chitosan, alginates, collagen, and hyaluronic acid were preferable as they are innately bioactive and biocompatible.[7-8] However, the non-ideal properties, such as non-tunable mechanical and biochemical properties, risk of contamination from animal resources, inherent batch-to-batch variability, and complex structures, could interfere with the specific cellular functions of interests.[9-10] Alternatively, synthetic hydrogels from the covalently-crosslinked polymer with high reproducibility and tunable mechanical property, such as polyethylene glycol (PEG), polyacrylamide (PA), and

polypeptide, are used as biologically inert materials for 3D cell culture.[11-13] Nevertheless, the preparation often requires rough synthetic conditions and further complex bioconjugation of natural components onto the polymer scaffolds is needed to enhance the biological activity of the synthetic hydrogel for 3D cell culture and tissue engineering application.

DNA-based hydrogels have thus attracted mounting attention for their inherent biocompatibility, biodegradability, and unique programmability that are suitable for biotechnology.[14] Notably, encoding the sequences of DNA building blocks could allow a versatile spectrum of gelation network via simple physical hybridization and loading of specific multiple exogenous molecules with quantitative and spatial controls.[15] DNA can be conjugated into the synthetic polymer scaffold as the crosslinker to assemble hydrogel with high mechanical stiffness to sustain cells suspension for 3D cell printing.[16] Alternatively, pure DNA hydrogels can be assembled by the "Y" tiles scaffold for stimuli-responsive hydrogels and cell application. [17-18]

However, biotoxicity concern still shadows the application of DNA-polymer hybrid hydrogel.[16, 19] In addition, although the pure DNA hydrogels showed excellent biocompatibility and self-healing property, thermal annealing and high DNA concentration are often needed to assemble hydrogel with suitable mechanical stiffness to support the cell growth, thus limits the in-situ cells encapsulation and temperature-sensitive factors such as proteins, antibody, and growth factor. In addition, complex sequence design of the X-/Y-tiles building block is required to introduce additional exogenous molecules or functionalization of the DNA hydrogel to suit the different needs of cell culture study.[20] Therefore, a pure DNA hydrogel with inherent biocompatibility, programmable for multi-modulus loading, and low gelation concentration is

desired to provide a new approach of versatile DNA-based hydrogel platform for cell culture.[21-22]

In this chapter, we design a dendritic DNA building block with simultaneous functions of biofunctionalization and hydrogel gelation by independently programming the dendritic DNA loading branch and gelation branches, respectively. In addition, efficient crosslinking of the dendritic DNA building blocks would be achieved and resulting in enhanced mechanical properties of the DNA hydrogel. This is due to the simplified hydrogel assembly of the dendritic DNA and linker molecules instead of mixing several ssDNA strands which would lead to a higher chance of crosslinking mismatch and preventing the optimum crosslinking condition.

2.2. Result and Discussion

2.2.1. Design of Self-assembled Dendritic DNA Hydrogel for 3D Cell Culture

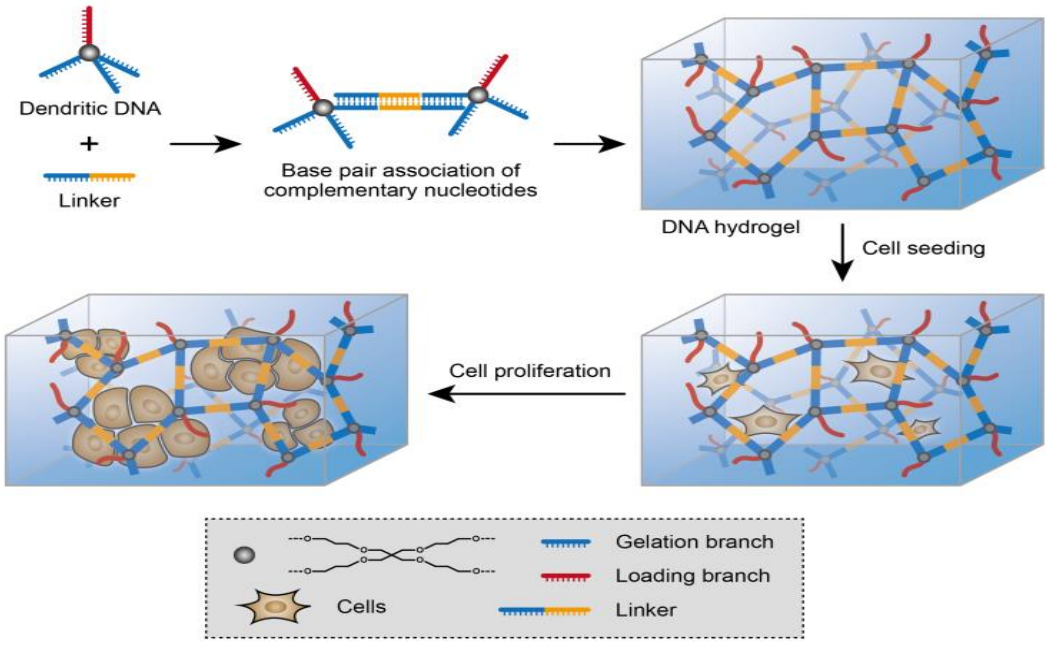

Scheme 2.1. Self-assembly of dendritic DNA building block and single-strand DNA linker into dendritic DNA hydrogel **DDH** for 3D cell culture platform. DNA branches and segments with the same color are complementary.

This chapter is a follow-up of the work done by Wu, J.[23] Herein we design a dendritic DNA building block (**D**) with four single-stranded DNA extended from the focal core. **D** possess inherent 3D conformation and fixed composition upon the synthesis. The solid phase oligonucleotide synthesis of **D** starts with the first arm (loading branch) followed by the addition of the focal core on the 5'-end. Then, the three arms of gelation branches can be synthesized simultaneously. Due to the nature of the synthesis process, **D** structure has two independent functions: 1) Hydrogel network formation (via three gelation branches) and 2) Loading of molecules (via gelation branch).

The dendritic DNA hydrogel (**DDH**) self-assembly is formed by crosslinking **D** with a single-stranded DNA linker (**L**) via hybridization between the complementary DNA base pairs. The structure and mechanical property of **DDH** can be tuned by either varying the concentration of the DNA or the ratio of **D** vs **L**. Furthermore, **DDH** assembly can be done isothermally to enable rapid in-situ cells encapsulation for 3D cell culture. Upon successful encapsulation, the cells proliferate to form complex cell morphologies such as cell clusters and spheroid with high cells viability. Subsequent cells harvesting and re-culture into a new **DDH** can be easily done due to the thixotropic nature of the hydrogel.

2.2.2. Dendritic DNA Synthesis and Characterization

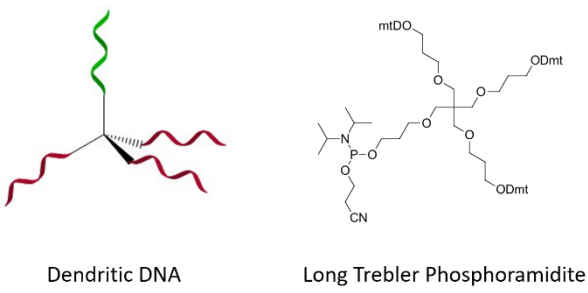

Figure 2.1. The structure of the dendritic DNA and the long trebler phosphoramidite.

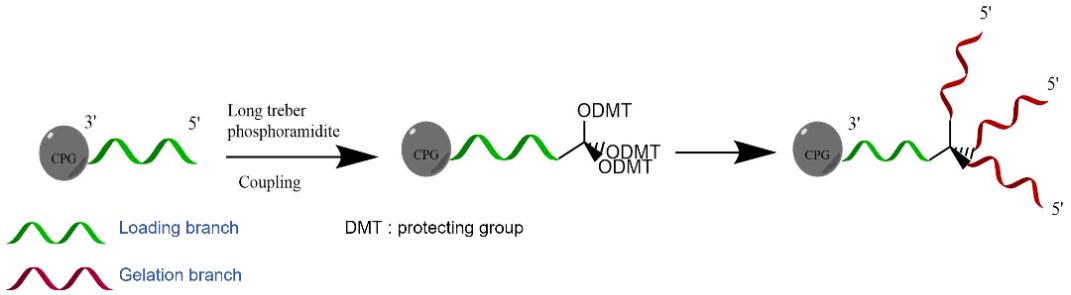

Scheme 2.2. Illustration of solid-phase oligonucleotide synthesis of **D**.

The DNA hydrogel consists of a dendritic DNA (**D**), a four branches ssDNA, and a

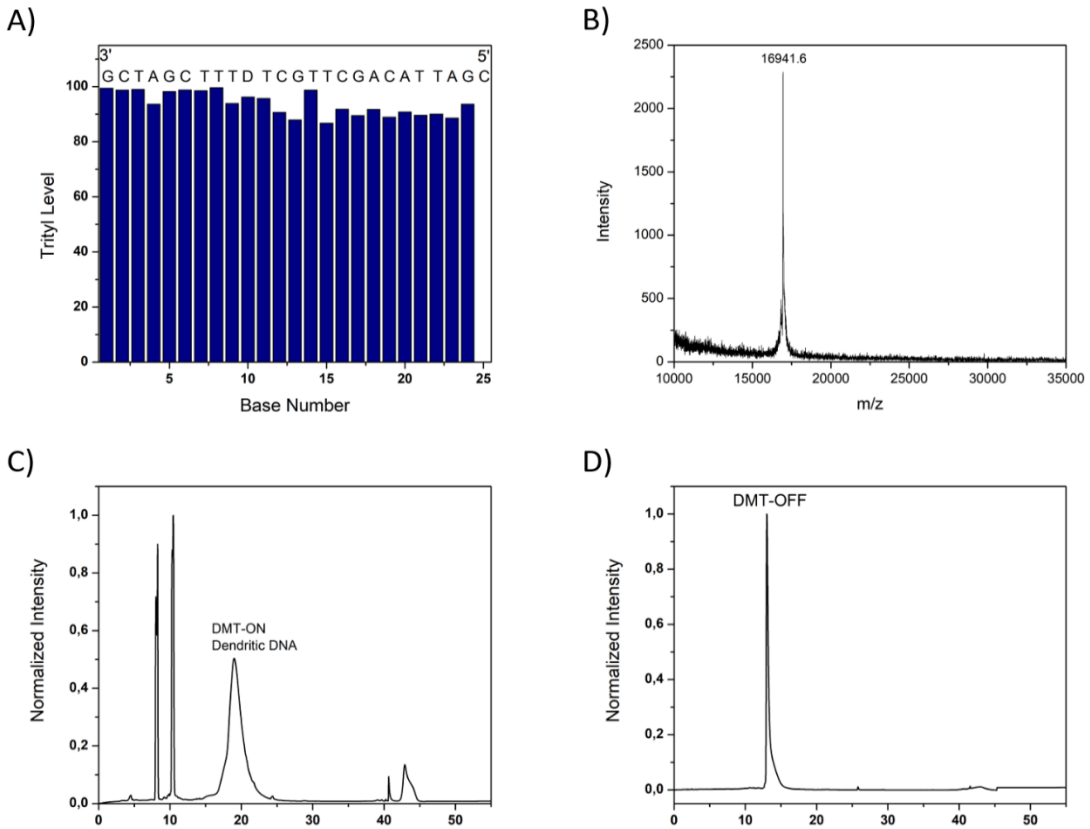

Figure 2.2. A) Trityl Bar of the oligonucleotide synthesis. B) MALDI-TOF mass spectrum of the **D**. C) HPLC chromatogram of the DMT-ON **D**. D) HPLC chromatogram of the DMT-OFF **D**

ssDNA linker (**L**) which form supramolecular structure upon self-assembly via hybridization. **D** consists of two parts, the loading branch (green) and three gelation branches (red) which are connected by the long trebler phosphoramidite (**Figure 2.1**). The synthesis of the dendritic DNA started from the 3'-end of the loading branch, followed by the addition of the long trebler phosphoramidite on the 5'-end. Upon successful coupling of the long trebler, the three gelation

branches began to grow simultaneously with each step of the synthesis. In the solid phase oligonucleotide synthesis, the yield of the resulting DNA is highly dependent on the coupling efficiency. The phosphoramidites have DMT protecting group, which upon detritylation produces DMT carbocation. The DMT carbocation absorbs at 495nm which produces orange color and can be used to monitor the coupling efficiency of the synthesis (**Figure 2.2A**). The trityl level must always be above 85% to ensure high coupling efficiency.

After cleavage from the solid support and deprotection of the phosphoramidites, the 5'-end of the dendritic DNA still has the DMT protecting groups. The DMT-ON dendritic DNA was purified by HPLC (**Figure 2.2C**) followed by cleavage of DMT and DMT-OFF purification (**Figure 2.2D**) to yield highly pure dendritic DNA **D**. The successful synthesis of **D** was further confirmed by MALDI-TOF MS (16,941.6 Da $(M+H)^+$, calc. 16945.16 Da) (**Figure 2.2B**).

2.2.3 Dendritic DNA Hydrogel Self-assembly

Table 2.1. DNA Sequence of the dendritic DNA and the linker

DNA	**Sequence (5' to 3')**
D	$(CGA\ TTA\ CAG\ CTT\ GCT)_3$ D TTT CGA TCG
L	AGC AAG CTG TAA TCG ACA ACG TTG T
L-FAM	FAM- AGC AAG CTG TAA TCG ACA ACG TTG T

The dendritic DNA (**D**) will hybridize with the linker (**L**) to form the supramolecular hydrogel **DDH** through the three gelation branches (**Scheme 2.1**). **D** consists of 54 nucleotides (nt) in total, 3x15nt for hybridization with the linker, and 9nt as the loading branch (**Table 1**). For the gelation sequence, the amount of GC-content is 47% to provide favorable thermostability for the crosslinking network due to the base stacking interaction.

Thermostability is important for the cell culture application as the hydrogel will be incubated at 37ºC. Moreover, the oligo(deoxythymidine) spacers are included before the addition of the relatively rigid organic focal core long trebler phosphoramidite (D) to provide more flexibility to the structure.

The linker **L** is a 25nt long ssDNA, 15 bases are complementary to the gelation branch of the **D**, while the rest 10nt are palindromic sequences to hybridize with another linker molecule. The design of the linker can be modified with an exogenous molecule for stimuli-responsive hydrogel. The gelation of the **D** and **L** can occur under room temperature within minutes, which is favorable for the loading of temperature-sensitive functions and the cell seeding for 3D cell culture application.

2.2.4. Tunable Mechanical Property of The Dendritic DNA Hydrogel

The mechanical property of the **DDH** was easily tunable by changing the ratio of **D** vs **L** concentration (**Figure 2.3**). In all different ratios of **D** vs **L**, the storage modulus G' was constantly higher than the loss modulus G" over time, showing that **DDH** was indeed a physical gel. The physical gels are dynamically cross-linked, changing their state between liquid and solid under different environmental factors.

D has three gelation branches for hybridization with L to form **DDH**. When **D** and **L** were mixed at a ratio of 1:3, all the gelation branches would hybridize with the linker to achieve optimum stiffness of the hydrogel (**Figure 2.3C**). As the ratio of **L** was increased from 1:1 to 1:3, both G' and G" values increased and became more stable. Furthermore, the increase of the G'/G" shows that the hydrogel is more solid like (**Figure 2.3E**), indicating that the **DDH**

mechanical stiffness increase by adding more hydrogel crosslinking network by addition of the linker **L** concentration to the **D** building block.

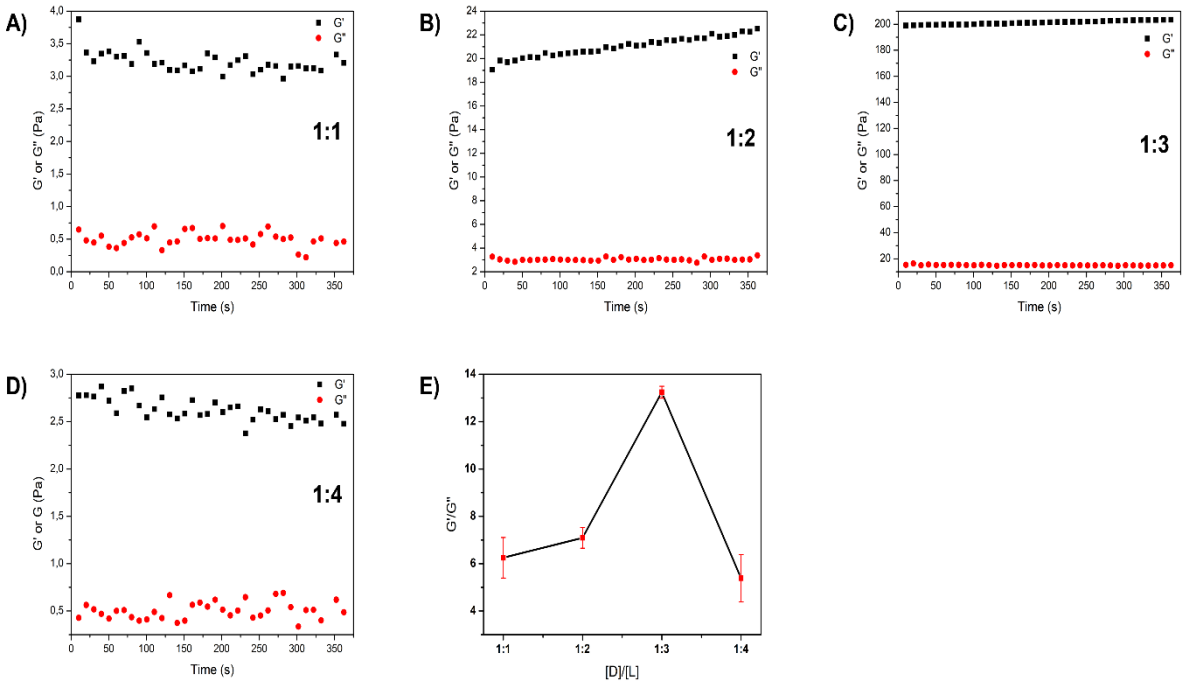

Figure 2.3. Storage modulus (G') and loss modulus (G") as a function of time for 100 µM **DDH** with ratio A) 1:1, B) 1:2, C) 1:3. D) 1:4, and E) G'/G" of **DDH** at different ratio.

However, when the **L** ratio reached 1:4, both G' and G" values decreased and more fluctuated, similar to ratio 1:1. Due to the existence of the palindromic site on the linker **L**, intramolecular hybridization such as hairpin formation may be preferred in an excess concentration of **L**, thus preventing the hybridization with **D** gelation branches to form the crosslinking network. Therefore, either increasing or decreasing the **L** equivalence would compromise the G'/G" value by hindering or providing insufficient crosslinking among **D** and **L**. Moreover, it can be concluded that **DDH** with the ratio of **D** vs **L** at 1:3 achieved optimum gelation concentration and mechanical stiffness. This restructuring property of **DDH** demonstrates that **DDH** is a soft material with tunable mechanical properties, which makes it favorable for various applications, such as 3D cell culture and drug delivery.

2.2.5. Dendritic DNA Hydrogel Structure

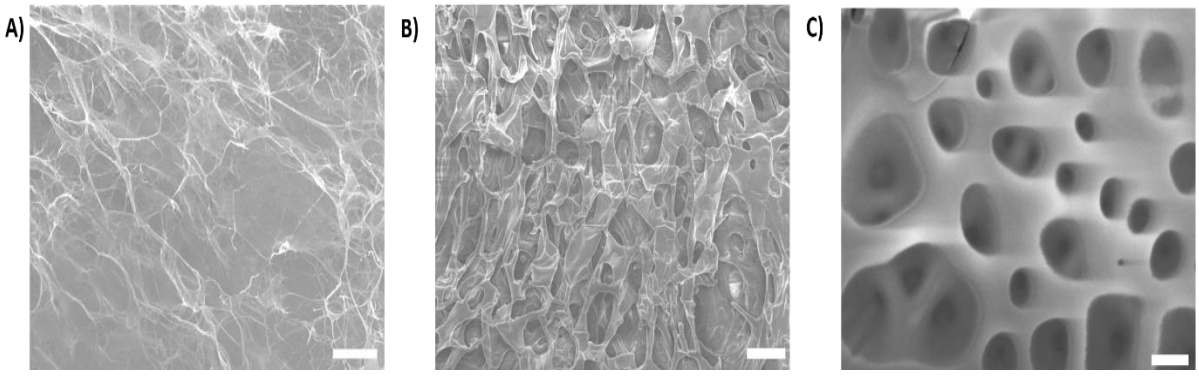

Figure 2.4. SEM image of the hydrogel with different [**D**] and [**D**] vs [**L**] ratio. A) [**D**] = 100nM, ratio 1:3. B) [**D**] = 200μM, ratio 1:2. C) [**D**] = 200μM, ratio 1:3. Scale bar: 10μm.

Scanning electron microscope (SEM) was employed to study the network structure of **DDH**. The DDH was freeze-dried prior to SEM. At nanomolar concentration of **D**, the gel was already formed with thin fibrous-like structures because of the low gelation concentration of **D** and **L** to assemble the hydrogel (**Figure 2.4A**). When the gelation concentration of **D** was increased to 200μM, more densely packed and uniform 3D crosslinked networks were present inside the hydrogel and expands both horizontally and vertically with most pore sizes below 10μm (**Figure 2.4B**). However, when the concentration of the linker decreased, there were insufficient linker molecules to fully crosslink with **D** gelation branches, hence showing larger pore size and decreased mesh density yet still maintaining the long-range interconnectivity (**Figure 2.4C**).

In all cases, the **DDH** structure has porous channels which are beneficial for nutrients traffic and provide more spaces for the cells to interact and proliferate. It is worth noting that by using a linker instead of direct hybridization of the dendritic DNA **D** building block, would allow to tune the mesh density of **DDH** microstructure and mechanical property by adjusting the linker ratio. Moreover, extra stimuli or functionalization can also be introduced via linker

sequence without altering the design of the **D** building block, hence reducing the synthetic demand.

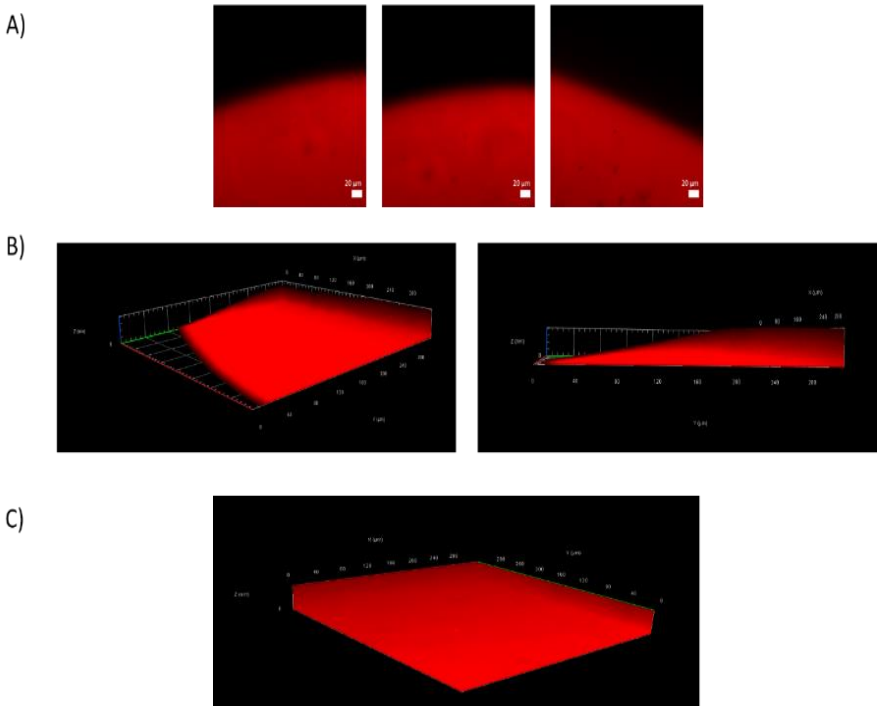

Figure 2.5. A) Confocal image of the hydrogel edge. Scale bar: 20µM. 3D construct image of the B) hydrogel edge, and C) middle part of the hydrogel.

To demonstrate the uniform crosslinking of the **DDH** network, the linker was modified with the FAM dye at the 5'-end (**L-FAM**) and the distribution was observed by the confocal fluorescence microscopy (**Figure 2.5**). The **DDH** was not dried and was still in swollen form when the experiment was conducted. From the brightness of the hydrogel, it could be seen that the hydrogel crosslinking was uniform. The 3D image was constructed by taking the images of the hydrogel for every 2µm over the height of 30µm. The hydrogel edge appears flatten and there is a clear line in the brightness of the hydrogel edge and the glass surface, indicating that the hydrogel formed was a soft gel.

2.2.6. Thermal Stability of The Dendritic DNA Hydrogel

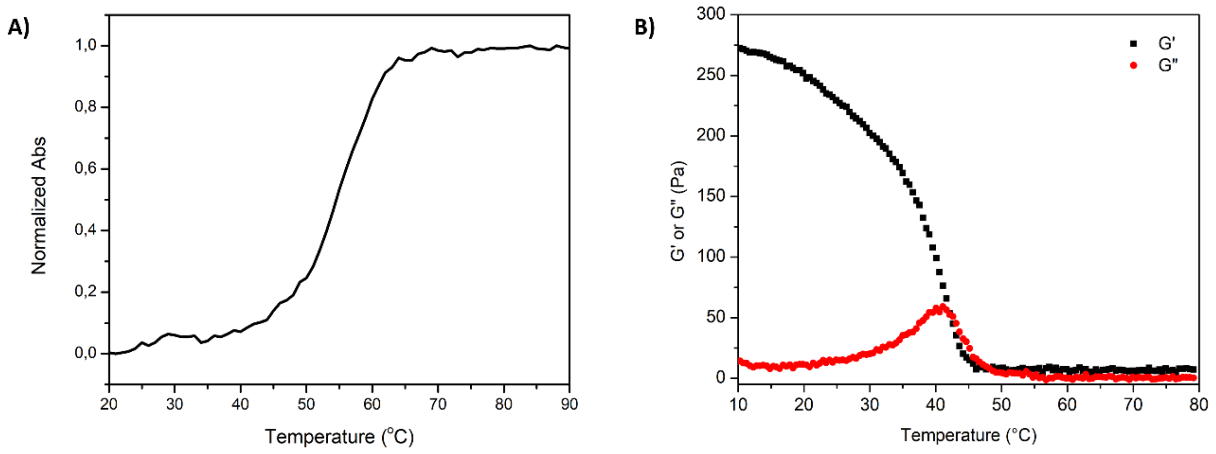

Figure 2.6. A) UV melting curve of **DDH**. [**D**] = 500 nM, [**L**] = 1.5µM. Ramp rate 1°C/min. B) Temperature ramp rheological analysis of the DNA hydrogels, from 10°C to 80°C, ramp rate 5°C/min, fixed frequency (1Hz) and strain (1%). G'= storage modulus, G" = loss modulus. [**D**] = 100µM, [**L**] = 300µM.

The thermal stability of **DDH** was assessed by UV spectroscopy and the temperature sweep analysis by rheometer. **DDH** showed a sigmoidal curve typical to the duplex DNA, indicating that the crosslinking between **D** and **L** was formed by DNA hybridization (**Figure 2.6A**). The melting point of the duplex DNA in the **DDH** crosslinking was at 54.5°C, indicating that **DDH** crosslinking could occur at room temperature.

To further confirm the thermal stability of bulk **DDH** hydrogel, on the macroscopic level, a study to determine the gel-to-sol transition was performed by conducting the temperature sweep rheometer experiment. The gel-sol transition temperature (Tgel) is determined as the intersection point between the G' and G" (**Figure2.6B**). The **DDH** was still a physical gel until it turned into quasi-sol 43°C. It is worth noting that for the cell culture experiment, the cells are incubated at 37°C. Hence, **DDH** can still maintain its gel state and provide structural support for cell encapsulation. Furthermore, the single sigmoidal curve

shown on both Tm and Tgel measurements indicated uniform crosslinking existed in **DDH**, as observed by the confocal microscopy study discussed in **Section 2.2.5**.

2.2.7. 3D Cell Culture in Dendritic DNA Hydrogel

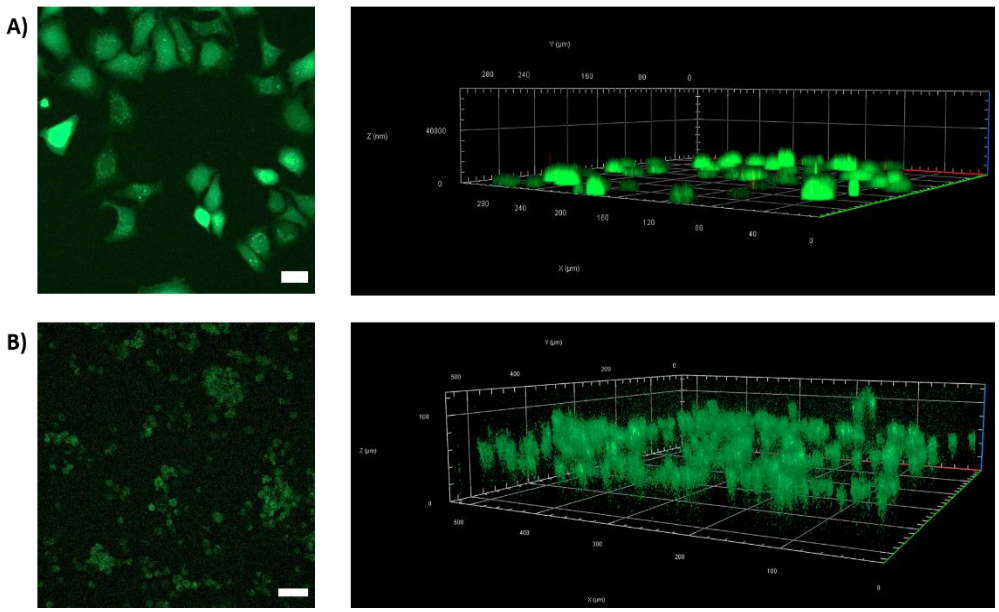

Figure 2.7. Merged fluorescent image (left) and the 3D construct (right) of A549 cells cultured in A) 2D monolayer solution, B) **DDH**. Scale bar: A) 20µm, B) 50µm

Figure 2.7. shows the merged fluorescent image of the 2D cell culture and 3D cell culture after 72 hours and 96 hours, respectively. It was observed that in 2D solution, the morphology of the cells appeared to be stretched and flattened. The cells settled on the bottom surface of the culture dish and occupied less than 10µm of height. (**Figure 2.7A**). On the other hand, the cells cultured in the **DDH** appeared spherical and exhibited cell-cell interaction to form cell colonies and aggregates. Moreover, the cells were encapsulated and distributed three-dimensionally in the DNA hydrogel over 100µm in height (**Figure 2.7B**).

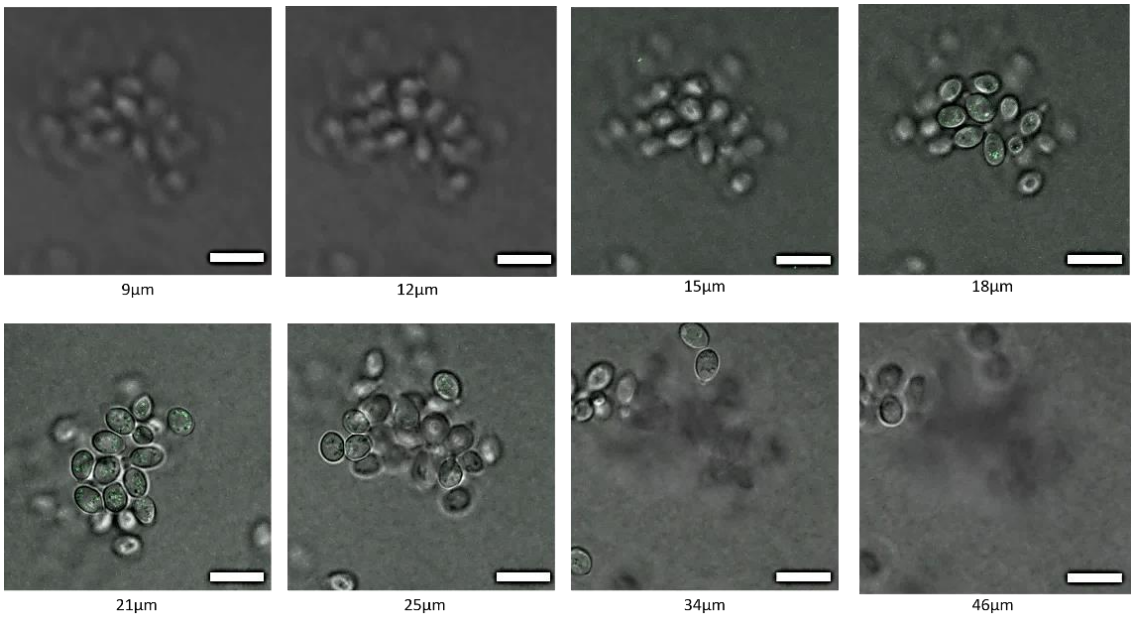

Figure 2.8. Merged fluorescent and bright field image of the spheroids at different height. Scale bar: 10µm.

In contrast to the 2D cell culture where the cells can be observed within one layer, unique defocus phenomena was observed in **DDH** due to the cell interaction three-dimensionally at different heights (**Figure 2.8**). The defocus phenomena observed in all cross-section images showed the cells interacted with the neighboring cells and adhered to form the slightly deformed spheroid. After staining the cells with the fluorescence dye, the membrane-stained cells appeared in all different cross-section images, indicating that small molecule such as dye can still access the cells inside-out, thus showing the feasibility of incorporating soluble factors such as growth molecules. Furthermore, the fluorescent live/dead assay indicated that the viability of the A549 cells in the 2D cell culture and **DDH** 3D cell culture was 97.2 ± 2.4% and 99.4 ± 1.7%, thus demonstrating the biocompatibility of the **DDH** as the 3D cell culture platform. Overall, the distinct cell morphologies achieved in the 2D cell culture and **DDH** showed that the **DDH** could provide mechanical stiffness to support the cell growth and mimic the cell environment *in vivo.*

2.2.8. Cell Harvesting and Regeneration

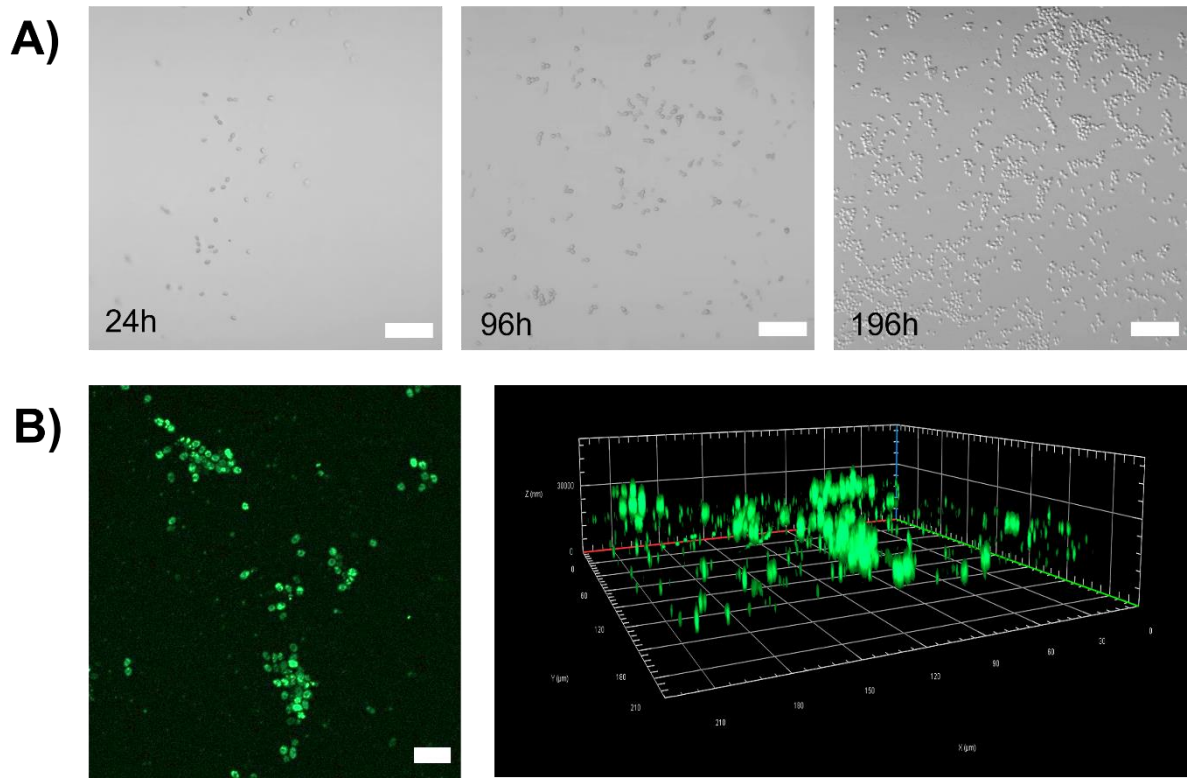

Figure 2.9. 2nd generation culture of A549 cell line in **DDH-2** after the cells were harvested from **DDH** ([**D**] = 200 μM)**.** A) Microscope images of A549 cells at different time over 8 days. Scale bar: 50μm. B) Fluorescence image of A549 cells in **DDH-2** at day 8. Left: confocal image; Right: reconstructed 3D image. Cells are stained with Calcein-AM (green – live cells) and PI (red – dead cells) to determine cell viability. Scale bar: 20μm.

Cell harvest and re-culture are necessary abilities for 3D cell culture. To demonstrate that feature in the DNA hydrogel, the cell was pipetted out from **DDH** when the medium was partially converted into solution upon gentle pipetting. The cell was then re-cultured by mixing with fresh cell medium solution, containing **D** and **L**. It took longer time for the cells to grow as the hydrogel with seeded cells would take time to merge and self-heal to form the newly cast DNA hydrogel **DDH-2** (**Figure 2.9A**)**.** After 8 days, the cells in **DDH-2** achieved similar morphology and cell viability (98.7±1.8%) as those in the precedent **DDH** (**Figure 2.9B**).

2.3. Conclusion

In summary, we designed and synthesized dendritic DNA as the building block for the supramolecular dendritic DNA hydrogel (**DDH**). The mechanical property and the mesh size of the **DDH** crosslinking network were tunable by adjusting the concentration and the ratio of the dendritic DNA and linker. Low gelation concentration was required to form the **DDH** with good mechanical property to support cell growth. The encapsulation of the cells within **DDH** occurred isothermally and rapidly under physiological conditions. Distinct cell morphologies such as spherical cell shape and cell colonies can be achieved with high viability. Additionally, with simple protocols, the cells can be harvested and re-cultured into a newly cast DNA hydrogel due to the dynamic crosslinking network in the supramolecular DNA hydrogel, endowing the self-healing property in **DDH**. The new DNA hydrogel design which incorporates the dendritic DNA would offer simple hydrogel assembly as well as loading and functionalization strategy for stimuli-responsive hydrogel, which could be further used for other biomedical applications such as tissue engineering, drug delivery, and 3D cell printing.

2.4. Experimental Details

Materials

Unless otherwise stated, all reagents and solvents were purchased from Sigma-Aldrich (Singapore). All the phosphoramidites and reagents for the solid phase DNA synthesis were purchased from Glen Research (Virginia, USA) and the Mermade column was purchased from Bioautomation (Texas, USA). All single-strand DNAs were purchased from Sangon Biotech (Shanghai, China). The buffer solution was purchased from 1st Base (Singapore). Ultrapure deionized (DI) water used in all experiments was obtained from a Millipore Milli-Q system (resistivity 18.2 MΩ.cm).

Methods

- **Solid Phase Dendritic DNA Synthesis**

Synthesis of the dendritic DNA was performed on Bioautomation Mermade 4. Fast deprotecting phosphoramidite and the long-trebler phosphoramidite (Glen Research, Cat no. 10-1925-90) was used to synthesize the dendritic DNA. The DNA cleavage from the solid support was done in 33% ammonium hydroxide solution at 25ºC for 90 minutes followed by deprotection at 60ºC for an hour. The DMT-ON DNA products were purified by HPLC (Shimadzu, Japan) equipped with reverse-phase (RP) column (Microsorb 100-5 C18 Dynamax 250x10 mm). The HPLC mobile phases were 0.1M TEAA buffer (pH 7) and ACN. The gradient method was used to collect the product. The concentration of the ACN was increased from 5% to 60% over 30 minutes at 3.5 mL/min flush speed. The DMT-ON dendritic DNA was flushed at 38-44% ACN. The collected product was freeze-dried by lyophilizer. The DMT protecting group on the dendritic DNA was cleaved by 80% acetic acid (200 µL) for 15 minutes at room

temperature. 1 mL cold ethanol was added to the solution followed by centrifugation at 13,500 xg for 10 minutes at 4ºC to precipitate the DNA. The solvent was removed by a vacuum concentrator.

The detitylated DMT-OFF dendritic DNA was purified by HPLC with the same method. The dendritic DNA was flushed at 23-26% ACN. The collected product was freeze-dried. The lyophilized dendritic DNA powder was dissolved in 1XTAE, 12.5mM $MgCl_2$ buffer (pH 7) and stored as the stock solution. The quantification of the dendritic DNA was done by measuring the absorption at wavelength 260 nm with Nanodrop 2000c spectrophotometer (Thermo Scientific, US).

- **Matrix Assisted Laser Desorption/Ionization Time-of-Flight (MALDI-TOF)**

  Matrix preparation :

  - *Matrix for myoglobin (M0630, Sigma)*. 10mg of sinapinic acid (SA) was dissolved in 500µL 50% acetonitrile solution with 0.1% TFA. The saturated solution was centrifuged to get the supernatant and stored in small aliquots (20 µL each).

  - *Matrix for DNA*. There are two matrix components; 3-HPA and ammonium citrate. **A** : 10mg 3-HPA in 200 µL 50% acetonitrile. **B**: 10mg ammonium citrate in 200 µL water. **A** was mixed with **B** at a volume ratio of 8 to 1.

The sample was diluted to 100pmole/µL and mixed with the matrix at sample to matrix volume ratio 1:1. 1µL of the sample mix was deposited on the spot of the MALDI plate and left to air-dry before being analyzed. The instrument (JMS-S3000, JEOL) was first calibrated with

myoglobin MW = 16,951.49. Linear positive mode and 55% laser intensity was used to get the mass spectrum.

- **DNA Hydrogel Assembly**

Dendritic DNA and linker with certain concentration and ratio were mixed in 1XTAE, 12.5 mM $MgCl_2$ buffer (pH 7). The solution was heated to 95℃ for 10 minutes in the heating block (AccuBlock™ Digital Dry Bath, Labnet International) to remove the initial DNA interaction. The heating block was turned off and the solution was slowly cooled down to room temperature to let the hydrogel assemble. The resulting DNA hydrogel was stored in the 4℃ fridge.

- **Fluorescent Imaging of The DNA Hydrogel**

Pre-calculated volume of dendritic DNA (**D**) and FAM-linker (L-FAM) was mixed in the buffer to form DNA hydrogel with [**D**] = 200μM and [L-FAM] = 600 μM. The solution was heated to 95℃ for 10 minutes and cooled down to room temperature. 5μL of the solution was drop-casted on top of the microscope glass cover. The image was collected on confocal microscope (Carl Zeiss LSM 800, Germany) with an oil-immersion 40x objective lens. FAM laser excitation wavelength was 488nm and emission was 520nm.

- **Scanning Electron Microscope (SEM)**

5μL of the DNA hydrogel was dropped on the silica wafer and freeze-dried overnight. Prior to SEM observation, the samples were coated with Pt at 20mA for 60s to get 12nm Pt height. The field emission SEM images were acquired using JEOL-JSM 6700F.

- **Mechanical Property by Rheometer**

The mechanical property measurement was carried out with Discovery Hybrid Rheometer (DHR-3, TA Instruments). The parallel plate (25mm diameter) was used and the sample gap was set to 300μm. 50μL DNA hydrogel was assembled for the experiment.

- *Time Sweep*

  The elastic modulus (G') and loss modulus (G") as a function of time were recorded at constant strain 1% and frequency 1Hz for 5 minutes.

- *Temperature Sweep*

  The elastic modulus (G') and loss modulus (G") was recorded against temperature change at constant strain 1% and frequency 1Hz.

- **UV Melting Temperature**

The UV melting temperature measurement was performed on UV spectroscopy (UV-1800, Shimadzu) equipped with the temperature controller. Three samples of 120μL DNA hydrogel [**D**] = 0.5μM, [**L**] = 1.5μM were loaded into the 8-microwell cuvette. The samples were first heated to 90°C and cooled down to 20°C with a ramp rate of 1°C/min. The UV melting curve was acquired by recording the absorbance at 260nm vs temperature. The melting temperature was obtained by fitting the data points into a sigmoidal equation.

- **Cell Line and Culture Condition**

The cell line used in all experiments was A549 human lung carcinoma. For 2D cell culture, the cell media was DMEM supplemented with 10% FBS and 1% penicillin. For the 3D

cell culture, the cell media was DMEM+Glutamax I supplemented with 1X Non-essential Amino Acid. All cells were incubated in a humidified atmosphere of CO_2/air (5%/95%) at 37℃.

- **Live/Dead Fluorescence Imaging**

2D Cell Culture. $5x10^4$ cells were seeded in µ-dish 35mm, high (ibidi, German) and incubated for 72 hours.

3D Cell Culture. 5000 cells in the cell media were mixed with the **D** and **L** to form 20µL DNA hydrogel ([**D**] = 200µM, [**L**] = 600µM). The solution was gently pipetted to ensure homogenous cell distribution in the hydrogel. The hydrogel was drop-casted in the middle of the µ-dish 35mm, high. After 3 hours, 50 µL of cell media was topped up on top of the hydrogel to ensure enough nutrients for the cells throughout the experiment. The cells in the hydrogel were incubated for 96 hours.

Live/Dead Cell Staining Kit (04511, Sigma) was used to determine the viability of the cell. The kit contains Calcein-AM which stains viable cells to generate green fluorescence (excitation:490 nm, emission 515nm) and Propidium Iodide (PI, excitation:535nm, emission:617nm) which stains dead cells to emit red fluorescence.

10 µL of solution A (Calcein-AM) and 5µL of solution B (PI) were added to 5mL PBS to prepare the assay solution. The cell media of the sample was firstly removed. Then, the sample was gently washed with PBS to remove residual esterase activity followed by staining with 100µL assay solution and incubation for 30 minutes at 37℃. All images were collected by the confocal microscope (Carl Zeiss LSM 800) using the 63x oil immersion and 20x objective lens. 488nm excitation was used as both Calcein-AM and PI can be excited using this excitation

wavelength. The 3D constructs were acquired with the z-step size of 2µm (20x lens) or 0.5µm (63x lens).

The cell viability was calculated by identifying cells using the Imaris (Bitplane, Northern Ireland) spot detection function. The relative proportion of live cells (green fluorescent) and dead cells (red fluorescent) at four different cross-section heights are determined to get the cell viability. The data are presented as mean values ± standard deviation.

2.5. References

1. Barralet, J. E.; Wang, L.; Lawson, M.; Triffitt, J. T.; Cooper, P. R.; Shelton, R. M., *Journal of Materials Science: Materials in Medicine* **2005,** *16* (6), 515-519.

2. Langhans, S. A., *Frontiers in Pharmacology* **2018,** *9* (6).

3. Zhang, Y. S.; Khademhosseini, A., *Science* **2017,** *356* (6337), eaaf3627.

4. Tibbitt, M. W.; Anseth, K. S., *Biotechnol Bioeng* **2009,** *103* (4), 655-63.

5. Lutolf, M. P.; Gilbert, P. M.; Blau, H. M., *Nature* **2009,** *462* (7272), 433-41.

6. Peppas, N. A.; Hilt, J. Z.; Khademhosseini, A.; Langer, R., *Advanced Materials* **2006,** *18* (11), 1345-1360.

7. Caliari, S. R.; Burdick, J. A., *Nature Methods* **2016,** *13* (5), 405-414.

8. Jose, G.; Shalumon, K. T.; Chen, J. P., *Curr Med Chem* **2020,** *27* (16), 2734-2776.

9. Serban, M. A.; Prestwich, G. D., *Methods* **2008,** *45* (1), 93-8.

10. Jabbari, E.; Leijten, J.; Xu, Q.; Khademhosseini, A., *Materials Today* **2016,** *19* (4), 190-196.

11. Wang, W.; Xiang, L.; Diaz-Dussan, D.; Zhang, J.; Yang, W.; Gong, L.; Chen, J.; Narain, R.; Zeng, H., *Chemistry of Materials* **2020,** *32* (24), 10545-10555.

12. Kang, H. W.; Tabata, Y.; Ikada, Y., *Biomaterials* **1999,** *20* (14), 1339-44.

13. Lee, C. C.; MacKay, J. A.; Fréchet, J. M. J.; Szoka, F. C., *Nature Biotechnology* **2005,** *23* (12), 1517-1526.

14. Dong, Y.; Yao, C.; Zhu, Y.; Yang, L.; Luo, D.; Yang, D., *Chemical Reviews* **2020,** *120* (17), 9420-9481.

15. Li, F.; Tang, J.; Geng, J.; Luo, D.; Yang, D., *Progress in Polymer Science* **2019,** *98*, 101163.

16. Li, C.; Faulkner-Jones, A.; Dun, A. R.; Jin, J.; Chen, P.; Xing, Y.; Yang, Z.; Li, Z.; Shu, W.; Liu, D.; Duncan, R. R., *Angewandte Chemie International Edition* **2015,** *54* (13), 3957-3961.

17. Wang, Y.; Shao, Y.; Ma, X.; Zhou, B.; Faulkner-Jones, A.; Shu, W.; Liu, D., *ACS Applied Materials & Interfaces* **2017,** *9* (14), 12311-12315.

18. Jin, J.; Xing, Y.; Xi, Y.; Liu, X.; Zhou, T.; Ma, X.; Yang, Z.; Wang, S.; Liu, D., *Advanced Materials* **2013,** *25* (34), 4714-4717.

19. Li, C.; Chen, P.; Shao, Y.; Zhou, X.; Wu, Y.; Yang, Z.; Li, Z.; Weil, T.; Liu, D., *Small* **2015,** *11* (9-10), 1138-1143.

20. Um, S. H.; Lee, J. B.; Park, N.; Kwon, S. Y.; Umbach, C. C.; Luo, D., *Nat Mater* **2006,** *5* (10), 797-801.

21. Wu, J.; Meng, Z.; Lu, Y.; Shao, F., *Chemistry* **2017,** *23* (56), 13980-13985.

22. Zhu, X.; Wu, J.; Shao, F.; Hu, X., *ACS Applied Bio Materials* **2018,** *1* (4), 1118-1123.

23. Wu, J. Dendritic DNA and its application to biological and biomedical technology. Nanyang Technological University, Singapore, 2017.

CHAPTER 3

Integrin-targeting Functionalized DNA Hydrogel to Control Cell Spreading and Attachment

3.1 Introduction

Members of the RGD peptide selectively recognize the integrin binding site via the amino acid sequence Arg-Gly-Asp (RGD) as the binding motif to the integrin subtype αvβ3, which plays a crucial role for the initial cell attachment.[1] Cell attachment is important to study several physiological processes and diseases developments, hence this peptide sequence is widely used for the cell study. The structure of the RGD peptide affects its cell attachment property with the cyclic peptide showed higher cell attachment affinity as compared to the linear RGD peptide sequence.[2-4]

The RGD-peptide motif has been widely used to improve cell attachment ability into the hydrogel scaffold, especially for the culture of fibroblast cells where the cells appear long, flatten, and stretched *in vivo*.[5-6] Additionally, the adherence property is also desired when manipulating the cell fate of the human mesenchymal stem cells (hMSCs) where the fate of the stem cells greatly differed depends on many cues in the cell microenvironment, including the cell shape and cytoskeletal integrity.[7-8] hMSCs that were allowed to adhere, flattened, and spread committed into osteoblast fate via osteogenesis, while the round and unspread cells committed into adipocytes via adipogenesis differentiation.[9]

Furthermore, fibroblasts has been gaining traction in the regenerative medicine field as the practical alternative for some cell therapy as compared to the mesenchymal stem cells due to ease of harvesting fibroblasts from the biological waste and the robustness of the fibroblasts cell expansion *in vitro*.[10] Therefore, designing a biocompatible hydrogel with the tailored cell

attachment ability to suit the different needs of 3D cell culture requirement is of utmost importance.

Modified DNA hydrogel that incorporates targeting and functional DNA such as aptamers, DNA-based nanomotors and nanosensors have been widely explored, yet the application of this hydrogels has not been much studied for the 3D cell culture application.[11-12] The programmability of the DNA allows the versatile design of the hydrogel for wide range application, but most DNA hydrogels require complicated DNA sequence design to offer multifunctionality of the hydrogels.[13] Therefore, developing a DNA hydrogel 3D cell culture platform that can easily incorporate controlled targeting ability while maintaining the substantial mechanical stiffness for optimal cell culture condition is of interest.

3.2 Result and Discussion

3.2.1 Design of The Integrin-targeting Functionalized DNA Hydrogel (D-RGD)

Table 3.1. Sequence for the assembly of integrin-targeting DNA hydrogel.

DNA	Sequence (5'-3')
D-R	(GCC ATC CGT CGA GCC TGC AG)$_3$ D TTT CCG TCG TGA GCA
L-R	CTG CAG GCT CGA CGG ATG GCA ATG CGC GCA TT
ssD-R	N_3 – TGC TCA CGA CGG AAA

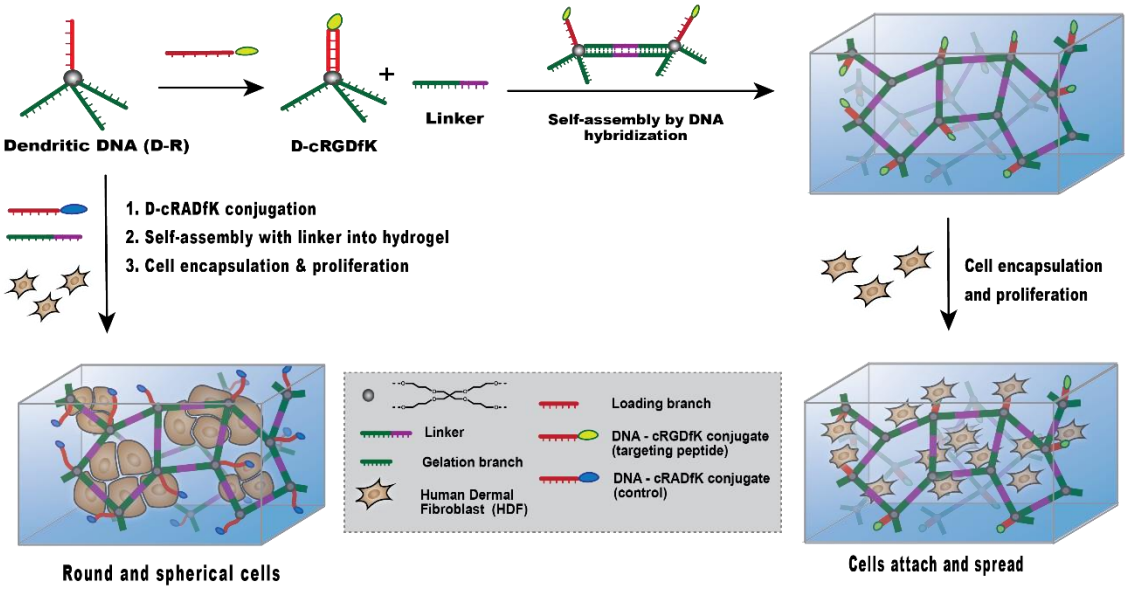

Scheme 3.1. Self-assembly of the integrin-targeting functionalized DNA hydrogel. Human dermal fibroblast cells encapsulated in the D-cRGDfK dendritic DNA (**D-RGD**) hydrogel appear stretched and spread, while the fibroblast cells encapsulated in the negative control D-cRADfK dendritic DNA (**D-RAD**) hydrogel appeared round and spherical. [**D-R**] = 0.5mM, [**L-R**] = 1.5mM, [**ssDNA-peptide**] = 0.5 mM.

Herein we designed a dendritic DNA (**D-R**) architecture with four single-stranded DNA (ssDNA) arms connected to the focal core. The three gelation branches on **D-R** serve as the crosslinking arms to hybridize with a linker (**L-R**) to further form the three-dimensional hydrogel network, while the fourth arm serves as the loading function. The independent sequence programmability of loading and network gelation in the dendritic DNA **D-R** allows the functionalization of bio-cue via the loading branch, and sequentially be attached to **D-R** framework to manipulate the cell attachment and spreading on the hydrogel scaffold (**Scheme 3.1**). The supramolecular self-assembly of the DNA hydrogel can form isothermally at room temperature, thus enabling the loading of temperature-sensitive cue such as peptide. A cyclic peptide cRGDfK can selectively bind to integrin αvβ3 which sequence was found on the integrin of the cell surface and thus enhancing the cell attachment to the DNA hydrogel scaffold. Meanwhile, the scrambled peptide cRADfK serves as the negative control as it provides non-binding selectivity to the cell integrin.

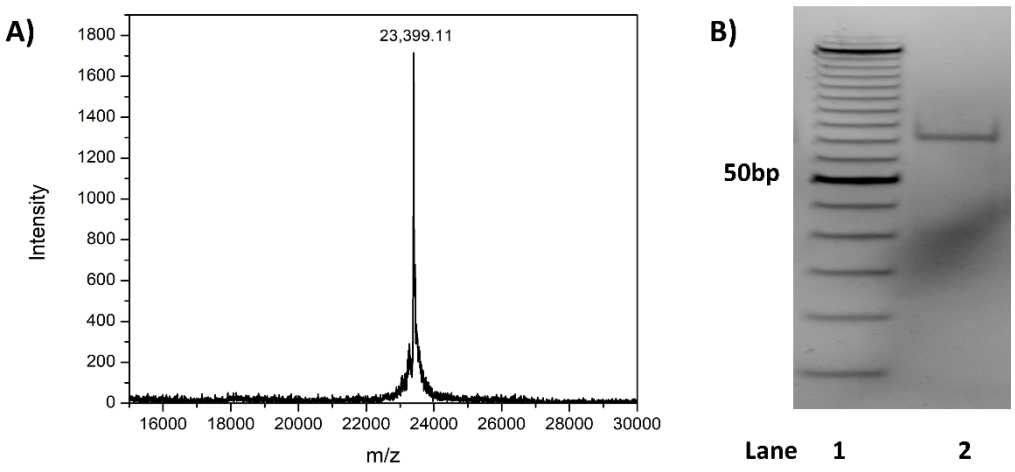

Figure 3.1. Characterization of dendritic DNA **D-R**. A) MALDI-TOF mass spectrum. B) PAGE-Gel analysis. Lane 1: 10bp DNA ladder. Lane 2: dendritic DNA **D-R**.

A single-strand DNA complementary to **D-R** loading branch was conjugated with the peptide via Copper-free click chemistry to form a DNA-peptide conjugate. The DNA-peptide conjugate was subsequentially hybridized with **D-R** loading branch to form the dendritic DNA **D-cRGDfK**. The dendritic DNA **D-R** loading branch was designed to provide stability for the duplex formation with the ssDNA-peptide conjugate by increasing the bp length and GC-content to 15bp and 70% GC-content, respectively. The addition of bp length and GC-content on the loading branch would increase the thermal stability of the duplex (Tm calculated = 50.6°C), which is crucial in the cell culture application where the cell would be incubated at 37°C over several days.

In this work, we modified the length and GC-content of **D-R** gelation branches to provide more stability to the hydrogel network to accommodate the fibroblast cells, considering the large size of fibroblast cells. In addition, raising the GC-content and bp length of the gelation branches would increase the melting temperature of the hydrogel network, preventing early degradation over the course of HDF cell culture, which is typically over 7 days. The

dendritic DNA **D-R** was synthesized via solid-phase oligonucleotide synthesis followed by purification with HPLC. The dendritic DNA mass was confirmed by MALDI-TOF and PAGE-Gel (**Figure 3.1**), (obtained. 23,399.11 Da $(M+H)^+$, calc. 23,403.80 Da)

Next, the peptide-functionalized DNA hydrogel (**D-RGD**) was fabricated by mixing the two components, **DD-cRGDfK** conjugate and linker **L-RGD** at ratio of 1:3 [**D-R**] = 0.5mM, [**L-R**]. Higher DNA concentration was chosen to accommodate the minimum requirement of the peptide concentration presence in the hydrogel.[5] The same protocol also applied for the formation of the negative-control (**D-RAD**) hydrogel. Upon cell encapsulation within the **D-RGD** hydrogel, the cell would attach and spread throughout the hydrogel framework.

3.2.2 DNA – peptide Conjugation

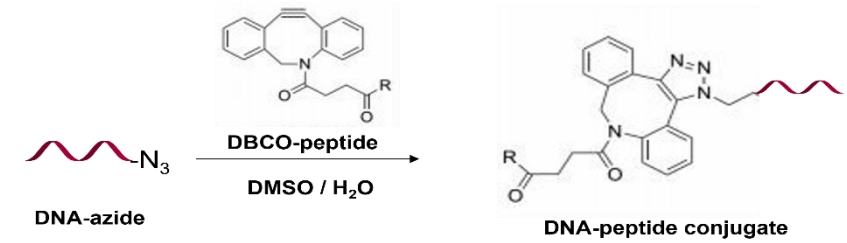

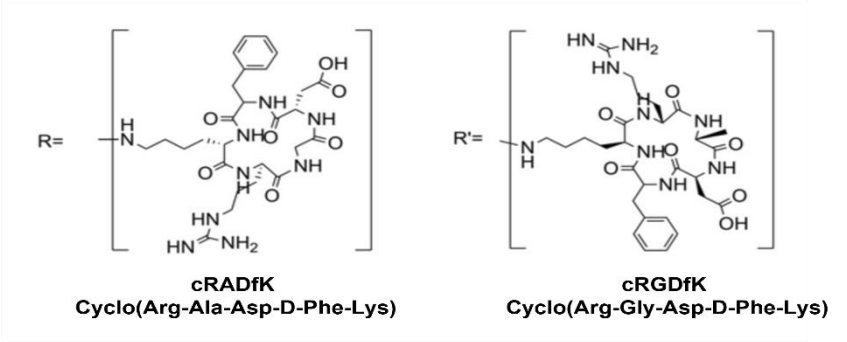

Scheme 3.2. Reaction pathway to form ssDNA-peptide conjugate via copper-free click chemistry.

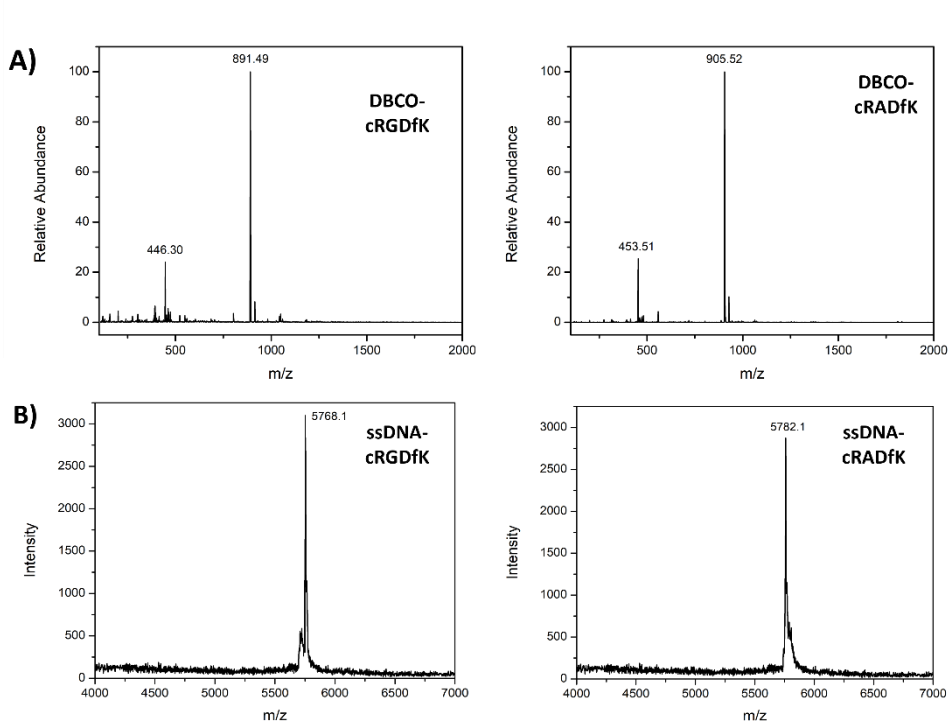

Figure 3.2. Characterization of the ssDNA-peptide conjugate. A) ESI-MS mass spectrum of DBCO-peptide. B) MALDI-TOF mass spectrum of ssDNA-peptide conjugate.

The conjugation of the ssDNA and the cyclic peptide was done by "copper-free" click chemistry reaction, as it provides a safer alternative to the copper-assisted click chemistry which requires the presence of the Cu(I) catalyst that is toxic to most organism in the biological system. The copper-free click chemistry is based on the reaction between an azide-labelled molecule with a cyclooctyne (DBCO) moiety under room temperature to form the stable triazole to crosslink the biomolecule via covalent bond.[14] Here we utilized an azide-labelled ssDNA complementary to the **D-R** loading branch and mixed with the DBCO-modified cyclic peptide to form the DNA-peptide conjugate (**Scheme 3.2**).

The cyclic peptide (cRGDfK and cRADfK) was first mixed with the DBCO-NHS for 2h followed by HPLC purification and mass spectroscopy to confirm the successful reaction and purity of the DBCO-peptide moiety (**Figure 3.2A**), (DBCO-cRGDfK : obtained. 891.49

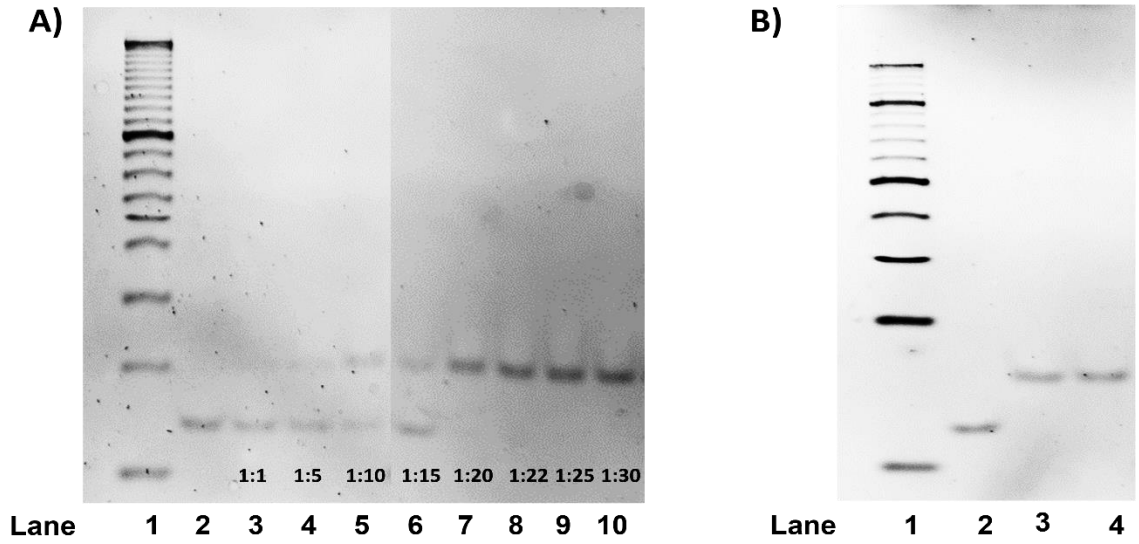

Figure 3.3. PAGE-Gel analysis of A) ratio of [ssDNA-N_3] vs [DBCO-peptide]. Lane 1: 5bp DNA ladder, Lane 2: DNA-N_3 control. B) ssDNA-peptide conjugate. Lane 1: 5bp DNA ladder, Lane 2: ssDNA, Lane 3: DNA-cRGDfK, Lane 4: DNA-cRADfK

$(M+H)^+$, 446.0 $(M+H)^{2+}$, calc. 891.07 $(M+H)^+$. DBCO-cRADfK : obtained. 905.52$(M+H)^+$, 453.51 $(M+H)^{2+}$, 905.11 $(M+H)^+$.)

Next, the copper-free click chemistry reaction was performed by adding the azide-labelled DNA with the modified DBCO-peptide for 12 hours at 37°C to promote successful reaction. The ratio of each component for the complete conjugation of DNA-peptide molecule was analysed by PAGE-gel (**Figure 3.3A**). With ratio of [ssDNA-N_3] vs [DBCO-peptide] at1:1 to 1:15, the reaction was still not completed as the DNA-N_3 molecule were still present in the solution. Upon addition of more DBCO-peptide to ratio 1:20, the ssDNA-N_3 completely reacted with the DBCO-peptide to form the ssDNA-peptide conjugate (**Figure 3.3B**). The mass of both DNA-cRGDfK and DNA-cRADfK conjugates were confirmed by MALDI-TOF (**Figure 3.2B**). (DBCO-cRGDfK : obtained. 5768.1 $(M+H)^+$, calc. 5767.80 $(M+H)^+$; DBCO-cRADfK: obtained. 5782.1 $(M+H)^+$, calc. 5781.8 $(M+H)^+$.

3.2.3 DNA Hydrogel Framework

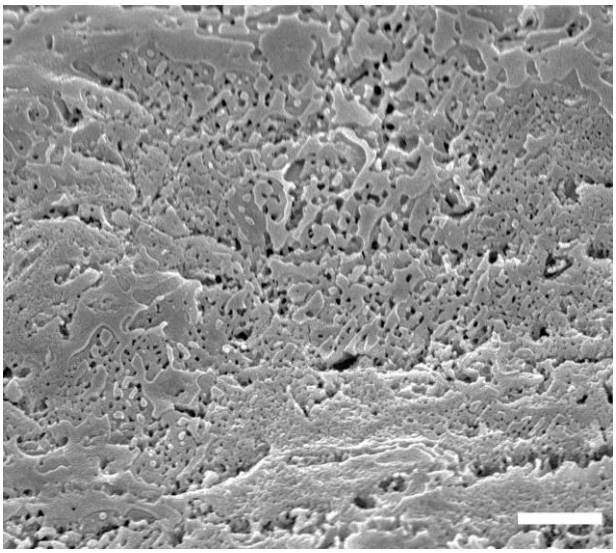

Figure 3.4. SEM image of DNA hydrogel. Scale bar: 1μm

After the self-assembly of dendritic DNA **D-R** and linker **L-R**, the framework structure of the DNA hydrogel was further characterized by scanning electron microscope (SEM) (**Figure 3.4**). The hydrogel framework appeared to be sheet-like with high mesh density and small pore size less than 1μm. The very dense structure is due to the rigid DNA composition in **D-R** gelation branches and the higher DNA concentration used in this work ([**D-R**] = 0.5mM, [**L-R**] = 1.5mM) as compared to the previous DNA hydrogel **DDH** used in **Chapter 2** ([**D**] = 0.2mM, [**L**] = 0.6mM). The uniform and dense inner structure could provide substantial mechanical support and anchor for cell adherence on the hydrogel framework.

3.2.4 Cell Adhesion in the Integrin-targeting DNA Hydrogel

The application of the integrin-targeting DNA hydrogel to provide cell attachment and control spreading was demonstrated by encapsulating human dermal fibroblast (HDF) cells in 2D cell culture, negative control **D-RAD** hydrogel, and integrin-targeting **D-RGD** hydrogel

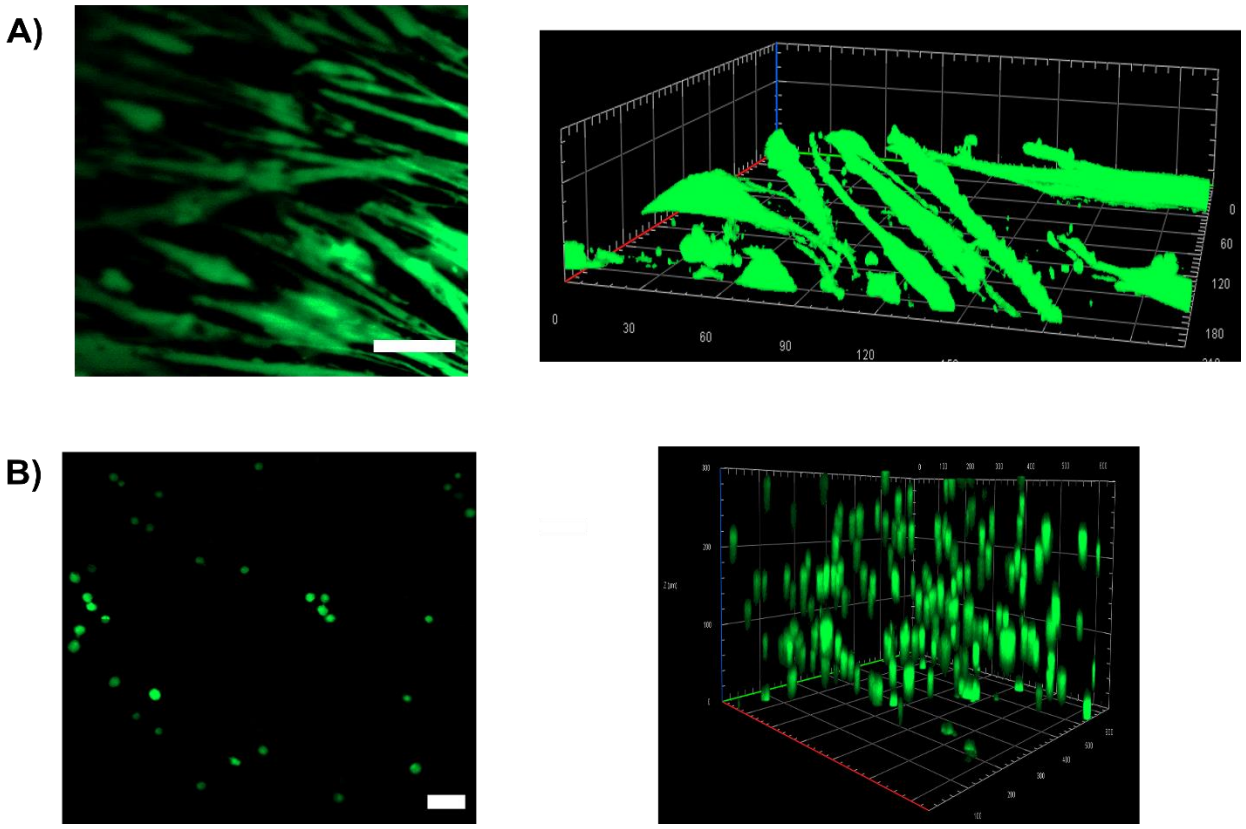

Figure 3.5. Confocal fluorescence image (left) and 3D construct (right) of HDF cells after 8 days cultured in A) 2D monolayer cell culture and B) negative control **D-RAD** hydrogel ([**D-cRADfK**] = 0.5mM, [**L-R** = 1.5mM]). HDF cells were stained with Calcein-AM (green-live) and PI (red-dead). Scale bar : 50µm.

over 8 days (**Figure 3.5 - 3.6**). The HDF cells cultured in these three different platforms showed distinct cell morphology. In 2D cell culture, the fibroblast cell adhered to the bottom of the culture flask flat surface appeared to be very stretched and flat, as normally seen in the fibroblast cultured in the monolayer 2D cell culture (**Figure 3.5A**). The range of elongated fibroblast cultured in 2D monolayer is at 50-90µm. In addition, the cell cultured in 2D monolayer did not occupy over 30µm height, as shown on the 3D construct image.

Meanwhile, the cells cultured in the negative control **D-RAD** hydrogel appeared to be spherical, confirming that the hydrogel did not provide cell attachment site for the HDF cells. In addition, the 3D construct image showed that the HDF cells were encapsulated throughout the hydrogel framework and occupied more than 300µm height. (**Figure 3.5B**).

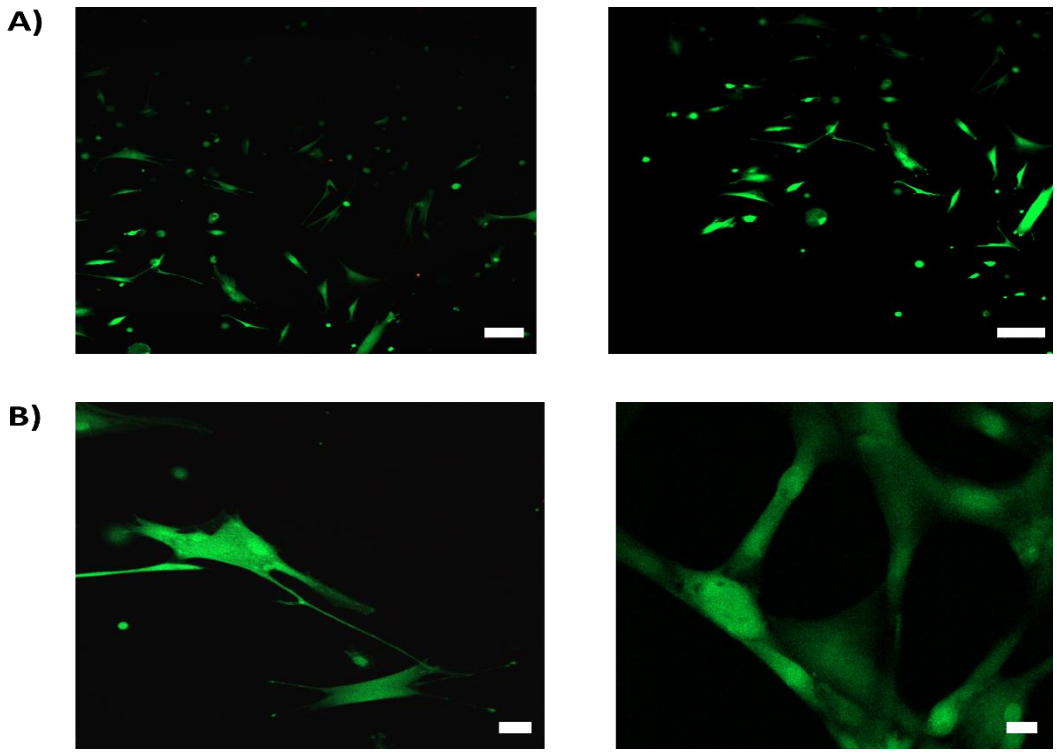

Figure 3.6. Confocal fluorescence image of HDF cells cultured in the integrin-targeting **D-RGD** hydrogel after 8 days. A) wide view, scale bar:100µm and B) closer view, scale bar: 20µm. ([**D-cRGDfK**] = 0.5mM, [**L-R** = 1.5mM]). HDF cells were stained with Calcein-AM (green-live) and PI (red-dead).

In **Figure 3.6**, most of the HDF cells cultured in **D-RGD** hydrogel appeared to be stretched and spread, proving that the RGD-functionalized DNA hydrogel provided cell attachment site on the framework by casting dendritic DNA **D-R** loading branch with integrin-targeting ligand (**Figure 3.6A**). However, few of the HDF cells still appeared in spherical shape and the interconnecting network of HDF cells as usually seen in the 3D cell culture environment was not observed in the **D-RGD** hydrogel. There was only a few of HDF cell that interconnected with each other. (**Figure 3.6B**). The inner structure of the lyophilized **D-RGD** hydrogel consists of dense mesh networks and small pore size below 1µm. The small pore size would exclude the fibroblast cells to be encapsulated in the DNA hydrogel 3D framework. In addition, the pore size would become smaller when the hydrogel was in swollen state, as compared to the large, flat, and elongated fibroblast (size 50-90µm), which may inhibit the cell-cell interaction to spread and form the interconnected cell network across the hydrogel.[15] Overall, these results demonstrated the feasibility of utilizing dendritic DNA **D-R** as a hydrogel

framework to form hydrogel with independent tunable biophysical and biochemical properties, which is an important feature to modulate and control the cell function in 3D cell culture microenvironment, yet still remains a challenge with the ECM-derived or the natural polymer hydrogel scaffold.

3.3 Conclusion

As a proof-of-concept, we designed and developed a DNA-based hydrogel system which offered simultaneous multifunction of bio-cue loading and hydrogel network formation by independently programmed the DNA sequence in the dendritic DNA building block. Temperature-sensitive peptide with integrin-targeting property was successfully conjugated into the complementary ssDNA of the loading branch by simple copper-free click chemistry reaction. Furthermore, the subsequent supramolecular self-assembly of the DNA hydrogel was fast and robust, allowing the cell encapsulation and casting of the temperature-sensitive peptide into the hydrogel framework without compromising the viability of the cells. Based on the preliminary results, the embedded fibroblast cell was suspended three-dimensionally and appeared to be stretched and spread as compared to the spherical shape of the cells in the negative control, hence confirming that the integrin-targeting hydrogel provided cell attachment site on the hydrogel framework. These promising results signified the feasibility utilizing the dendritic DNA hydrogel to design a versatile 3D cell culture tool. By carefully taking into consideration the different needs of 3D cell culture study, the dendritic DNA system can be programmed to exhibit tunable mechanical property and biochemical property based on-demand.

3.4 Future Work

More investigations are still required to further develop the integrin-targeting functionalized dendritic DNA hydrogel design as the on-demand 3D cell culture platform to control the cell attachment and spreading of fibroblast cells. The future studies will focus mainly on these aspects:

1) Designing the dendritic DNA sequence that would offer suitable hydrogel inner structure and substantial mechanical strength to support 3D cell culture for fibroblast cells.
2) Enhancement of the cell attachment throughout the DNA hydrogel framework. Some strategies can be further employed such as:
    a) Systematic study to find the optimum concentration of targeting peptide to be conjugated with the dendritic DNA
    b) Increasing the spacer length between the cyclic peptide and DBCO moiety. Increased spacer length would provide more accessibility for the ligand association between the integrin-targeting peptide and the cell surface despite the tightly crosslinked hydrogel network.

3.5 Experimental details

Materials

Product	Manufacturer
Phosphoramidites and reagents for solid-phase DNA synthesis	Glen Research (Virginia, USA)
Mermade columns (1μmol, 2000Å)	Bioautomation (Texas, USA)
Single strand oligonucleotide	Sangon Biotech (Shanghai, China)
Cyclic Peptide	Peptide International (US)
Acrylamide	Invitrogen (Carlsbad, CA, USA)
N,N-methylenebisacrylamide	Sigma-Aldrich (Singapore)
TEMED	Bio-Rad Laboratories (Singapore)
5bp and 10bp DNA ladder	Thermo Fisher (Singapore)
Ethidium bromide solution, 10mg/ml	Bio-Rad Laboratories (Singapore)
6x DNA loading dye	Thermo Fisher (Singapore)
10X Tris-borate-EDTA (TBE) buffer	Vivantis (Malaysia)
10X Tris-acetate-EDTA (TAE) buffer	Vivantis (Malaysia)

Unless otherwise stated, all reagents and solvents were purchased from Sigma-Aldrich (Singapore) with analytical grade or molecular biology grade. Ultrapure deionized (DI) water used in all experiments was obtained from a Millipore Milli-Q system (resistivity 18.2 MΩ.cm).

Methods

- **Solid Phase Dendritic DNA Synthesis**

Synthesis of the dendritic DNA was performed on Bioautomation Mermade 4. Fast deprotecting phosphoramidite and the long-trebler phosphoramidite (10-1925-90) was used to synthesize the dendritic DNA. The DNA cleavage from the solid support was done in 33%

ammonium hydroxide solution at 25ºC for 90 minutes followed by deprotection at 60ºC for an hour. The DMT-ON DNA products were purified by HPLC (Shimadzu, Japan) equipped with reverse-phase (RP) column (Microsorb 100-5 C18 Dynamax 250x10 mm). The HPLC mobile phases were 0.1M TEAA buffer (pH 7) and ACN. The gradient method was used to collect the product. The concentration of the ACN was increased from 5% to 60% over 30 minutes at 3.5 mL/min flush speed. The DMT-ON dendritic DNA were flushed at 38-44% ACN. The collected product was freeze dried by lyopholizer. The DMT protecting group on the dendritic DNA was cleaved by 80% acetic acid (200 µL) for 15 minutes at room temperature. 1 mL cold ethanol was added to the solution followed by centrifugation at 13,500 xg for 10 minutes at 4ºC to precipitate the DNA. The solvent was removed by vacuum concentrator.

The detitylated DMT-OFF dendritic DNA was purified by HPLC with the same method. The dendritic DNA was flushed at 23-26% ACN. The collected product was then freeze dried. The lyophilized dendritic DNA powder was dissolved in 1XTAE, 12.5mM $MgCl_2$ buffer (pH 7) and stored as the stock solution. The quantification of the dendritic DNA was done by measuring the absorption at wavelength 260 nm with Nanodrop 2000c spectrophotometer (Thermo Scientific, US).

- **Matrix Assisted Laser Desorption/Ionization Time-of-Flight (MALDI-TOF)**

  Matrix preparation :

  - *Matrix for myoglobin (M0630, Sigma)*. 10mg of sinapinic acid (SA) was dissolved in 500µL 50% acetonitrile solution with 0.1% TFA. The saturated solution was centrifuged to get the supernatant and stored in small aliquots (20 µL each).

- *Matrix for DNA*. There are two matrix components; 3-HPA and ammonium citrate. **A** : 10mg 3-HPA in 200 µL 50% acetonitrile. **B** : 10mg ammonium citrate in 200 µL water. **A** was mixed with **B** at volume ratio 8 to 1.

The sample was diluted to 100pmole/µL and mixed with the matrix at sample to matrix volume ratio 1:1. 1µL of the sample mix was deposited on the spot of the MALDI plate and left to air-dried before being analysed. The instrument (JMS-S3000, JEOL) was first calibrated with myoglobin MW = 16,951.49. Linear positive mode and 55% laser intensity was used to get the mass spectrum.

- **Polyacrylamide Gel electrophoresis**

15 % non-denaturing polyacrylamide gel was prepared with 142.5 g acrylamide, 7.5 g N,N'-methylenebisacrylamide and DI water forming 1 L solution. By adding 4 µl 6 × DNA loading dye to 20 µl samples (mass DNA= 300ng), the mixtures were rapidly loaded on a 15 % nondenaturing polyacrylamide gel. Gel electrophoresis were conducted at 300 V in 1 × TBE buffer solution for 4 h. Then polyacrylamide gels were stained in 1 × TBE buffer of ethidium bromide for 30 min. Data was analyzed by using G:BOX iChemi gel documentation system (Syngene).

- **DBCO-modified Cyclic Peptide**

DBCO-NHS ester (Sigma, 761524), cyclic peptide, and EDC were mixed in 1 equivalent each in DMSO for 2 hours under room temperature. The sample was then purified by HPLC and the mass was confirmed by ESI-MS.

- **ssDNA-peptide Conjugation**

ssDNA-azide was mixed with the DBCO-cyclic peptide (1:20 equiv) in PBS solution for 12h at 37°C. The sample was then purified with Amicon® Ultra-4 3K (Merck, Singapore) to remove unreacted peptide and concentrated the ssDNA-peptide conjugate.

- **DNA Hydrogel Assembly**

ssDNA-peptide conjugate was mixed with dendritic DNA **D-R** at 1:1 equivalent in the 1XTAE, 12.5 mM $MgCl_2$ buffer (pH 7) and left overnight at room temperature. The sample was then purified with Amicon® Ultra-4 10K (Merck, Singapore) to remove unbounded DNA. The **D-cRGDfK** quantification was determined by UV absorbance from wavelength 200nm to 300nm. The **D-cRGDfK** was mixed with **L-R** in the buffer solution ([**D-cRGDfK**] = 0.5mM, [**L-R**] = 1.5mM with gentle pipetting.

- **Scanning Electron Microscope (SEM)**

5µL of the DNA hydrogel was dropped on the silica wafer and freeze-dried overnight. Prior to SEM observation, the samples were coated with Pt at 20mA for 60s to get 12nm Pt height. The field emission SEM images were acquired using JEOL-JSM 6700F.

- **Cell Line and Culture Condition**

The cell line used in all experiments HDF human dermal fibroblast. The cell media was DMEM supplemented with 10% FBS and 1% penicillin. All cells were incubated in a humidified atmosphere of CO_2/air (5%/95%) at 37℃. Cells were incubated for 8 days.

- **Fluorescence Imaging**

2D Cell Culture. $5x10^4$ cells were seeded in µ-dish 35mm, high (ibidi, German)

3D Cell Culture. 5000 cells in the cell media was mixed with the **D-cRGDfK** or **D-cRADfK** and **L-R** to form 20µL DNA hydrogel. The solution was gently pipetted to ensure homogenous cell distribution in the hydrogel. The hydrogel was drop-casted in the middle of the µ-dish 35mm, high. After 3 hours, 50 µL cell media was topped up on top of the hydrogel to ensure enough nutrients for the cells throughout the experiment. The cells in the hydrogel was incubated for 8 days and cell media was changed every two days.

Live/Dead Cell Staining Kit (04511, Sigma) was used to determine the viability of the cell. The kit contains Calcein-AM which stains viable cells to generate green fluorescence (excitation:490 nm, emission 515nm) and Propidium Iodide (PI, excitation :535nm, emission:617nm) which stains dead cells to emit red fluorescence.

10 µL of solution A (Calcein-AM) and 5µL of solution B (PI) was added to 5mL PBS to prepare the assay solution. The cell media of the sample was firstly removed. Then, the sample was gently washed with PBS to remove residual esterase activity followed by staining with 100µL assay solution and incubation for 30 minutes at 37℃. All images were collected by the confocal microscope (Carl Zeiss LSM 800) using the 63x oil immersion and 20x objective lense. 488nm excitation was used as both Calcein-AM and PI can be excited using this excitation wavelength. The 3D constructs were acquired with z-step size of 2µm (20x lens) or 0.5µm (63x lens).

3.6 References

1. Pallarola, D.; Bochen, A.; Boehm, H.; Rechenmacher, F.; Sobahi, T. R.; Spatz, J. P.; Kessler, H., *Adv Funct Mater* **2014,** *24* (7), 943-956.

2. Dou, X.; Nomoto, T.; Takemoto, H.; Matsui, M.; Tomoda, K.; Nishiyama, N., *Scientific Reports* **2018,** *8* (1), 8126.

3. Kämmerer, P. W.; Heller, M.; Brieger, J.; Klein, M. O.; Al-Nawas, B.; Gabriel, M., *Eur Cell Mater* **2011,** *21*, 364-72.

4. Patel, P. R.; Kiser, R. C.; Lu, Y. Y.; Fong, E.; Ho, W. C.; Tirrell, D. A.; Grubbs, R. H., *Biomacromolecules* **2012,** *13* (8), 2546-2553.

5. Pereira, R. F.; Barrias, C. C.; Bártolo, P. J.; Granja, P. L., *Acta Biomaterialia* **2018,** *66*, 282-293.

6. Li, B.; Chen, J.; Wang, J. H., *J Biomed Mater Res A* **2006,** *79* (4), 989-98.

7. Kilian, K. A.; Mrksich, M., *Angewandte Chemie International Edition* **2012,** *51* (20), 4891-4895.

8. Kang, S.-W.; Cha, B.-H.; Park, H.; Park, K.-S.; Lee, K. Y.; Lee, S.-H., *Macromolecular Bioscience* **2011,** *11* (5), 673-679.

9. McBeath, R.; Pirone, D. M.; Nelson, C. M.; Bhadriraju, K.; Chen, C. S., *Dev Cell* **2004,** *6* (4), 483-95.

10. Ichim, T. E.; O'Heeron, P.; Kesari, S., *Journal of Translational Medicine* **2018,** *16* (1), 212.

11. Gačanin, J.; Synatschke, C. V.; Weil, T., *Advanced Functional Materials* **2020,** *30* (4), 1906253.

12. Morya, V.; Walia, S.; Mandal, B. B.; Ghoroi, C.; Bhatia, D., *ACS Biomaterials Science & Engineering* **2020,** *6* (11), 6021-6035.

13. Shao, Y.; Jia, H.; Cao, T.; Liu, D., *Accounts of Chemical Research* **2017,** *50* (4), 659-668.

14. Baskin, J. M.; Prescher, J. A.; Laughlin, S. T.; Agard, N. J.; Chang, P. V.; Miller, I. A.; Lo, A.; Codelli, J. A.; Bertozzi, C. R., *Proceedings of the National Academy of Sciences* **2007,** *104* (43), 16793-16797.

15. Ginzberg, M. B.; Kafri, R.; Kirschner, M., *Science* **2015,** *348* (6236), 1245075.

CHAPTER 4

Self-assembly of Supramolecular Double Network DNA Hydrogel with Enhanced Mechanical Property

Adapted from manuscript prepared by Bella Rosa Liyarita and Xiao Hu.

4.1. Introduction

Nucleic acid materials have gained significant attention over the past decades due to the inherent biocompatibility and the unique sequence programmability of the DNA building block to exhibit on-demand properties. The development of the DNA building block to assemble a programmable DNA nanostructure have been widely explored and recently more efforts are done to study the DNA as a material for the assembly of a larger scale polymeric biomaterial, particularly to form functional DNA hydrogels with a wide range of potential application in drug delivery[1], 3D cell culture platform[2], biosensor[3], and cancer therapy[4]. By exploiting the unique biochemical property of specific interaction via the base pair hybridization, DNA hydrogels have been designed to incorporate specific stimuli such as temperature, pH, and competitive DNA strand replacement.[4-6] Careful consideration and precise design of the DNA sequence allows real-time modulation of the mechanical, structural, and biochemical function of the DNA hydrogels, which gives a big advantage over other types of biopolymer hydrogel which is mostly static by nature.[7-8]

However, despite the unique properties the DNA hydrogels presented, the application of pure DNA hydrogel as the platform for 3D cell culture to stimulate cells environment *in vivo* is still hindered with the low mechanical property of DNA hydrogels as compared to other existing polymer hydrogel.[9-10] For example, in the study of cancer cell culture, spheroid model gives more deeper understanding of the cells interaction and behaviour. It remains a challenge to develop a DNA-based hydrogel platform that can provide optimal inner structure and substantial mechanical strength to facilitate the spheroid formation and proliferation. Most DNA hydrogels exhibit low mechanical property in the range of hundreds Pa and would require a very high DNA concentration up to 9% w/v to form a DNA hydrogel in the range of few

thousands Pa.[6, 11] There are some factors to consider when designing DNA hydrogel with controlled mechanical property such as the thermal stability of the hybridized duplex DNA, structural rigidity and flexibility, and focal crosslinking points of the DNA chain. However, the total DNA content in the hydrogel should be optimized to avoid the high production cost of the large scale DNA synthesis.[12] Therefore, a new approach to form DNA hydrogel with tunable and high mechanical property is needed for 3D cell culture application.

One approach to enhance the DNA mechanical property is by incorporating the double network hydrogel strategy where two existing networks in the hydrogel system exhibits contrasting physical properties, one is rigid network while the second network is flexible, soft and ductile.[13-14] However, most study on the double network hydrogels property are on the covalent or hybrid crosslinked networks and the supramolecular double-network study has not yet been done on pure DNA hydrogels.[15-19] Therefore, it is of a great interest to incorporate this strategy on the dendritic DNA hydrogel system by systematically design the dendritic DNA framework to exhibit rigid and flexible mechanical property as the two networks for the double-network DNA hydrogel self-assembly.

4.2. Result and Discussion

Table 4.1. DNA sequence for the single-network DNA hydrogel assembly

Code	Sequence (5'-3')
D1	$(TTAATAATATAAAAT)_3$ D TTT CGA TCG
D2	$(CGA\ TTA\ CAG\ CTT\ GCT)_3$ D TTT CGA TCG
D3	$(GAG\ GTG\ GAC\ CGA\ GGA)_3$ D TTT CGA TCG
D4	$(CCG\ GCC\ GGG\ CGC\ GCC)_3$ D TTT CGA TCG
D5	$(CCA\ GCT\ GCC\ A)_3$ D TTT CGA TCG
D6	$(GCC\ ATC\ CGT\ CGA\ GCC\ TGC\ AG)_3$ D TTT CGA TCG
D7	$(GTC\ CAC\ GTC\ CTG\ CTC\ GCC\ GTC\ GTC\ CCG\ ATC\ ACG\ CCA\ CTG\ G)_3$ D TTT CGA TCG
L1	ATT TTA TAT TAT TAA ATA CGC GCG TAT
L2	AGC AAG CTG TAA TCG ATA CGC GCG TAT
L3	TCC TCG GTC CAC CTC ATA CGC GCG TAT
L4	GGC GCG CCC GGC CGG ATA CGC GCG TAT
L5	TGG CAG CTG G ATA CGC GCG TAT
L6	CTG CAG GCT CGA CGG ATG GCA ATG CGC GCA TT
L7	CCA GTG GCG TGA TCG GGA CGA CGG CGA GCA GGA CGT GGA C ATA CGC GCG TAT

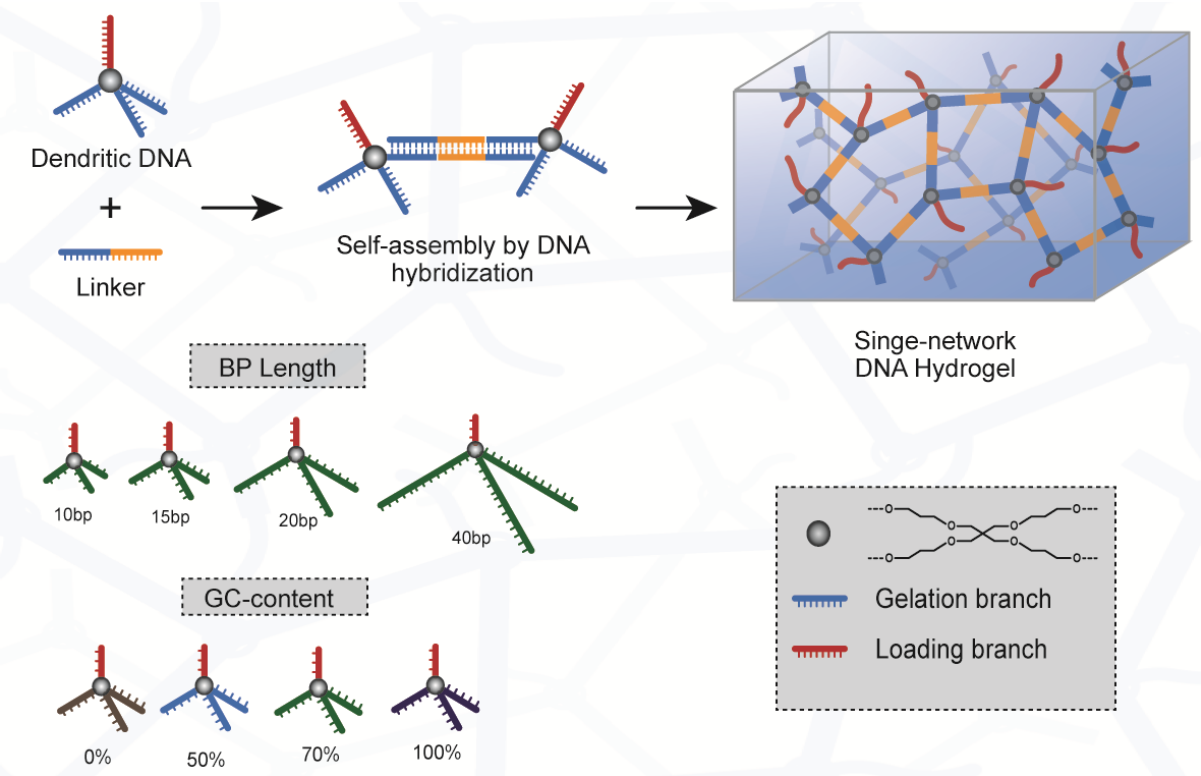

Scheme 4.1. Self-assembly of single-network dendritic DNA hydrogel. Base pair length and the GC-content on **D** gelation branch is varied.

We first optimized the design of each single network dendritic DNA (**D**) to determine the two hydrogel network which exhibits flexible and rigid mechanical property, respectively. The mechanical property of the hydrogel network, the elasticity and modulus, are determined by the flexibility and length of the polymer chains between the two crosslinking points. For the supramolecular DNA hydrogel formed by the DNA self-assembly, the length between the two adjacent crosslinking points can be easily programmed by changing the DNA base pair (bp) length of the DNA chain. Furthermore, the rigidity and flexibility of the DNA chains can also be controlled by varying the guanine-cytosine (GC) content on the DNA sequence. DNA chain with GC-rich sequence is more rigid and less flexible than the one with the AT-rich chain. [20]

The dendritic DNA molecule **D** consists of four single-stranded DNA arms connected to the focal core. **D** simultaneously serves as the crosslinking network via hybridization with

the three gelation branches, and the loading of exogeneous entity via the loading branch. To assemble the single network hydrogel, the single-strand DNA linker (**L**) is used to crosslink each **D** molecule to form the hydrogel network over three-dimension space (**Scheme 4.1**). The linker consists of two parts 1) DNA sequence complementary to the **D** gelation branches for the network crosslinking, 2) palindromic site consists of 12nt t associate with another **L** molecule. Here, we design the dendritic DNA building block with the gelation branches of varied bp length and GC-content. The bp length of the gelation branches is varied from 10-40bp, whereas the GC-content is from 0-100%. Meanwhile, the DNA sequence of palindromic site in **L** is kept the same (**Table 4.1**). Once **D** and **L** is mixed at ratio 1:3, all the available gelation branches will hybridize with **L** and crosslink with another **D** molecule to self-assemble into DNA hydrogel with optimal mechanical property, as discussed in ***Chapter 2***.

4.2.2. UV Melting Temperature of The Single Network DNA Hydrogels

Table 4.2. Melting temperature of the single-network DNA hydrogel based on the base pair length and content of GC base in the gelation branches.

Code	BP Length	%GC	Tm (°C)
D1	**15**	**0**	**43.9**
D2/D-A	**15**	**50**	**54.5**
D3	**15**	**70**	**62.7**
D4	**15**	**100**	**-**
D5	**10**	**70**	**60.1**
D6/D-B	**20**	**70**	**70.2**
D7	**40**	**70**	**73.1**

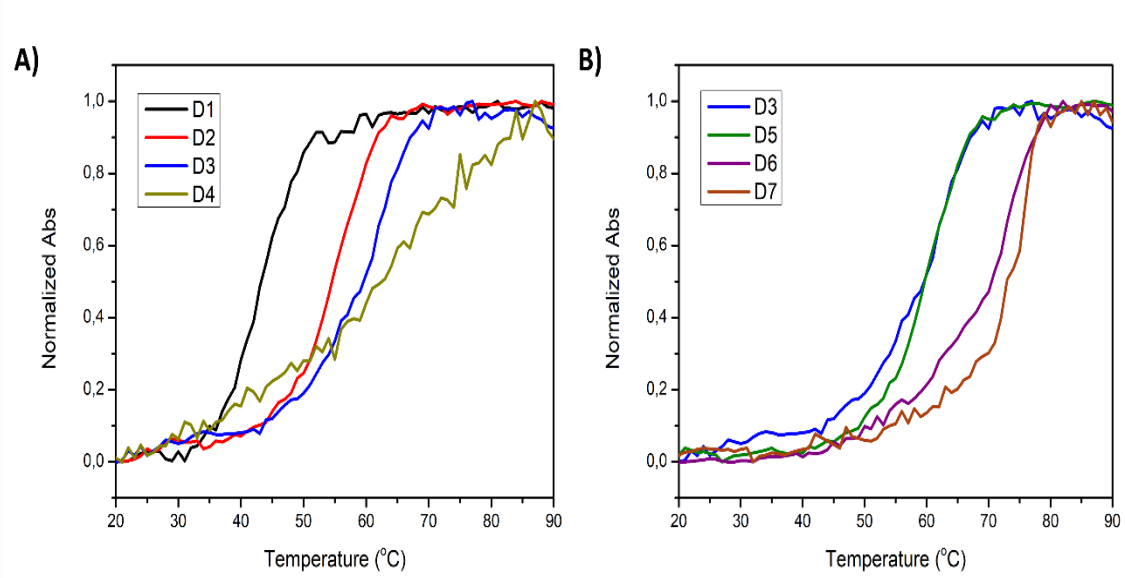

Figure 4.1. UV melting curve of the DNA hydrogels formed by D1 to D7. A) varied GC-content on **D** gelation branches from 0% to 100% (**D1-D4**). B) varied base pair length on **D** gelation branches from 10bp to 20bp (**D3, D5-D7**). [**D**] = 0.5μM, [**L**] = 1.5μM. Ramp rate = 1°C/min

The melting temperature of each DNA hydrogels was determined by UV spectroscopy (**Figure 4.1**). Figure **4.1A** compares the thermal stability of the DNA hydrogels by varying the GC-content on the **D** gelation branch from 0% to 100% (**Table 4.2**). As the percentage of GC-content increase from 0% to 70% (**D1 – D3**), the melting temperature of the hydrogel shifts to higher temperature from 43.9°C to 62.7°C due to stronger base pairing interaction formed by the three hydrogen bonds in the G-C base pairing, as compared to the two hydrogen bonds interaction in the A-T base pairing. In addition, the base stacking within the nucleobases also strengthens the interaction of the G-C base pairs.[21-22]

However, the melting temperature curve of **D** with 100% GC-content (**D4**) shows linear increase in the absorbance instead of the sigmoidal increase typical to the duplex DNA UV melting temperature curve. This suggests that the duplex formation of dendritic DNA **D4** and linker **L4** is not fully successful and does not subsequently form the optimal network crosslinking. GC-rich regions on the DNA strands are more likely to mis-pair with other GC-

rich region on the complementary strand. In addition, using the palindromic sequence on the linker increase the tendency of the GC-rich linker strand to form hairpin by self-dimerization, hence preventing the optimum crosslinking between the complementary DNA strands. **Figure S4.1** shows the hairpin formation and its corresponding melting temperature of **L4**. The lowest and highest hairpin melting temperature is at 45.1°C and 64.3°C, respectively. This hairpin formation of **L4** and its corresponding high melting temperature blocks the base pair hybridization of **D4** and **L4** to form the DNA duplex and hydrogel network crosslinking.

Figure 4.1B shows the comparison of thermal stability of DNA hydrogel with varied length of the dendritic DNA gelation branches from 10bp to 40bp (**D3**, **D5**-**D7**) while GC-content is kept at 70%. Increasing the bp length from 10bp to 20bp raises the melting temperature of the hydrogel by 13°C. However, increasing the bp length from 20bp to 40bp only raised the melting temperature by 3°C, showing that increasing the bp length on the DNA strand to more than 20bp does not significantly increase the thermal stability of the DNA hydrogel.

4.2.3. Mechanical Strength of The Single Network DNA Hydrogels

The mechanical strength of bulk single network DNA hydrogels is characterized by rheometer. The concentration of dendritic DNA and linker for all hydrogels are kept the same at [**D**] = 100 µM and [**L**] = 300µM. **Fig 4.2** compares the mechanical strength of the single network hydrogels assembled by **D1** to **D7**. In all DNA hydrogels, the G' is higher than G" value, indicating that **D1** – **D7** are indeed in gel form. Adjusting the GC-content on the **D** gelation branches from 0% to 70% (**D1**-**D4**) increase the mechanical strength by 2-fold due to the increased in DNA structural rigidity provided by the higher GC-content in the DNA hydrogel network (**Fig 4.2A**). Similar to UV melting temperature result, **D4** hydrogel shows G'

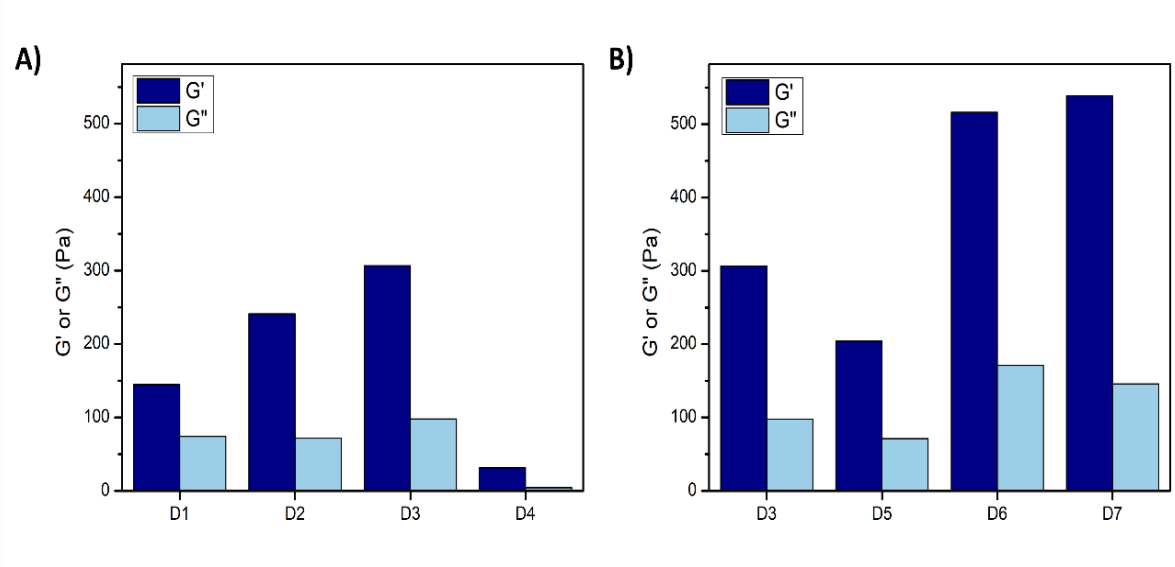

Figure 4.2. Comparison of the mechanical strength of the single-network hydrogels. G'= storage modulus, G" = loss modulus. A) varied GC-content on **D** gelation branches from 0% to 100% (**D1-D4**). B) varied base pair length on **D** gelation branches from 10bp to 20bp (**D3, D5-D7**. The total concentration of hydrogel components are maintained at [**D**] = 100µM, [**L**] = 300µM in each hydrogels. Rheological test condition at 25°C, 1Hz, 1% strain.

= 31,5 Pa and G" = 4,1 Pa, indicating **D4** forms hydrogel with very low mechanical strength (4,7-fold lower than **D1**). Due to the high melting temperature of the **L4** hairpin formation, most of **L4** molecules are in single strand DNA or hairpin form and thus subsequently disrupting the self-assembly of the hydrogel network.

Fig 4.2B shows the comparison of mechanical strength of the single network DNA hydrogels formed by varying the bp length of the DNA gelation strands from 10bp to 40bp while maintaining the GC-content at 70% (**D3, D5-D7**). The G' value of the DNA hydrogel increases by 2,6-fold with varying bp length from 10bp to 40bp. Meanwhile, increasing the bp length from 20bp to 40bp does not significantly increase the mechanical strength of the hydrogels (**D6**, **D7**). The longer DNA chain between the two adjacent crosslinking points may result in more flexibility of the DNA crosslinking network. In addition, the high GC-content in the long DNA chain **L7** may cause the DNA base pairs to be much more prone to mismatch with another GC-rich region of the other **L7** molecule.

4.2.4. Design of Double Network DNA Hydrogel

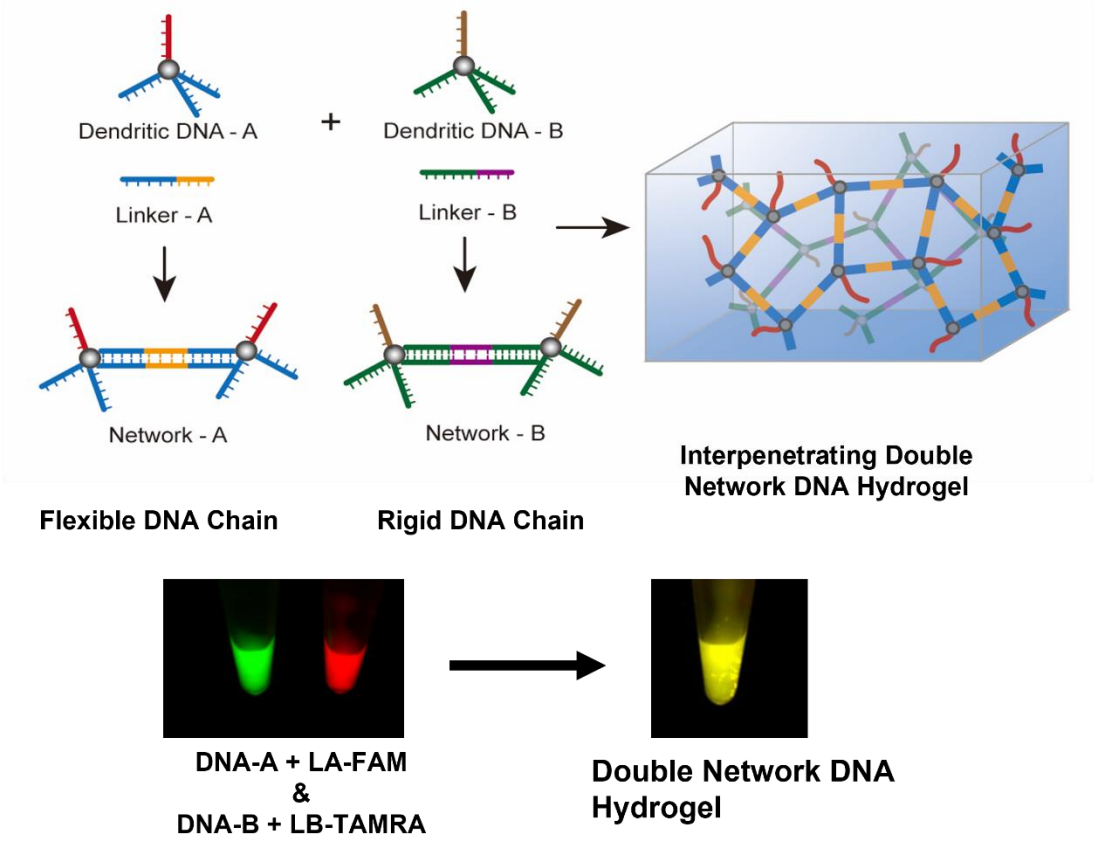

Scheme 4.2. Top: self-assembly of double network DNA (**DN**) hydrogel. DNA with the same color code is complementary to each other. Bottom: visualization of **FAM-DA** and **TAMRA-DB** single network hydrogels to assemble homogeneous double network **DN** hydrogel.

Code	Sequence (5'-3')
D-A	$(CGA\ TTA\ CAG\ CTT\ GCT)_3$ D TTT CGA TCG
D-B	$(GCC\ ATC\ CGT\ CGA\ GCC\ TGC\ AG)_3$ D TTT CGA TCG
L-DA	AGC AAG CTG TAA TCG ACA ACG TTG T
LA-FAM	FAM - AGC AAG CTG TAA TCG ACA ACG TTG T
L-DB	CTG CAG GCT CGA CGG ATG GCA ATG CGC GCA TT
LB-TAMRA	TAMRA - CTG CAG GCT CGA CGG ATG GCA ATG CGC GCA TT
L-DB2	CTG CAG GCT CGA CGG ATG GCA AT CCC | GGG ATT

Table 4.2. DNA sequence used for the formation of the double network DNA hydrogel

In double network hydrogel, there are two existing networks in the hydrogel which have contrasting mechanical property, one is more flexible while the other is more rigid. To assemble the double network DNA hydrogel (**DNH**), dendritic DNA **D2/D-A** (15bp, 50% GC), **D6/D-B** (20bp, 70%), and their respective linker **L2/L-DB** and **L6/L-D6** are chosen as the components for the double network formation. **D-A** and **D-B** serves as the flexible and rigid chain respectively for the following reasons:

1) **D-A** have a balanced GC-content on its gelation branches (50% GC) to provide thermal stability of the hydrogel first network for further application in 3D cell culture. The cells incubation occurs at 37°C over a few days, hence each single network hydrogels should have a good thermal stability at least 10°C above the incubator temperature to prevent early degradation of the hydrogel.
2) **D-B** dendritic DNA with 70% GC-content provides structural rigidity to the second network. In addition, with 20bp length on the DNA chain, the second network length would still match the length of the first network (15bp) to optimize the self-assembly of **DNH**.
3) **D-B** hydrogel (**D-BH**) provides similar mechanical strength compared to the hydrogel assembled by **D7** (40bp, 70% GC). With lower bp length, **D-B** would benefit from better overall yield and purity as compared to **D7**. The DNA synthesis overall yield depends on the length of the DNA chain. The coupling efficiency of the solid phase oligonucleotide synthesis would decrease with higher bp length. The cumulative effect of a series of poor coupling would give result to a synthesized dendritic DNA with poor overall yield and difficult to purify.

As shown in **Scheme 4.2**, the self-assembly of **DNH** formed by the gelation of the first network dendritic DNA **D-A** with its linker **L-DA** and the second network dendritic DNA **D-B** and its linker **L-DB.** The palindromic site on both linkers contains different DNA sequence to prevent cross talking between the first and second network. Hence, the design of the first hydrogel network **D-A** would exist independently without disrupting the formation of the second hydrogel network **D-B.** Notably, **D** architecture structure would allow dual function of loading and gelation simultaneously. The loading branch of **D-A** and **D-B** could be independently modified to exhibit two or more functionalization as programmed by the DNA sequence.

4.2.5. Self-assembly of Double Network Hydrogel

To investigate the effect of each single network crosslinking on the mechanical strength of **DNH**, we first optimized the ratio of the components in the first and second network. In all **DNH**, the ratio of [**D**] vs [**L**] is 1:3 and the total concentration of each component is kept constant at [**D**] = 100μM and [**L**] = 300μM.

Fig 4.3 shows the effect of varying the ratio of **D-A** and **D-B** crosslinking network on the mechanical strength of **DNH**. In the single network hydrogel, **D-AH** modulus is at G'=241 Pa, G"=71Pa and **D-BH** modulus at G'= 624 Pa, G"=183 Pa. All double network hydrogels showed enhanced mechanical strength as compared to the single network hydrogel **D-AH.** At ratio 3:2, the **DNH** shows higher mechanical strength than both single network hydrogels (3,5-fold higher than **D-AH** and 1,4-fold higher than **D-BH**). Interestingly, **DNH** with balanced

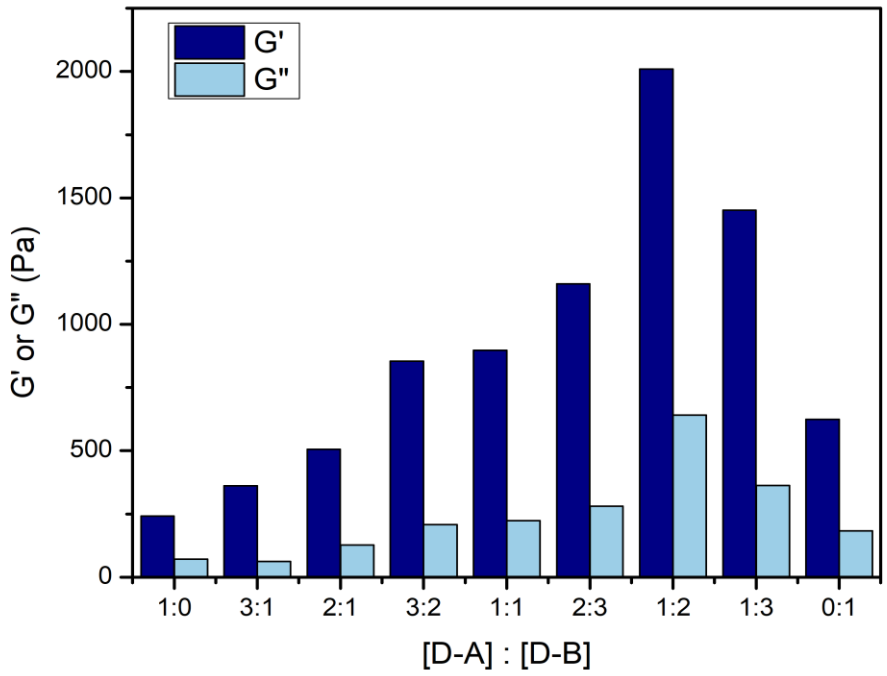

Figure 4.3. Comparison of the mechanical strength of the hydrogels. G'= storage modulus, G" = loss modulus on the double network DNA hydrogel formed by D-A and D-B at different ratio. The total concentration of hydrogel components are maintained at [**D**] = 100µM, [**L**] = 300µM in each hydrogels. Rheological test condition at 25°C, 1Hz, 1% strain.

ratio of **D-A** and **D-B** at 1:1 shows similar mechanical strength **DNH** with ratio 3:2, indicating that the second network **D-B** is more dominant. This further confirmed by the greater enhancement of the **DNH** mechanical strength with increased **D-B** components. However, **DNH** with ratio 1:3 shows lower mechanical strength despite the highest percentage of the stronger **D-B** components. The lower percentage of **D-A** components in the **DNH** ratio 1:3 may have caused the decrease in the efficiency of the interpenetrating network, hence resulting in less optimal mechanical strength. Notably, **DNH** with ratio of 1:2 show the highest mechanical strength among all double-network hydrogel at G' = 2010 Pa, G"= 641 Pa (8,4-fold higher than **D-AH** and 3,2-fold higher than **D-BH**). Therefore, **DNH** with ratio of [**D-A**] vs [**D-B**] at 1:2 was selected for further investigation as it exhibited the highest mechanical strength among all reported double network DNA hydrogels.

The enhanced mechanical strength of the interpenetrating network of flexible **D-AH** and rigid **D-BH** is due to the formation of the double networks and caused by the stress transfer between the two interpenetrating double network, instead of the stress being confined into the smaller crosslinking in the single-network hydrogel.[13-15, 18, 23] More extensive double networks and enhanced mechanical property in **DNH** are only formed when substantial amount of both **D-A** and **D-B** components are present. Therefore, the trend of enhanced mechanical property is due to the degree on interpenetration between the two single networks **D-AH** and **D-BH** in **DNH.**

4.2.6 Mechanical Property of Double Network DNA Hydrogel

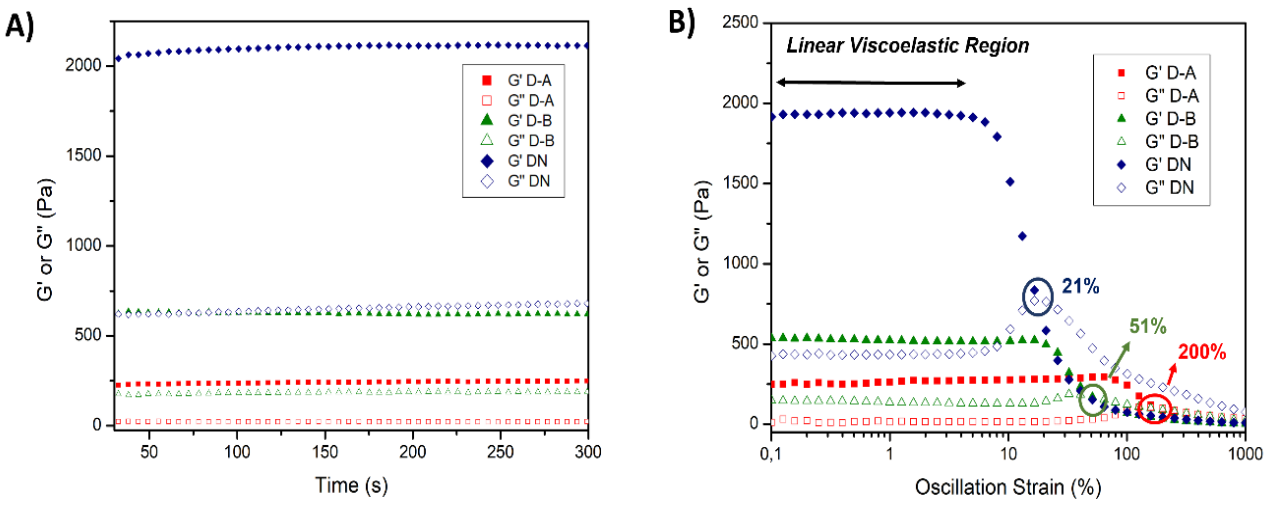

Figure 4.4 Rheological characterization of the single network D-A, D-B, and double network DN hydrogel. G' = storage modulus, G" = loss modulus. A) Time sweep from 0 to 300s, 1Hz, 1% strain. B) Amplitude sweep from 0.1 to 1000%, 1Hz. . Total [**D**] = 100μM, [**L**] = 300μM in each hydrogels. Ratio of [D-A] : [D-B] = 1:2 in DN hydrogel

To explore the mechanical properties of the double-network **DN** hydrogel, the rheological properties of the hydrogels were investigated in detail as shown in **Figure 4.5** Both single-network hydrogels **D-A**, **D-B**, and double-network hydrogel **DN** maintained stable gel state over 300s (**Figure 4.4A**). As discussed in **Section 4.2.5**, the **DN** hydrogel showed non-

linear enhancement in the mechanical stiffness as compared to the single-network **D-A** and **D-B** hydrogels (8.4-fold higher than **D-A** hydrogel and 3.2-fold higher than **D-B** hydrogel) due to the interpenetrating network of the flexible **D-A** and rigid **D-B** DNA chains. However, there is no increase in order of magnitude of the G' and G" modulus as reported in the pure chemically crosslinked doble-network hydrogels due to the weaker interactions of the supramolecular non-covalent crosslinking in DNA hydrogels where the physical crosslinks can be easily sheared as the two networks experience stress.[13]

The viscoelasticity of the DNA hydrogel was further studied by oscillation strain sweep from 0.1% to 1000% as shown in **Figure 4.4B**. The flexible **D-A** hydrogel showed broader range of linear viscoelasticity region up to 90% oscillation strain followed by the rapid decrease of G' value and reached the crossing point with G" at 200%, indicating the transitioned of gel to sol state. The more rigid **D-B** hydrogel exhibited shorter range of linear viscoelasticity region up to 16% and reached the critical strain at 51% upon the collapse of the gel state. Meanwhile, the double-network **DN** hydrogel showed the shortest linear viscoelastic region up to 6% and critical strain point at 21% despite the presence of the flexible **D-A** network in the hydrogel. The broader range of linear viscoelasticity region indicates that the hydrogel is more flexible and able to withstand network destruction at higher deformation as demonstrated by **D-A** hydrogel. On the other hand, lower critical strain point indicates that the hydrogel network is stiffer and breakdowns at a lower deformation. It is worth noting that the DNA hydrogels covered a broad range of viscoelasticity region, hence corroborate demonstrating that the mechanical property of the DNA hydrogels can be easily tuned by programming the DNA chain based on-demand.

4.2.7. Structure of DNA Hydrogels

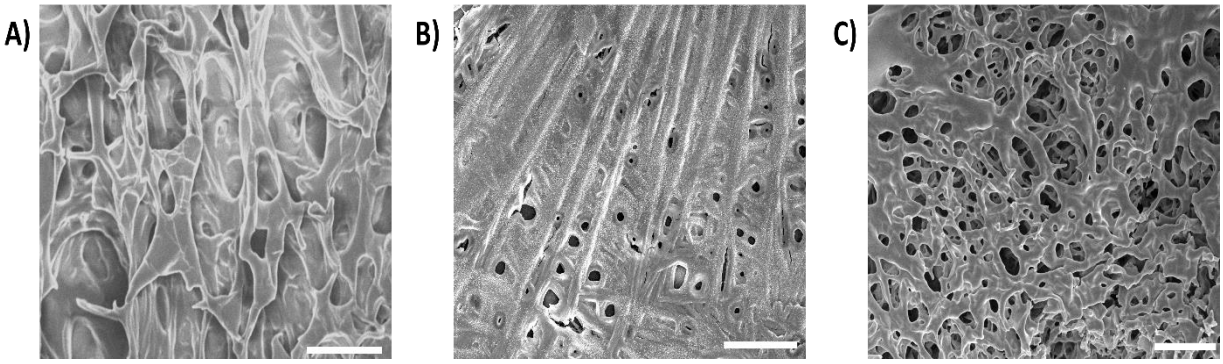

Figure 4.5. SEM images of lyophilized DNA hydrogels. A) **D-A** hydrogel, B) **D-B** hydrogel, C) **DN** hydrogel. . Ratio of [**D-A**] : [**D-B**] = 1:2 in **DN** hydrogel. Scale bar: 10μm.

Internal structure of the 3D framework in single network hydrogels **D-AH**, **D-BH**, and double network hydrogel **DNH** was further characterized by scanning electron microscope (SEM) as shown in **Figure 4.6.** The more flexible **D-A** hydrogel exists as larger porous network structure with long-range continuity. Meanwhile, the more rigid **D-B** hydrogel shows a much denser sheet-like structure and smaller pore size due to the difficulty adjusting the DNA chains. Comparing the two single-network hydrogels and the double-network hydrogel, **DN** hydrogel shows more ordered and uniformed structure with long-range interconnectivity of the 3D framework, leading to a better mechanical property of the hydrogel.

4.2.8. Dynamic Nature of Double Network DNA Hydrogel

The dynamic nature of the double network hydrogel was further investigated by assessing the thermal behaviour of the DNA hydrogels as shown in **Figure 4.6**. To determine the melting temperature (Tm) of the hydrogels, we recorded the DNA absorbance (λ=260nm) against the temperature by UV spectroscopy. To study the gel-sol transition temperature (Tgel), we recorded the value of G' and G" against the temperature change. Tgel is determined as the

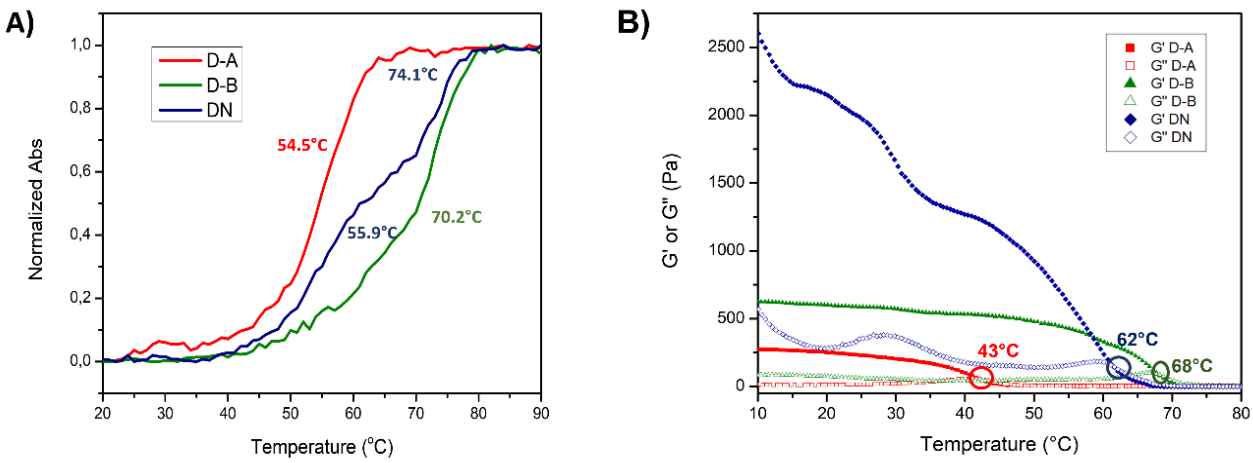

Figure 4.6. A) UV melting curve of **D-A**, **D-B**, and **DN** hydrogel. [**D**] = 500 nM, [**L**] = 1.5µM. B) Temperature ramp rheological analysis of the DNA hydrogels, from 10°C to 80°C, ramp rate 5°C/min, fixed frequency (1Hz) and strain (1%). G'= storage modulus, G" = loss modulus. Total [**D**] = 100µM, [**L**] = 300µM in each hydrogels. Ratio of [**D-A**] : [**D-B**] = 1:2 in **DN** hydrogel.

intersection point when the G' (storage modulus) is lower than G" (loss modulus), indicating that the DNA hydrogel is no longer a physical gel.

In UV melting temperature study, the temperature was first raised to 90°C for annealing and unfolding of the duplex DNA in the hydrogel into single-stranded DNA. As the temperature decrease, the single-stranded DNA hybridize with the complementary base pairs to form the duplex DNA and subsequently crosslink to form the hydrogel network. **Figure 4.6A** compares the thermal stability of the single-network hydrogels **D-A**, **D-B**, and double-network hydrogel **DN.** Both **D-A** and **D-B** hydrogels show single sigmoidal curve with Tm at 54.5°C and 70.2°C, respectively. This suggest that the single-network DNA hydrogels were formed by uniform crosslinking structure.

On the other hand, **DN** hydrogel shows double sigmoidal curve, indicating there are two melting temperature points at 74.1°C and 55.9°C. As the temperature cooled down from 90°C to 65°C, the second network **D-B** has overcome its melting temperature (Tm=70.2°C) to

form the duplex DNA whereas the first network **D-A** (Tm=54.5°C) is still in unfolded form. As the temperature further decrease to 40°C, the first network **D-A** starts to assemble to duplex DNA as it has overcome its melting temperature. At 25°C, both first and second network **D-A** and **D-B** are in duplex DNA structure and form the **DN** hydrogel.

To further corroborate the self-assembly of the **DN** hydrogel, a study of the gel-sol transition was performed by rheometer. The G' decreases with increasing temperature and further intersects with G" at the gel-sol transition point (Tgel) as shown in **Figure 4.6B**. All DNA hydrogels have single gel-sol transition point as the hydrogel network disassembled above 70°C. The transition temperature of the single-network hydrogels **D-A**, **D-B**, and double-network **DN** hydrogel were 43°C, 68°C, and 62°C respectively. Both single-network hydrogels **D-A** and **D-B** exhibited single sigmoid decrease against the temperature. Meanwhile, the **DN** hydrogel shows two points of sigmoidal decrease. At 35°C, some of the first network **D-A** disintegrated while most of the second network **D-B** remained intact. As the temperature increase, the second network **D-B** starts to disintegrate until it completely transitioned from gel to sol at 62°C. Furthermore, the transition point difference between **DN** hydrogel and single-network hydrogels **D-A** and **D-B** is 6°C and 19°C, respectively. The slight difference between **DN** hydrogel and **D-B** hydrogel indicating that the second network **D-B** is more dominant in the double-network hydrogel as discussed in section **4.2.5**, **4.2.6**. Notably, the mechanical strength of the **DN** hydrogel was always significantly higher than both single-network hydrogels until 57°C at which its mechanical strength became lower than **D-B** hydrogel, again demonstrating that the two interpenetrating networks in **DN** hydrogel strengthening the mechanical property of the DNA hydrogel.

4.2.9. Controllable Responsiveness of Double Network DNA Hydrogel

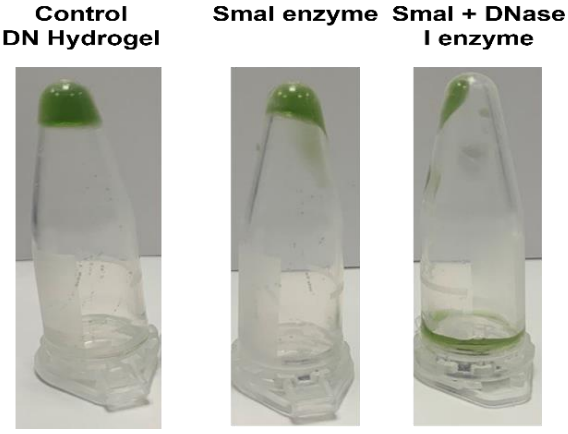

Figure 4.7. Enzyme degradation study of the double network hydrogels : SamI enzyme can digest DNA backbone at specific sequence CCC | GGG on the L-DB2 to cleave the D-B network. Dnase I enzyme can digest single-and double-stranded DNA to cleave both network. Total [**D**] = 50µM, [L] = 150µM with ratio of [**D-A**] : [**D-B**] = 1:2 in DN hydrogel

Enzyme degradation study was done to assess the controllable responsiveness of the double-network **DN** hydrogel. Benefiting from the wide selection of restriction enzyme tools that can cleave the DNA at specific sites, the **DN** hydrogel can be programmed to exhibit controlled responsiveness based on-demand. In this study, the linker **L-DB** palindromic site was sequenced to contain CCC | GGG sequence which can be cleaved specifically by SmaI enzyme. The components for the first network **D-A** remained the same. **DN** hydrogel was digested by SmaI enzyme at room temperature over 24h, cleaving the second network **D-B** yet still maintaining the first network **D-A** in the system (**Figure 4.7**), hence decreasing the mechanical strength of **DN** hydrogel.

Additionally, full degradation of the **DN** hydrogel can be achieved by addition of both restriction enzyme SmaI and endonuclease DNase I, which targeting DNA at non-specific sites. Upon addition of both enzymes to the system, the **DN** hydrogel network was fully degraded and converted to solution in a one-way gel to sol transition. The programmable responsiveness

of the **DN** hydrogel system is beneficial in the application of 3D cell culture drug screening. The **DN** hydrogel can serves both as the scaffold to maintain the cells structural integrity and also as the vehicle to deliver the bio-cue or drugs cargo to the 3D cell culture system in controlled manner.

4.2.10. 3D Cell Culture in Double Network DNA Hydrogel

Encouraged by the enhanced mechanical property and structural integrity exhibited by the double network **DN** hydrogel, we further investigated its application as the 3D cell culture platform by encapsulating A549 cells in both single-network and double-network hydrogels (**Figure 4.9**). The A549 cells were incubated over period of 96h to allow sufficient time for the cells to proliferate and assemble into multicellular spheroid formation. The formation of spheroids, the three-dimensional cell culture arrangement into sphere-like formation, is beneficial to provide better information regarding the cells interaction in the microenvironment *in vivo*. Thus, optimizing the hydrogel mechanical property that can sustain the spheroid formation is crucial for the development of DNA hydrogel as 3D cell culture platform.

In all hydrogels the cells morphology appeared to be spherical instead of stretched as in 2D cell culture, hence confirming that the cells were suspended three-dimensionally in the DNA hydrogels. Interestingly, the spheroid in the three different DNA hydrogels showed variability in size and shape despite the same amount of incubation time. Both single-network **D-A** and **D-B** hydrogels (**Figure 4.8A-B**) showed non-spherical spheroid shape. In single-network **D-A** hydrogel the cell spheroid appeared to be in ellipsoidal shape with the size of

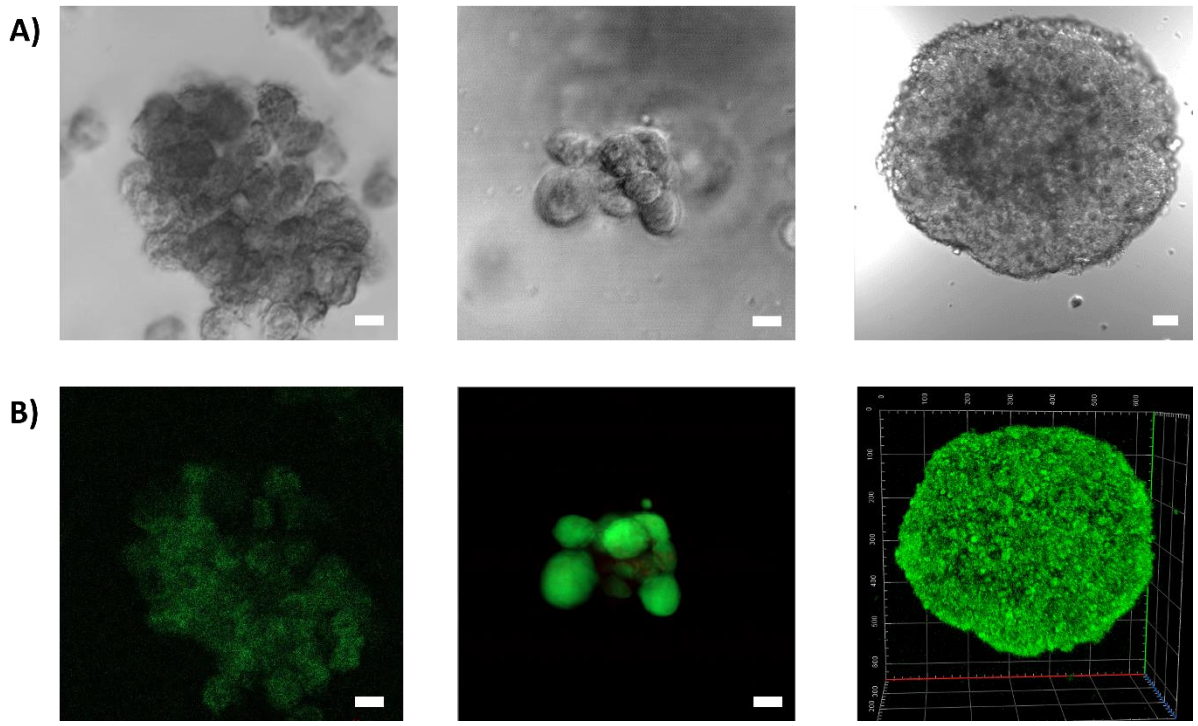

Figure 4.8. A549 cells cultured in single network **D-A**, **D-B**, and double network **DN** hydrogel after 96 hours. A) microscope image, and B) fluorescence image of the cells in **D-A** (left), **D-B** (middle), **D-N** (right). Cells were stained with Calcein-AM (live cells-green) and PI (dead cells-red). Scale bar 50µm. Grit 100µm.

112µm, indicating that the spheroid was still in the tight aggregation arrangement. The cell viability in **D-A** hydrogel was 99.3±06%. The spheroid morphology in **D-B** hydrogel appeared to be like Figure 8-shaped with the size half of the spheroid in **D-A** hydrogel. The smaller spheroid size in **D-B** hydrogel may be due to the tightly crosslinked and rigid structure of the **D-B** hydrogel. The small porosity and pore interconnectivity of the **D-B** hydrogel would diminish the efficient nutrient diffusion and waste exchange in the cell culture system, hence lowering the cell proliferation rate in the spheroid.[24] The cell viability in **D-B** hydrogel was 97.1±0.4%

Remarkably, the spheroid in double-network **DN** hydrogel appeared to be in a spherical shape with over 500µm size and viability of 95.3±0.9%. The structure and enhanced mechanical property in **DN** hydrogel provided the optimal condition for the spheroid formation. The **DN** porous and long-range interconnectivity structure allowed facile nutrient, gas, and

waste diffusion in the cells microenvironment and provided sufficient space for the cells to grow and interact. Furthermore, the enhanced mechanical stiffness exhibited by the **DN** hydrogel provided structural integrity for the cells microenvironment to sustain the spheroid formation into compact spheroid. The **DN** hydrogel showed robust and better performance as the *in vitro* 3D cell culture platform to host, support, and sustain the spheroid formation for the study of the tumour model or drug screening.

4.3. Conclusion

In this work, we proposed the strategy to enhance DNA hydrogel mechanical strength by designing a DNA hydrogel system with two networks which exhibit flexible and rigid DNA structure. Systematic study to design a flexible and rigid dendritic DNA hydrogel was performed by varying the bp length and GC-content on the dendritic DNA gelation branches. The self-assembled supramolecular hydrogel was entirely based on DNA hybridization, which is distinctly different from the previously reported supramolecular double-network hydrogel system. The extensive rheology study further confirmed that the two DNA networks were interpenetrating and bound within each other, leading to the enhanced mechanical properties of the DNA hydrogel. Furthermore, the double-network DNA hydrogel demonstrated dynamic nature of the supramolecular hydrogel and programmable responsiveness against temperature and restriction enzyme. In addition, cells cultured in the double network DNA hydrogel grow into a distinct compact spheroid arrangement due to the optimal mechanical stiffness and porous structure to sustain the spheroid formation. This approach demonstrated the versatile functionality of the dendritic DNA design which could be harnessed as a promising tool for the on-demand 3D cell culture platform and further application in drug release, drug screening, tissue engineering, and other biomedical application.

4.4 Experimental Details

Materials

Unless otherwise stated, all reagents and solvents were purchased from Sigma-Aldrich (Singapore). All the phosphoramidites and reagents for the solid phase DNA synthesis were purchased from Glen Research (Virginia, USA) and the Mermade column was purchased from Bioautomation (Texas, USA). All single strand DNAs were purchased from Sangon Biotech (Shanghai, China). The buffer solution was purchased from 1st Base (Singapore). SmaI and DNase I enyme were purchased from New England Biolab (Singapore). Ultrapure deionized (DI) water used in all experiments was obtained from a Millipore Milli-Q system (resistivity 18.2 MΩ.cm).

Methods

- **Solid Phase Dendritic DNA Synthesis**

Synthesis of the dendritic DNA was performed on Bioautomation Mermade 4. Fast deprotecting phosphoramidite and the long-trebler phosphoramidite (10-1925-90) was used to synthesize the dendritic DNA. The DNA cleavage from the solid support was done in 33% ammonium hydroxide solution at 25ºC for 90 minutes followed by deprotection at 60ºC for an hour. The DMT-ON DNA products were purified by HPLC (Shimadzu, Japan) equipped with reverse-phase (RP) column (Microsorb 100-5 C18 Dynamax 250x10 mm). The HPLC mobile phases were 0.1M TEAA buffer (pH 7) and ACN. The gradient method was used to collect the product. The concentration of the ACN was increased from 5% to 60% over 30 minutes at 3.5 mL/min flush speed. The DMT-ON dendritic DNA were flushed at 38-44% ACN. The collected product was freeze dried by lyopholizer. The DMT protecting group on the dendritic DNA was cleaved by 80% acetic acid (200 µL) for 15 minutes at room temperature. 1 mL cold ethanol

was added to the solution followed by centrifugation at 13,500 xg for 10 minutes at 4ºC to precipitate the DNA. The solvent was removed by vacuum concentrator.

The detitylated DMT-OFF dendritic DNA was purified by HPLC with the same method. The dendritic DNA was flushed at 23-26% ACN. The collected product was freeze dried. The lyophilized dendritic DNA powder was dissolved in 1XTAE, 12.5mM $MgCl_2$ buffer (pH 7) and stored as the stock solution. The quantification of the dendritic DNA was done by measuring the absorption at wavelength 260 nm with Nanodrop 2000c spectrophotometer (Thermo Scientific, US).

- **Single-network DNA Hydrogel Assembly**

Dendritic DNA and linker with ratio of 1:3 [**D**] = 100μM, [**L**] = 300μM were mixed in 1XTAE, 12.5 mM $MgCl_2$ buffer (pH 7). The solution was heated to 95℃ for 10 minutes in the heating block (AccuBlock™ Digital Dry Bath, Labnet International) remove the initial DNA interaction. The heating block was turned off and the solution was slowly cooled down to room temperature to let the hydrogel assemble. The resulting DNA hydrogel was stored in the 4℃ fridge.

- **Double-network DNA Hydrogel Assembly**

All components of the double network hydrogel (**D-A, D-B, L-DA, L-DB**) were mixed in 1XTAE, 12.5 mM $MgCl_2$ buffer (pH 7) at different ratio. The total ratio of dendritic DNA vs Linker is always 1:3. The total concentration of dendritic DNA components (**D-A**+**D-B**) is 100μM and linker (**L-DA+L-DB**) is 300μM. The solution was vortexed to ensure homogeneous solution and heated to 95℃ for 10 minutes in the heating block (AccuBlock™ Digital Dry Bath, Labnet International) to remove the initial DNA interaction. The heating block was turned off

and the solution was slowly cooled down to room temperature to let the hydrogel assemble. The resulting DNA hydrogel was stored in the 4℃ fridge.

- **UV Melting Temperature**

The UV melting temperature measurement was performed on UV spectroscopy (UV-1800, Shimadzu) equipped with the temperature controller. 120μL DNA hydrogels with total concentration of [**D**] = 0.5μM, [**L**] = 1.5μM were loaded into the 8-microwell cuvette. The samples were first heated to 90°C and cooled down to 20°C with ramp rate of 1°C/min. The UV melting curve was acquired by recording the absorbance at 260nm vs temperature. The melting temperature was obtained by fitting the data points into a sigmoidal equation.

- **Scanning Electron Microscope (SEM)**

5μL of the DNA hydrogel was dropped on the silica wafer and freeze-dried overnight. Prior to SEM observation, the samples were coated with Pt at 20mA for 60s to get 12nm Pt height. The field emission SEM images were acquired using JEOL-JSM 6700F.

- **Mechanical Property by Rheometer**

The mechanical property measurement was carried out with Discovery Hybrid Rheometer (DHR-3, TA Instruments). The parallel plate (25mm diameter) was used and the sample gap was set to 300μm. 50μL DNA hydrogel was assembled for the experiment.

- *Time Sweep*

  The elastic modulus (G') and loss modulus (G") as a function of time were recorded at constant strain 1% and frequency 1Hz for 5 minutes.

- *Temperature Sweep*

  The elastic modulus (G') and loss modulus (G") was recorded against temperature change at constant strain 1% and frequency 1Hz.

- *Amplitude sweep*

  The elastic modulus (G') and loss modulus (G") was recorded against increasing oscillation strain from 0.1% to 1000% at constant strain 1% and frequency 1Hz.

- **Enzyme Digestion**

40μL of **DN** hydrogel was assembled in the corresponding enzyme reaction buffer with total [**D**] = 50μM, [L] = 150μM with ratio of [**D-A**] : [**D-B**] = 1:2 in DN hydrogel. After annealing, the gel was stained with 4μL 6x DNA loading dye (Thermo Fisher, Singapore) for visualization.

For partially digested hydrogel, the hydrogel was incubated with 15U SmaI enzyme. For fully digested hydrogel, the hydrogel was incubated with 15U of both SmaI and DNase I enzyme. The incubation occurred at room temperature for 24 hours and was inactivated by addition of 1μL 0.5M EDTA to the hydrogel. The sample was then vortexed and placed upside down.

- **Cell Line and Culture Condition**

The cell line used in all experiments was A549 human lung carcinoma. For the 3D cell culture, the cell media was DMEM+Glutamax I supplemented with 1X Non-essential Amino Acid. All cells were incubated in a humidified atmosphere of CO_2/air (5%/95%) at 37℃.

- **Live/Dead Fluorescence Imaging**

3D Cell Culture. 5000 cells in the cell media was mixed with the **D** and **L** to form 20μL DNA hydrogel. Total concentration of the dendritic DNA is [**D**] = 100μM, and linker [**L**] = 300μM) with ratio of 1:3. For the double network DNA hydrogel, the ratio of [**D-A**] vs [**D-B**] components is 1:2. The solution was gently pipetted to ensure homogenous cell distribution in the hydrogel. The hydrogel was drop-casted in the middle of the μ-dish 35mm, high. After 3 hours, 50 μL cell media was topped up on top of the hydrogel to ensure enough nutrients for the cells throughout the experiment. The cells in the hydrogel was incubated for 96 hours and cell media was changed every two days.

Live/Dead Cell Staining Kit (04511, Sigma) was used to determine the viability of the cell. The kit contains Calcein-AM which stains viable cells to generate green fluorescence (excitation:490 nm, emission 515nm) and Propidium Iodide (PI, excitation :535nm, emission:617nm) which stains dead cells to emit red fluorescence.

10 μL of solution A (Calcein-AM) and 5μL of solution B (PI) was added to 5mL PBS to prepare the assay solution. The cell media of the sample was firstly removed. Then, the sample was gently washed with PBS to remove residual esterase activity followed by staining with 100μL assay solution and incubation for 30 minutes at 37℃. All images were collected by the confocal microscope (Carl Zeiss LSM 800) using the 63x oil immersion and 20x objective lense. 488nm excitation was used as both Calcein-AM and PI can be excited using this excitation wavelength. The 3D constructs were acquired with z-step size of 2μm (20x lens) or 0.5μm (63x lens).

The cell viability was calculated by identifying cells using the Imaris (Bitplane, Northern Ireland) spot detection function. The relative proportion of live cells (green fluorescent) and dead cells (red fluorescent) are determined to get the cell viability. The data is presented as mean values ± standard deviation.

4.5 Supporting Information

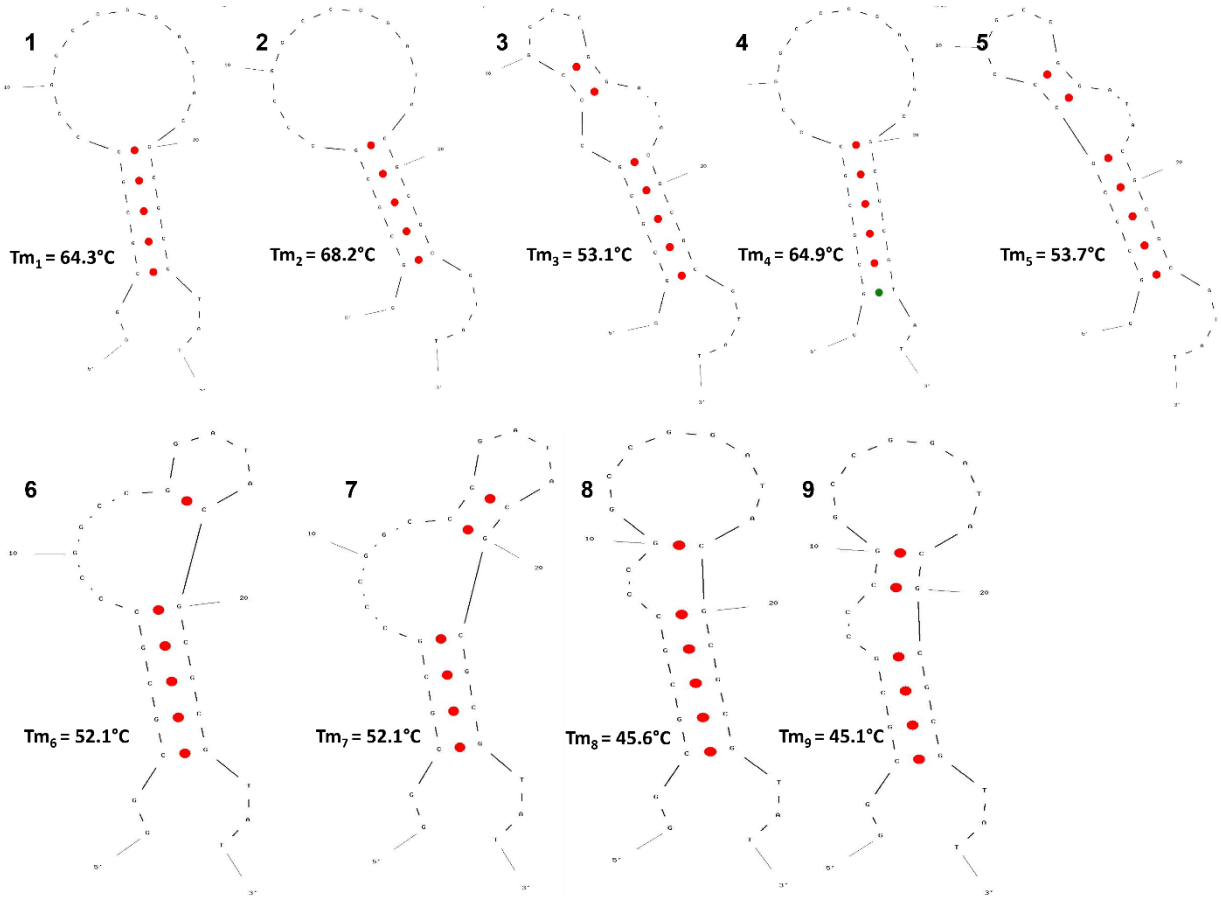

Figure S4.1. Formation of hairpin on the linker **L4** and its high melting temperature preventing the duplex formation and further hydrogel crosslinking network. Figures and melting temperature calculation retrieved from : sg.idtdna.com/calc/analyzer

4.6 References

1. Gačanin, J.; Kovtun, A.; Fischer, S.; Schwager, V.; Quambusch, J.; Kuan, S. L.; Liu, W.; Boldt, F.; Li, C.; Yang, Z.; Liu, D.; Wu, Y.; Weil, T.; Barth, H.; Ignatius, A., *Advanced Healthcare Materials* **2017,** *6* (21), 1700392.

2. Li, F.; Lyu, D.; Liu, S.; Guo, W., *Advanced Materials* **2020,** *32* (3), 1806538.

3. Nishikawa, M.; Ogawa, K.; Umeki, Y.; Mohri, K.; Kawasaki, Y.; Watanabe, H.; Takahashi, N.; Kusuki, E.; Takahashi, R.; Takahashi, Y.; Takakura, Y., *J Control Release* **2014,** *180*, 25-32.

4. Kang, H.; Liu, H.; Zhang, X.; Yan, J.; Zhu, Z.; Peng, L.; Yang, H.; Kim, Y.; Tan, W., *Langmuir* **2011,** *27* (1), 399-408.

5. Yue, L.; Wang, S.; Wulf, V.; Willner, I., *Nature Communications* **2019,** *10* (1), 4774.

6. Merindol, R.; Delechiave, G.; Heinen, L.; Catalani, L. H.; Walther, A., *Nature Communications* **2019,** *10* (1), 528.

7. Zhou, X.; Li, C.; Shao, Y.; Chen, C.; Yang, Z.; Liu, D., *Chem Commun (Camb)* **2016,** *52* (70), 10668-71.

8. Liu, H.; Cao, T.; Xu, Y.; Dong, Y.; Liu, D., *International Journal of Molecular Sciences* **2018,** *19* (6), 1633.

9. Walia, S.; Morya, V.; Gangrade, A.; Naskar, S.; Teja, A. G.; Dalvi, S.; Maiti, P. K.; Ghoroi, C.; Bhatia, D., *bioRxiv* **2021**, 2021.07.31.454582.

10. Wang, Y.; Shao, Y.; Ma, X.; Zhou, B.; Faulkner-Jones, A.; Shu, W.; Liu, D., *ACS Applied Materials & Interfaces* **2017,** *9* (14), 12311-12315.

11. Topuz, F.; Okay, O., *Macromolecules* **2008,** *41* (22), 8847-8854.

12. Bush, J.; Hu, C.-H.; Veneziano, R., *Applied Sciences* **2021,** *11* (4), 1885.

13. Gong, J. P.; Katsuyama, Y.; Kurokawa, T.; Osada, Y., *Advanced Materials* **2003,** *15* (14), 1155-1158.

14. Gong, J. P., *Science* **2014,** *344* (6180), 161-162.

15. Gong, J. P., *Soft Matter* **2010,** *6* (12), 2583-2590.

16. Gu, Z.; Huang, K.; Luo, Y.; Zhang, L.; Kuang, T.; Chen, Z.; Liao, G., *WIREs Nanomedicine and Nanobiotechnology* **2018,** *10* (6), e1520.

17. Cao, T.; Jia, H.; Dong, Y.; Gui, S.; Liu, D., *ACS Applied Materials & Interfaces* **2020,** *12* (4), 4185-4192.

18. Li, C.; Chen, P.; Shao, Y.; Zhou, X.; Wu, Y.; Yang, Z.; Li, Z.; Weil, T.; Liu, D., *Small* **2015,** *11* (9-10), 1138-1143.

19. Liu, G.; Zhou, C.; Teo, W. L.; Qian, C.; Zhao, Y., *Angewandte Chemie International Edition* **2019,** *58* (28), 9366-9372.

20. Scipioni, A.; Anselmi, C.; Zuccheri, G.; Samori, B.; De Santis, P., *Biophysical Journal* **2002,** *83* (5), 2408-2418.

21. Geggier, S.; Vologodskii, A., *Proceedings of the National Academy of Sciences* **2010,** *107* (35), 15421-15426.

22. Hormeño, S.; Ibarra, B.; Carrascosa, J. L.; Valpuesta, J. M.; Moreno-Herrero, F.; Arias-Gonzalez, J. R., *Biophys J* **2011,** *100* (8), 1996-2005.

23. Zhao, Y.; Liu, G.; Zhou, C.; Teo, W.; Qian, C., *Angewandte Chemie International Edition* **2019,** *58*.

24. Zanoni, M.; Piccinini, F.; Arienti, C.; Zamagni, A.; Santi, S.; Polico, R.; Bevilacqua, A.; Tesei, A., *Scientific Reports* **2016,** *6* (1), 19103.

CHAPTER 5

Summary and Future Outlook

Nucleic acid has arisen as the outstanding building block material for the hydrogel assembly due to its unique properties such as sequence programmability, multifunctional tunability, precise recognition, structural rigidity, and biocompatibility. The DNA hydrogel self-assembly is formed purely by the supramolecular interaction between the complementary DNA base pairs which results to the dynamic interaction in the hydrogel and confers to the thixotropic properties and designable responsiveness of the hydrogel. Thus, allowing the DNA building block as the competitive alternative in formation of hydrogel with tailored function and precise molecular structure design. However, some challenges still need to be addressed to further employ the supramolecular DNA hydrogel for practical use in tissue engineering, such as complex DNA building block design to load functionalities into the hydrogel and the low mechanical strength of the pure DNA hydrogel. In this thesis, we focus on the development of self-assembled dendritic DNA hydrogel design to offer bio-functionality and enhanced mechanical property for versatile application in 3D cell culture.

Chapter 1 introduces the background information of 3D cell culture significance and the ongoing research towards developing the biomimetic 3D cell culture platform. The different platforms of 3D cell culture technique were described, and particular interest lies on the hydrogel scaffold. The development of the different type of hydrogel scaffold was explained, and the challenges were discussed. Finally, the current development towards designing DNA hydrogel was further explored as well as the challenges that it faces.

Chapter 2 reports the self-assembly of dendritic DNA and linker to form the supramolecular dendritic DNA hydrogel (**DDH**), which was subsequently applied for 3D cell culture. A study was done to control and tune the inner structure and mechanical properties of the DNA hydrogel. Distinct cell morphology with high viability was achieved in **DDH**.

Additionally, due to the dynamic nature of the supramolecular hydrogel, the cells can be harvested and re-cultured into a new DNA hydrogel, owing to the thixotropic and self-healing property of **DDH**. The dendritic DNA hydrogel offers simultaneous dual function of bio-cue casting to the loading branch and the hydrogel crosslinking via the gelation branches, thus offer simple strategy to functionalize the hydrogel to cater for the different needs of 3D cell culture platform.

Chapter 3 demonstrates the potential application of functionalizing dendritic DNA hydrogel with the integrin-targeting cyclic peptide ligand, cRGDfK, to control the attachment to the DNA hydrogel framework. The dendritic DNA offers simultaneous multifunction of bio-cue loading and gelation to form the hydrogel network by independently programming the loading and gelation branch on the dendritic DNA building block. The temperature-sensitive peptide was conjugated with a ssDNA complementary to the loading branch and subsequently casted into the dendritic DNA framework via base pair hybridization without compromising the effectiveness of the targeting peptide and the cell viability. The embedded fibroblast cells in the functionalized hydrogel appeared to adhere and spread on the hydrogel framework and showed distinct cell morphology as compared to the negative control. The dendritic DNA hydrogel offers a versatile tool to design a hydrogel with controlled mechanical and biochemical property based on-demand.

Chapter 4 presents a strategy to enhance the mechanical property of the DNA hydrogel by incorporating interpenetrating double network with flexible and rigid structure into the DNA hydrogel. Systematic study was performed to study the effect of DNA base pair length and GC-content composition on the mechanical property of a single network DNA hydrogel, before further incorporating two networks with flexible and rigid mechanical property into a double

network DNA hydrogel. The extensive rheology study further confirmed that the two DNA networks were bound within each other, leading to the enhanced mechanical property of the double network DNA hydrogel. In addition, the double network DNA hydrogel showed programmable responsiveness against temperature and restriction enzyme, endowing the controlled responsiveness design of the DNA hydrogel. Furthermore, application to 3D cell culture showed that the cells in double network DNA hydrogel were able to grow and form a distinct compact spheroid arrangement due to the optimum mechanical stiffness and porous structure of the hydrogel.

Future direction of the dendritic DNA hydrogel focuses on incorporating the hydrogel for co-culture to better mimic the cell microenvironment *in vivo*. Due to the dynamic nature of the supramolecular network, the DNA hydrogel offers self-healing and thixotropic property which enable two different hydrogels merge and re-assemble into one. Therefore, cell migration study of two cell lines can be performed. Additionally, stimuli-responsive dendritic DNA hydrogel can be designed to incorporate a therapeutic agent into the dendritic DNA framework. The therapeutic agent can be released based on-demand over the course of cell culture, thus allowing for further application in drug release, drug screening, tissue engineering, and other biomedical application.